UNIVERSIDADE DE SÃO PAULO

INSTITUTO DE ASTRONOMIA, GEOFÍSICA E CIÊNCIAS ATMOSFÉRICAS

JAIRO FRANCISCO SAVIAN

Magnetostratigrafia e reconstrução paleoambiental de sucessões marinhas do Oceano Neo-Tétis: novas perspectivas acerca dos principais eventos paleoclimáticos do Paleógeno

Magnetostratigraphy and palaeoenvironmental record of marine sucessions from the Neo-Tethys Ocean: New insights into the main Paleogene palaeoclimatic events

São Paulo

2013

JAIRO FRANCISCO SAVIAN

Magnetostratigrafia e reconstrução paleoambiental de sucessões marinhas do Oceano Neo-Tétis: novas perspectivas acerca dos principais eventos paleoclimáticos do Paleógeno

Magnetostratigraphy and palaeoenvironmental record of marine sucessions from the Neo-Tethys Ocean: New insights into the main Paleogene palaeoclimatic events

Tese apresentada ao Instituto de Astronomia, Geofísica e Ciências Atmosféricas da Universidade de São Paulo como requisito parcial para a obtenção do título de Doutor em Ciências.

Área de concentração: Geofísica

Orientador: Prof. Dr. Ricardo Ivan Ferreira da Trindade

Co-Orientador: Prof. Dr. Luigi Jovane

São Paulo

2013

DEDICATÓRIA

Dedico essa tese a Valdomiro Fermino Savian e Antoninha Angelina Ponte Savian, meus pais, com carinho, admiração e gratidão pelo incansável apoio, compreensão e carinho ao longo de toda minha vida.

AGRADECIMENTOS

Table of contents

Resumo

SAVIAN, J.F. **Magnetostratigrafia e reconstrução paleoambiental de sucessões marinhas do Oceano Neo-Tétis: novas perspectivas acerca dos principais eventos paleoclimáticos do Paleógeno**, 2013. 145 pp. Tese (Doutorado) - Instituto de Astronomia, Geofísica e Ciências Atmosféricas, Universidade de São Paulo, São Paulo, 2013.

O intervalo que compreende o Paleoceno, Eoceano e Oligoceno (65,5-23,03 Ma) testemunhou importantes mudanças paleoclimáticas e paleogeográficas. Dados de isótopos estáveis ($\delta^{18}O$ e $\delta^{13}C$) em foraminíferos pelágicos mostram uma tendência de resfriamento de longo período, que termina com o evento abrupto Oi-1 (~34 Ma), próximo à transição Eoceno/Oligoceno, coincidente com a principal fase de glaciação da Antártida. Sobreposta a essa tendência de resfriamento lenta, observa-se curtos intervalos de aquecimento global extremos. Estes eventos *hipertermais* tem duração inferior a 300 kyrs e correspondem a variações de temperatura de 5° a 6° C. Na metade do Eoceno (~ 49-34 Ma), os registros isotópicos também indicam um forte evento de aquecimento transiente há ~40,0 Ma, o Ótimo Climatico do Eoceno Médio (MECO, na sigla em inglês). Nesta Tese apresentamos a magnetoestratigrafia, bioestratigrafia (nanofósseis e foraminíferos), litoestratigrafia, magnetismo ambiental, geoquímica e dados de isótopos de carbono e oxigênio em carbonato e em foraminíferos bentônicos ao longo do intervalo Eoceno-Oligoceno de sucessões do Oceano Indico (testemunho ODP 711A) e Neo-Tétis Oriental (seções de Monte Cagnero e Contessa). Os principais eventos climáticos globais do Paleoceno foram reconhecidos nestas seções. Este estudo mostra que as seções ODP 711A, Monte Cagnero (MCA), e Contessa (CHW–CR) oferecem um registro completo e integrado desde o Paleoceno até o Oligoceno da magnitude dos eventos hipertermais e do MECO, bem como as variações biogeoquímicas que os acompanharam. A seção de Monte Cagnero registra os mais importantes eventos climáticos do Eoceno-Oligoceno Inferior, incluindo a transição E-O em ~34 Ma e o MECO em ~40 Ma. Uma análise integrada e de alta resolução de isótopos estáveis, geoquímica, micropaleontologia e magnetismo ambiental neste seção ao longo do MECO revelou um intervalo de alta produtividade marcado por uma grande abundância de magnetofósseis, compreendendo o pico de temperatura do MECO e o período imediatamente posterior. O

mesmo sinal foi observado em Contessa e no testemunho ODP 711A. Nós especulamos que durante o MECO, um período mais quente, ocorreu um aumento na quantidade de hematita levada aos oceanos por meio de transporte eólico gerando fertilização e um consequente aumento de produtividade nos oceanos. A ocorrencia ubiqua de magnetofósseis em períodos quentes ao longo de todo o Eoceno sugere que mecanismos similares tenham sido responsáveis pelos picos de produção e preservação de magnetossomas.

Abstract

SAVIAN, J.F. **Magnetostratigraphy and palaeoenvironmental records in marine sedimentary sucessions from Neo-Tethys Ocean: New insights into the main Paleogene palaeoclimate events**, 2013. 145 pp. Thesis (Doctorate) - Instituto de Astronomia, Geofísica e Ciências Atmosféricas, Universidade de São Paulo, São Paulo, 2013.

The interval comprising the Paleocene, Eocene and Oligocene (65.5 to 23.03 Ma) has witnessed major changes in paleoclimate and paleogeography. Stable isotope records (δ^{18}O and δ^{13}C) from pelagic foraminiferal show a long-term cooling trend starting at ~55 Ma, which ends abruptally at the Oi-1 event (~34 Ma), near the Eocene/Oligocene transition, which is interpreted as the main episode of glaciation of Antarctica. Superimposed on this cooling trend, brief intervals of extreme warmt occur globally. These hyperthermal events last for less than 300 kyrs and may correspond to a global temperature increase of 5° to 6°C. In the middle to late Eocene, a strong transient warming event has been recognized in the oceanic record at ~40.0 Ma, the Middle Eocene Climate Optimum (MECO). The amplitude of the MECO warming is similar to that of hyperthermals, but it durations if two times longer; its origin and global nature being still debated. In this thesis we present a magnetostratigraphic analysis, integrated with biostratigraphy (calcareous nannofossils and foraminifera), lithostratigraphy, environmental magnetism, wt.% $CaCO_3$ and isotope records on bulk carbonate and on benthic foraminifera through the Paleogene interval from sedimentary successions from the Indian Ocean (ODP Hole 711A) and Eastern Neo-Tethys (Monte Cagnero and Contessa sections). The main global climatic events in the Paleogene were recognized in these sections. This study shows that the ODP 711A, Monte Cagnero (MCA), and Contessa (CHW–CR) sections are a complete and integrated record of hyperthermals, the MECO and the biogeochemical changes that occurred during the Paleocene to Oligocene interval. The Monte Cagnero section likely records the most important middle Eocene–early Oligocene climate events, such as the E-O climate transition at ~34 Ma and the MECO event at ~40 Ma. An integrated and high-resolution analysis of stable isotopes, geochemistry, micropaleontology and environmental magnetism of this section through the MECO interval shows an interval of very high productivity comprising

the MECO peak and its aftermath marked by a higher abundance of fossil magnetotactic bacteria. The same signal has also been found in Contessa and ODP 711A. We speculate that eolian hematite durint the MECO event may have promoted iron fertilization of the oceans during the warming event increasing significantly the primary productivity in the ocean. The widespread occurrence of magnetofossils in other warming periods suggest a common mechanism linking climate warming and the enhancement of magnetossome production and preservation.

Chapter 1. Introduction

1.1. A Brief Summary of the Paleogene Climate

The Paleogene (Paleocene to Oligocene, 65.5 to 23.03 Ma) is a period of the Earth's history that includes gradual trends of warming and cooling climatic conditions driven by tectonic process (10^5 to 10^7 years), periodic cycles driven by orbital process (10^4 to 10^6 years), and rapid shifts with extreme climate transients events (10^3 to 10^5 years) (e.g., Zachos et al., 2001; 2008). The study of sedimentary achives of this age around in the Tethys Realm contributes to better understand the continuous changes esperienced by the Earth's climate system. This period is also ideal to better understand the relationships between carbon cycling and climate in the absence of anthropic influence (Zachos et al., 2008).

Deep-sea stable isotope records indicate a general cooling trend over the last 50 Ma (Figure 1.1), since the early Eocene climatic optimum (EECO). The early Cenozoic was characterized by higher concentrations of greenhouse gases and much warm mean global temperature (Zachos et al., 2001; 2008). The Paleogene was a key transition in Earth history during which global climate changed from warm comparatively ice-free conditions to the colder, more glaciated state of the Cenozoic (Zachos et al., 2001).

Global temperatures during the Paleogene were aproximatly 12°C higher than today, especially during the EECO, 51-53 Ma ago, when the global climate system experienced the highest temperatures and pCO$_2$ concentration during the Cenozoic (Zachos et al., 2008). The EECO was followed by a long trend toward cooler conditions as expressed by a 3.0‰ rise in δ^{18}O with much of the change occurring over the early middle (50 to 48 Ma) and late Eocene (40 to 36 Ma), culminating in the Oi-1 glaciation (~33.4 Ma; Kennett and Shackeleton, 1976; Miller et al., 1991; Zachos et al., 2001; Coxall et al., 2005; Katz et al., 2008; Figure 1.1), was a critical part of the shift from a greenhouse climate to an icehouse climate. The long-term decline during the Paleogene in Earth's temperature is coupled to a long-term decline in the CO$_2$ concentration of the atmosphere (Figure 1.1) (Pearson and Palmer, 2000; Royer et al., 2001; Pagani et al., 2005).
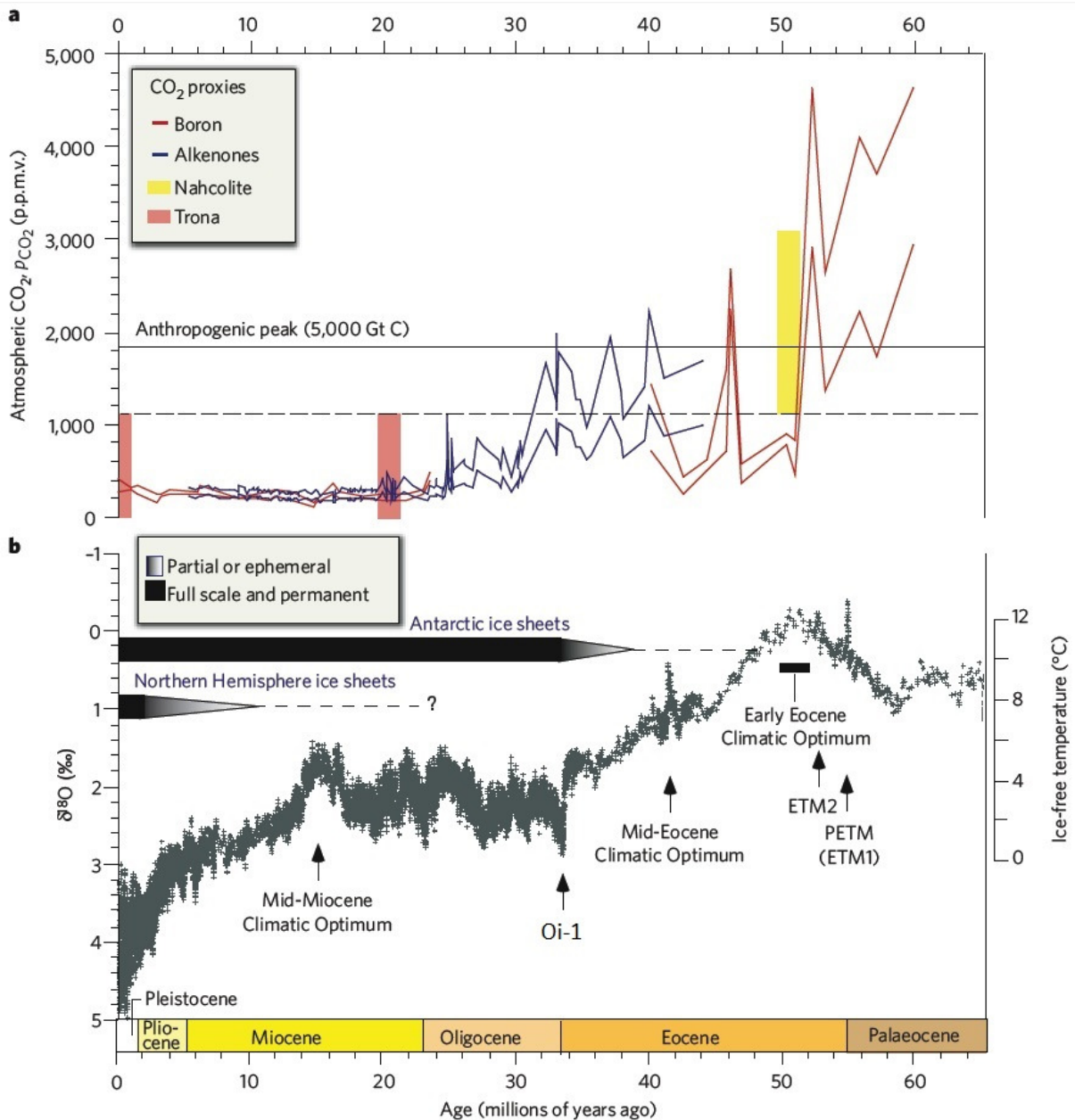
Figure 1.1. (a) Cenozoic pCO₂ for the last 65 Ma from marine and lacustrine proxy records. (b) δ¹⁸O and temperature variation for the same period. The figure also show the mainly climatic events during the Cenozoic, as the short-lived Paleocene Eocene Thermal Maximum (PETM), Eocene Thermal Maximum 2 (ETM2), Early Eocene Climatic Optimum (EECO), Middle Eocene Climatic Optimum (MECO), Oi-1 cooling event, and the Mid-Miocene Climatic Optimum (Modified from Zachos et al., 2008).

The long-term warming trend from the Palaeocene through the early Eocene, was punctuated by a series of abrupt, but short-lived (<300 ka) episodes of widespread warming. These transient events, termed ''hyperthermals'' (Thomas et al., 2000), are associated with major perturbations in the Earth's carbon cycle, major ecologically controlled biotic turnovers, temporary shoaling of the lysocline and carbonate compensation depth (CCD) inducing carbonate dissolution, and accelerated hydrological cycle (e.g., Kennett and Stott, 1991; Zachos et al., 2001; Bralower et al., 2002; Cramer et al., 2003; Bowen et al., 2006; Sluijs et al., 2007; Quillévéré et al., 2008; Westerhold et al., 2008). The Palaeocene–Eocene thermal maximum (PETM) was an important event of temperature warming by 5-7 °C over approximately 30,000 years at around 56 Ma that constitutes one of the most widely used analogues for global change (Dickens, 1999; Bains et. al., 2000). The contribution of the Paleogene paleogeographic, paleoclimatic, and paleoceanographic features suggests that the Paleogene was not a time of stable climate but may have recorded several shifts and the ocean-climate system was controlled by factors very different from today.

Superimposed on the period of cooling trend after the EECO, the middle Eocene climatic optimum (MECO) (Bohaty and Zachos, 2003; Jovane et al., 2007b; Bohaty et al., 2009), around 40 Ma, represents ~500 kyr increase in global surface and bottom water ocean temperatures of up to 4°C. These long-term cooling trend culminating in the Oi-1 glaciation (~33.4 Ma; Miller et al., 1991, Figure 1.1), more glaciated state of the Neogene that was a critical part of the shift from a greenhouse climate to an icehouse climate. The Eocene-Oligocene transition (E/O) transition reveals an abrupt stepwise onset of Antarctic glaciations with global shifts in the distribution of marine biogenic sediments, an overall increase in ocean fertility, a major drop in the CCD, and onset of Atlantic thermohaline circulation (Coxall et al., 2005; Via and Thomas, 2006; Billups, 2008). During this interval, Antarctica grew a large ice sheets, ≥ 50% the size of the present day volume (Coxall et al., 2005; Katz et al., 2008). Whether the opening of Southern ocean gateways was the catalyst for this dramatic climate change is still debated (Kennett, 1977; Scher and Martin, 2006; Backer et al., 2007; Lyle et al., 2007). Alternative and/or perhaps complementary hypotheses call upon other factors, including decreasing greenhouse gases (DeConto and Pollard, 2003; Pagani et al., 2005), and opening or closure of oceans gateways (DeConto and Pollard, 2003; Jovane et al., 2009; Allen and Armstrong, 2008).

One of the most important climatic event that brief reversal of the long-term Eocene cooling trend (Bohaty and Zachos, 2003) that eventually culminated in large-scale Antarctic glaciation and global cooling at the Eocene–Oligocene boundary, was namened Meddle Eocene Climatic Optimum (MECO). The MECO event is a transient warming event occurred gradually over ~500 ka, bigning at ~40.6-40.5 Ma with peak temperatures at ~40 Ma (Bohaty et al., 2009) (Figure 1.2). The MECO warming event was described initially in Southern Ocean drillcore records from Maud Rise and the Kerguelen Plateau (Bohaty and Zachos, 2003). Subsequently studies shown that MECO event to have been a global event because was recorded in South Atlantic, southwest Pacific, and subtropical North Atlantic cores (Bijl et al., 2009, 2010; Bohaty et al., 2009; Edgar et al., 2010; Witkowski et al., 2012), in Tethyan sections in Italy (Jovane et al., 2007b; Luciani et al., 2010; Spofforth et al., 2010; Toffanin et al., 2011, Savian et al., submitted), and also in the high-latitude North Atlantic (Polling et al., 2011). The MECO is defined by a large negative ~1.0–1.5‰ excursion in both benthic foraminiferal and fine-fraction $\delta^{18}O$ records (Bohaty and Zachos, 2003; Bohaty et al., 2009). The MECO warming event is also associated with a brief ~0.5‰ decrease in benthic and fine-fraction $\delta^{13}C$ during peak warming, which is superimposed on a long-term increase in $\delta^{13}C$ (Bohaty et al., 2009). The oxygen isotope ($\delta^{18}O$) records indicate warming of ~4–6 °C that lasted for approximately 500 kyr (Bohaty et al., 2009; Edgar et al., 2010). Increased CO_2 outgassing from volcanic or metamorphic sources were postulated as the most likely causes for a transient increase in the atmospheric CO_2 levels (pCO_2) that led to the greenhouse warming during the MECO event (Bohaty and Zachos, 2003; Zachos et al., 2008; Bohaty et al., 2009; Bijl et al., 2010). The rapid termination of this event has been linked to increased rates of organic carbon burial and resultant lowering of atmospheric pCO_2 (Spofforth et al., 2010).
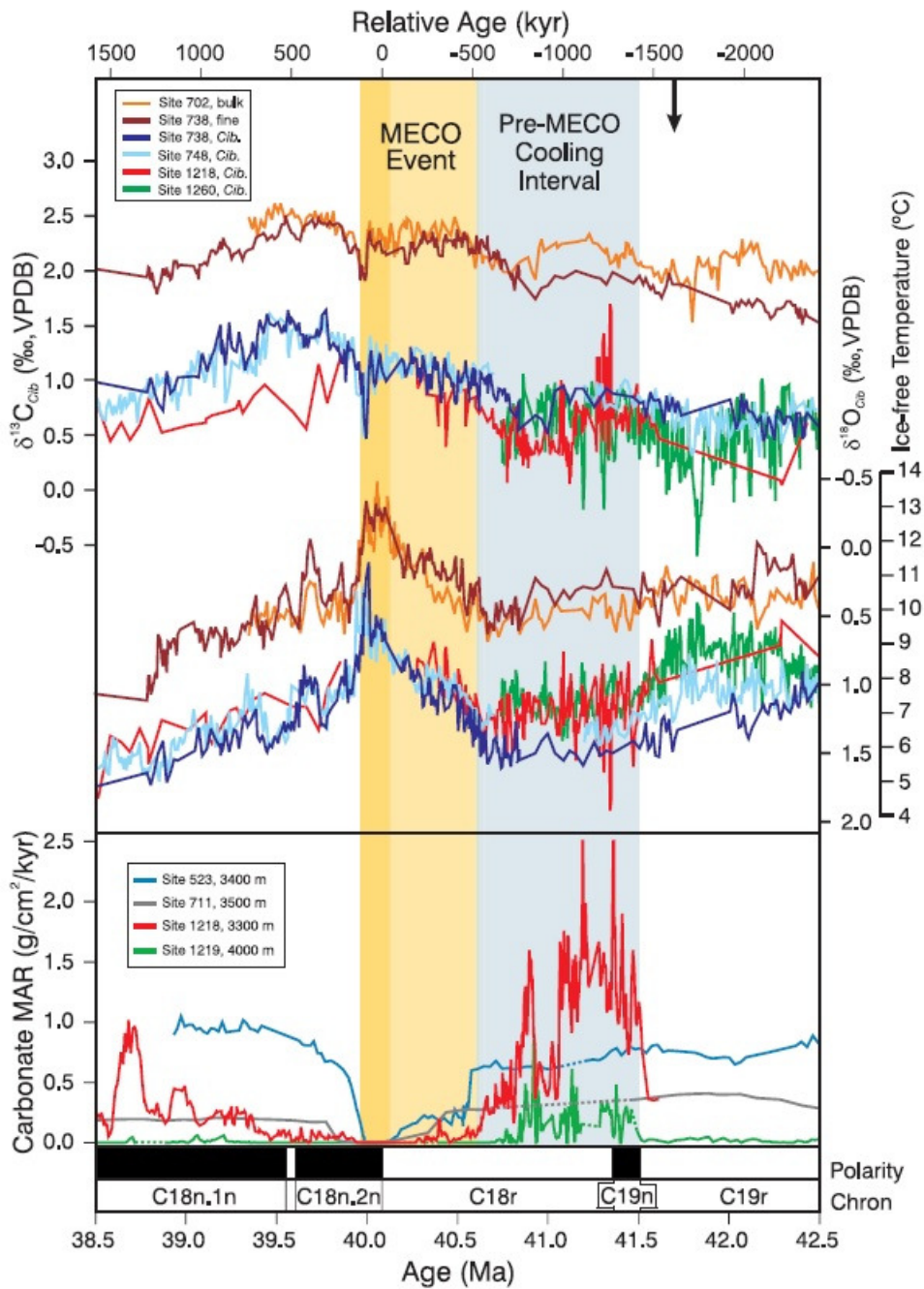
Figure 1.2. *Definition of the MECO event based on Late middle Eocene compilation of benthic foraminiferal stable isotope data, selected bulk/fine-fraction records, and carbonate mass accumulation rate (MAR) records (After Bohaty et al., 2009).*

1.2. The Neo-Tethys in the Paleogene: Magneto- and Biostratigraphy

Extensive outcrops in the Umbria–Marche basin of central Italy include some of the most complete successions of Paleogene sediments known in the Tethyan Realm. These successions could improve the magneto–, bio–, and chronostratigraphic framework of the classical southern Tethyan zonations enabling regional and supraregional correlations to construct a record of reliable Paleogene tropical to subtropical Cenozoic climatic conditions.

Neo-Tethys is defined as the ocean dividing Eurasia to the north from Africa and Arabia to the south (Dercourt et al., 1993). Neo-Tethys was denominated for differentiate the Neo-Tethys Ocean closed through the Alpine-Himalayan orogeny from the Paleo-Tethys Ocean closed along the Hercynian orogeny. In addition to the Neo-Tethys and the Paleo-Tethys, the Para-Tethys is defined as a series of basins north of the Alpine-Himalayan collision, which remained isolated from ocean circulation. Before the Alpine-Himalayan orogeny and the opening of the Red Sea, the Neo-Tethys was a wide ocean separating the Asian-European plate from the African-Arabian plate (Dercourt et al., 1993; Popov et al., 2004). The first Indo-Asian collision is dated at around 55 Ma, and continent-continent collision began at around ~34 Ma (Aitchison at al., 2007). Recently, Allen and Armstrong (2008) showed that the Arabian-Eurasian closure occurred at around the E/O boundary. The Arabian-Eurasia collision extends from the Aegean Sea to Iran, and is mostly concentrated in Turkey and Iran (Allen et al., 2004).

In the 1970's, a new interest in the nearly continuous and complete Paleogene sequences attracted a group of Paleomagnetic researchers to the Umbria-Marche Basin, central Italy. Alvarez et al. (1977) conducted a Paleomagnetic investigation on the Bottaccione Gorge section at Gubbio, at the Cretaceous-Paleogene Scaglia Formation, a succession of continuosly deposited pelagic limestones and marls that provided the magnetic reversal stratigraphy for the Upper Cretaceous and most of the Paleogene (Figure 1.3).
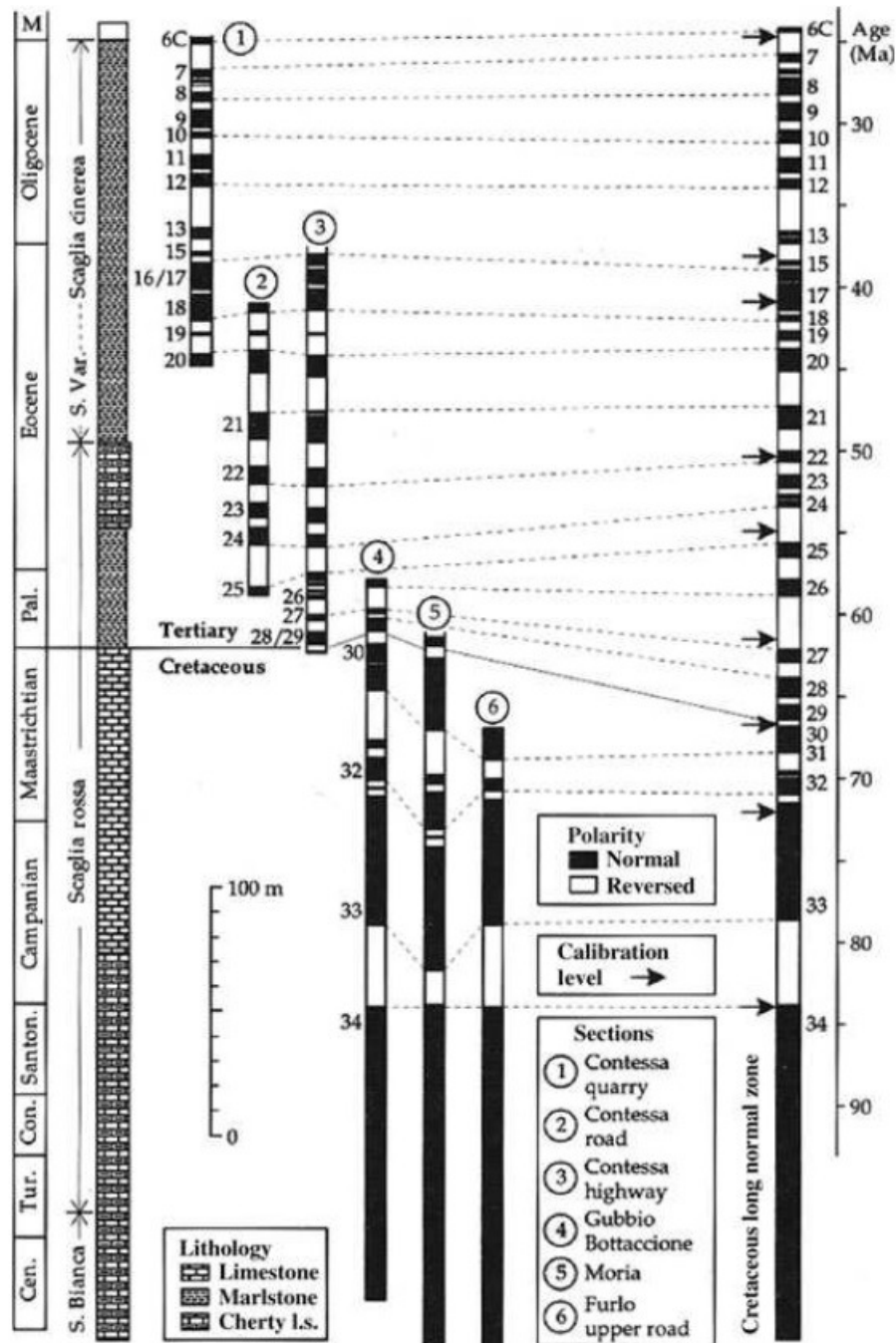
Figure 1.3. Magnetic polarity stratigraphy in the pelagic carbonate rocks of the Umbria-Marche Apennines (Lowrie & Alvarez, 1981).

Successive works of Lowrie et al. (1982) and Napoleone et al. (1983) provided a Paleogene magnetic stratigraphy in the Umbrian pelagic carbonates from Contessa section and Bottaccione Gorge, respectively. The work of William Lowrie and co-authors

independently confirmed the Paleogene geomagnetic polarity history first deduced from the oceanic magnetic anomalies. Also during the 1980s, the magnetostratigraphy of the Massignano section was studied by Bice and Montanari (1988). During the 1990s, the paleomagnetism of the Massignano section was studied by W. Lowrie and L. Lanci (Lowrie and Lanci, 1994; Lanci et al., 1996; Lanci and Lowrie, 1997; Lanci et al., 1998).

The Palaeogene carbonate succession of the Umbria–Marche (U–M) Basin is probably the most thoroughly studied in the Tethyan Realm, thanks to the accessibility of numerous well-exposed outcrops throughout this region, and its remarkable record of many crucial aspects of Earth's history from the Cretaceous–Palaeogene (K–Pg) boundary until the uppermost Oligocene (Coccioni et al. 1986, 1988, 1989, 1994, 2000, 2008, 2009, 2010a, b, 2012; Cresta et al. 1989; Bellagamba and Coccioni, 1990; Mattias et al. 1992; Brinkhuis and Biffi 1993; Premoli Silva and Jenkins 1993; Lowrie and Lanci 1994; Montanari et al. 1994, 1997; Galeotti et al. 2000, 2004, 2010; Montanari and Koeberl 2000; Spezzaferri et al. 2002; Coccioni and Galeotti 2003; Bodiselitsch et al. 2004; Jovane et al. 2004, 2006, 2007a, b, 2009, 2010; Brown et al. 2009; Giusberti et al. 2009; Hyland et al. 2009; Pross et al. 2010, and references therein).

A complete U–M Palaeogene pelagic composite succession (PPCS) was constructed from six well-exposed and thoroughly studied sections magnetobiostratigraphically calibrated and radioisotopically dated from several interbedded volcanosedimentary layers, which provides an improved integrated chronostratigraphy for the Palaeogene time scale, from the K–Pg boundary at 65.5 Ma to the uppermost Oligocene at 23 Ma (Coccioni et al., 2012).

The Monte Cagnero Lower section (lat. 43°38′51″ N; long. 12°28′24″ E) extends from the lower Bartonian to the lower Rupelian and is 70 m–thick (Figure 1.4). It consists of calcareous marls and marls with subordinate marly limestones white, greenish–grey, grey and pink to red in colour. Discrete biotite–rich layers occur at 107.55, 112.2 and 122.8 m (Parisi et al., 1988; Hyland et al., 2009). The transition between the Scaglia Variegata and the Scaglia Cinerea contains deformations possibly related to soft sediment slumping and/or faulting. Twenty reliable biohorizons were recognized, ten of which based on planktonic foraminifera, six to calcareous nannofossils, and four to dinocysts.
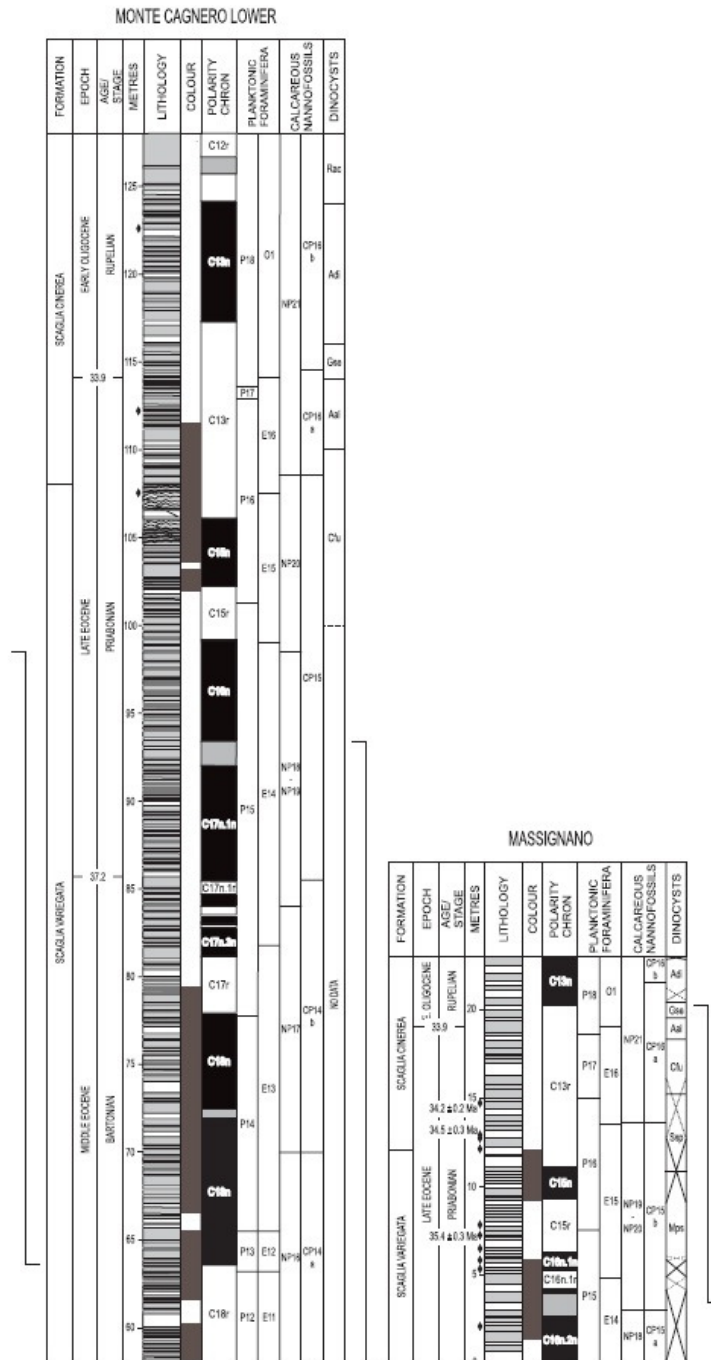
Figure 1.4*. Integrated stratigraphy of the Monte Cagnero Lower and Massignano sections. Chronostratigraphy is after Ogg et al. (2008). Correlation between Contessa Highway Upper and Monte Cagnero Lower sections is tied to the base of Chron C18n and that between Monte Cagnero Lower and Massignano sections to the base of Chron C16n. Planktonic foraminiferal Zones and Subzones are after Berggren et al. (1995) (codified as P) and Berggren and Pearson (2006) and Wade et al. (2011) (codified as E and O). Calcareous nannofossil Zones and Subzones are after Martini (1971) (codified as NP) and Okada and Bukry (1980) (codified as CP).*

21

Following Parisi et al. (1988), Brinkhuis and Biffi (1993), Verducci and Nocchi (2004), Hyland et al. (2009) and Jovane et al. (2013), the Monte Cagnero Lower section spans calcareous nannofossil Zones and Subzones NP16 to NP21 of Martini (1971) and CP14a to CP16b of Okada and Bukry (1980), planktonic foraminiferal Zones P12 to P18 of Berggren et al. (1995) and Zones E11 to O1 of Berggren and Pearson (2006) and Wade et al. (2011), dinocyst Zones Cfu to Rac of Brinkhuis and Biffi (1993), and the middle part of Chron C18r to the lowermost part of Chron C12r (Figure 1.4). The correlation between the Contessa Highway Upper section and the Monte Cagnero Lower section is tied to the base of Chron C18n (Figure 1.4).

The Monte Cagnero Middle section (lat. 43°38'51" N; long. 12°28'24" E) extends within the lower to middle Rupelian (Figure 1.5). It is currently 36 m–thick and consists of calcareous marls and marls with subordinate marly limestones greenish–grey, grey and reddish–violet in colour. Discrete biotite–rich layers occur at 122.8, 142.8, 145.8, 146.6, and 147 m. Volcaniclastic biotite at 146.6 m provided an age of 31.5±0.2 Ma (Coccioni et al., 2008). Fourteen reliable biohorizons were recognized, two of which based on planktonic foraminifera, eight to calcareous nannofossils, and four to dinocysts. According to Coccioni et al. (2008), Hyland et al. (2009) and Pross et al. (2010), the Monte Cagnero Middle section spans calcareous nannofossil Zones and Subzones NP21 to NP23 of Martini (1971) and CP16a to CP17–CP18 of Okada and Bukry (1980), planktonic foraminiferal Zones P18 to P19 of Berggren et al. (1995) and Zones E16 to O2 of Berggren and Pearson (2006) and Wade et al. (2011), dinocyst Zones Gse to Hpu of Brinkhuis and Biffi (1993), and the upper part of Chron C13r to the upper Chron C12n (Figure 1.5). The correlation between the Massignano section and the Monte Cagnero Middle section is tied to the base of Chron C13n (Figure 1.5).

Monte Cagnero Upper section (lat. 43°38'51" N; long. 12°28'24" E) has been proposed by Coccioni et al. (2008) as the GSSP for the Rupelian/Chattian boundary. It is currently 66 m–thick and the Rupelian/Chattian boundary falls at m 189 (Figure 1.5). This section consists of calcareous marls and marls with subordinate marly limestones greenish–grey and grey in colour. Discrete biotite–rich layers occur at 145.8, 146.6, 147, 151.65, 174.5, 208.7 and 209.1 m. Biotite from layer at 146.6 m provided an age of 31.5±0.2 Ma and those from layers at 208.7 and 209.1 m provided an age of 26.7 ±0.2 Ma (Coccioni et al., 2008). Twenty–one

reliable biohorizons were identified, five of which based on planktonic foraminifera, ten to calcareous nannofossils, and six to dinocysts.
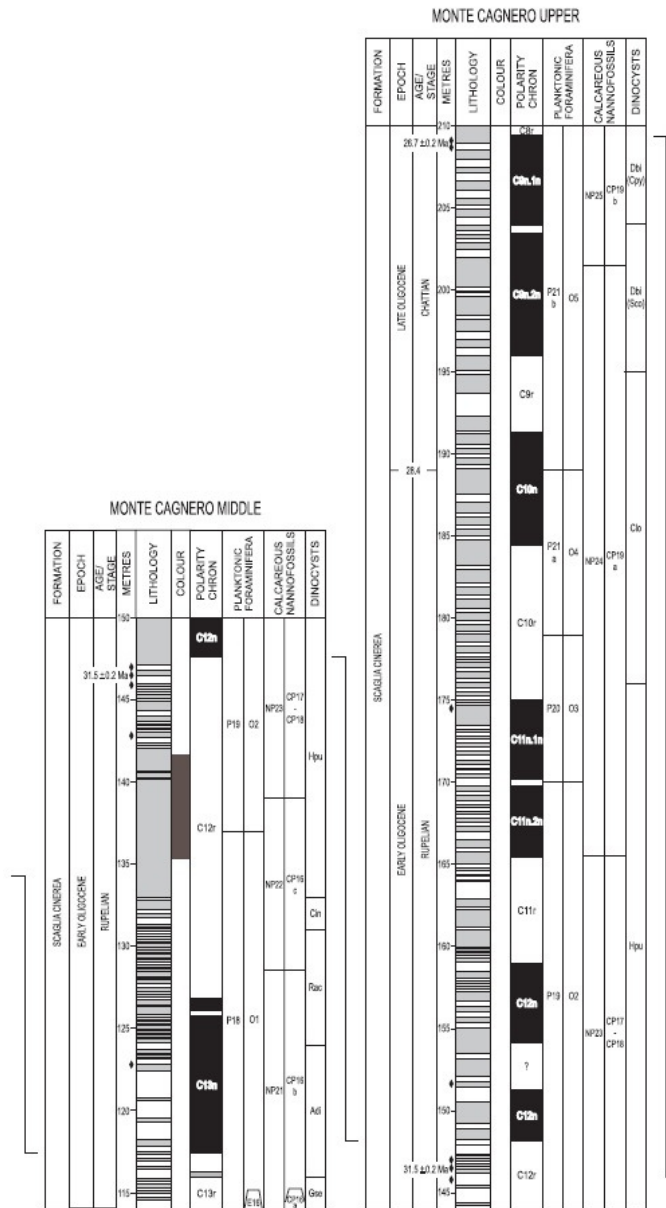
Figure 1.5. Integrated stratigraphy of the Monte Cagnero Middle and Monte Cagnero Upper sections. Chronostratigraphy is after Coccioni et al. (2008) and Ogg et al. (2008). Correlation between Massignano and Monte Cagnero Middle sections is tied to the base of Chron C13n and that between Monte Cagnero Middle and Monte Cagnero Upper sections to the base of Chron C12n. Planktonic foraminiferal Zones and Subzones are after Berggren et al. (1995) (codified as P) and Berggren and Pearson (2006) and Wade et al. (2011) (codified as E and O). Calcareous nannofossil Zones and Subzones are after Martini (1971) (codified as NP) and Okada and Bukry (1980) (codified as CP).

23

Following Coccioni et al. (2008), Hyland et al. (2009) and Pross et al. (2010), the Monte Cagnero Upper section spans calcareous nannofossil Zones and Subzones NP23 to NP25 of Martini (1971) and CP17–CP18 to CP19b of Okada and Bukry (1980), planktonic foraminiferal Zones and Subzones P19 to P21b of Berggren et al. (1995) and Zones O2 to O5 of Berggren and Pearson (2006) and Wade et al. (2011), dinocyst Zones and Subzones Hpu to Dbi (Cpy) of Pross et al. (2010), and the upper part of Chron C12r to the lowermost part of Chron C8r. The correlation between the Monte Cagnero Middle section and the Monte Cagnero Upper section is tied to the base of Chron C12n (Figure 1.5).

Other important section in the Tethyan realm at the Umbria-Marche basin is the Contessa Section. In the Contessa Valley, which cuts a NE-dipping, half-anticlinal structure a few kilometres NW of the Medieval city of Gubbio, the Scaglia Rossa, Scaglia Variegata and Scaglia Cinerea formations are well exposed in continuous fresh road-cuts and quarry faces several metres high (Lowrie et al. 1982; Cresta et al. 1989; Montanari et al. 1997; Galeotti et al. 2000, 2004, 2010; Jovane et al. 2007a, 2010; Giusberti et al. 2009; Coccioni et al. 2010b, 2012; Pross et al. 2010) (Figures 1.6 and 1.7).

The Contessa Highway Lower section extends from the Danian to the lowermost Thanetian. This section spans calcareous nannofossil Zones NP1–NP5 of Martini (1971) and CP1a–CP4 of Okada and Bukry (1980), planktonic foraminiferal Zones P0–Pa to P4a–P4b of Berggren et al. (1995) and Zones P0–Pa to P4b of Berggren and Pearson (2005) and Wade et al. (2011), and the upper part of Chron C29r to the lowermost part of Chron C26n (Figure 1.6) (Lowrie et al., 1982; Cresta et al., 1989; Fornaciari et al., 2007; Coccioni et al., 2010).

The Contessa Road section extends from Upper Danian to the Middle Ypresian. The Contessa Road section spans calcareous nannofossil Zones NP4–NP13 of Martini (1971) and CP3–CP11 of Okada and Bukry (1980), planktonic foraminiferal Zones P2 to P7–P9 of Berggren et al. (1995) and Berggren and Pearson (2005) and Zones E1–E7a of Berggren and Pearson (2006) and Wade et al. (2011), and the base of Chron C26n to the Middle part of Chron C22r (Figure 1.6). The correlation between the Contessa Highway Lower section and the Contessa Road section is tied to the base of Chron C26n (Figure 1.6) (Lowrie et al., 1982; Aubry, 1995; Galeotti et al., 2000, 2004, 2010; Raffi et al., 2005; Angori et al., 2007; Giusberti et al., 2009; Agnini et al., 2006).

Contessa Highway Middle section extends from the Middle Ypresian to the Middle Lutetian. Contessa Highway Middle section spans calcareous nannofossil Zones and Subzones NP12–NP15a of Martini (1971) and CP11–CP13a of Okada and Bukry (1980), planktonic foraminiferal Zones P7–P8 to P9 of Berggren et al. (1995) and Zones E5–E6 to E8 of Berggren and Pearson (2006) and Wade et al. (2011), and Chron C23n.1n to lowermost part of Chron C20r (Figure 1.7). The correlation between the Contessa Road section and the Contessa Highway Middle section is tied to the top of Chron C23n.1n (Figures 1.6 and 1.7) (Lowrie et al., 1982; Cresta et al., 1989; Jovane et al., 2007a; Agnini et al., 2006).

Contessa Highway Upper section extends from the Middle Lutetian to the Lower Bartonian Contessa Highway Upper section spans calcareous nannofossil Zones and Subzones NP15a–NP17 of Martini (1971) and CP13a–CP14b of Okada and Bukry (1980), planktonic foraminiferal Zones P9–P14 of Berggren et al. (1995) and Zones E8–E13 of Berggren and Pearson (2006) and Wade et al. (2011), and the uppermost part of Chron C21n to Chron C18n.2n (Figure 1.7). The correlation between the Contessa Highway Middle section and the Contessa Highway Upper section is tied the top of Chron C21n (Figure 1.7) (Lowrie et al., 1982; Cresta et al., 1989; Jovane et al., 2007a, 2010; Aubry, 1991).
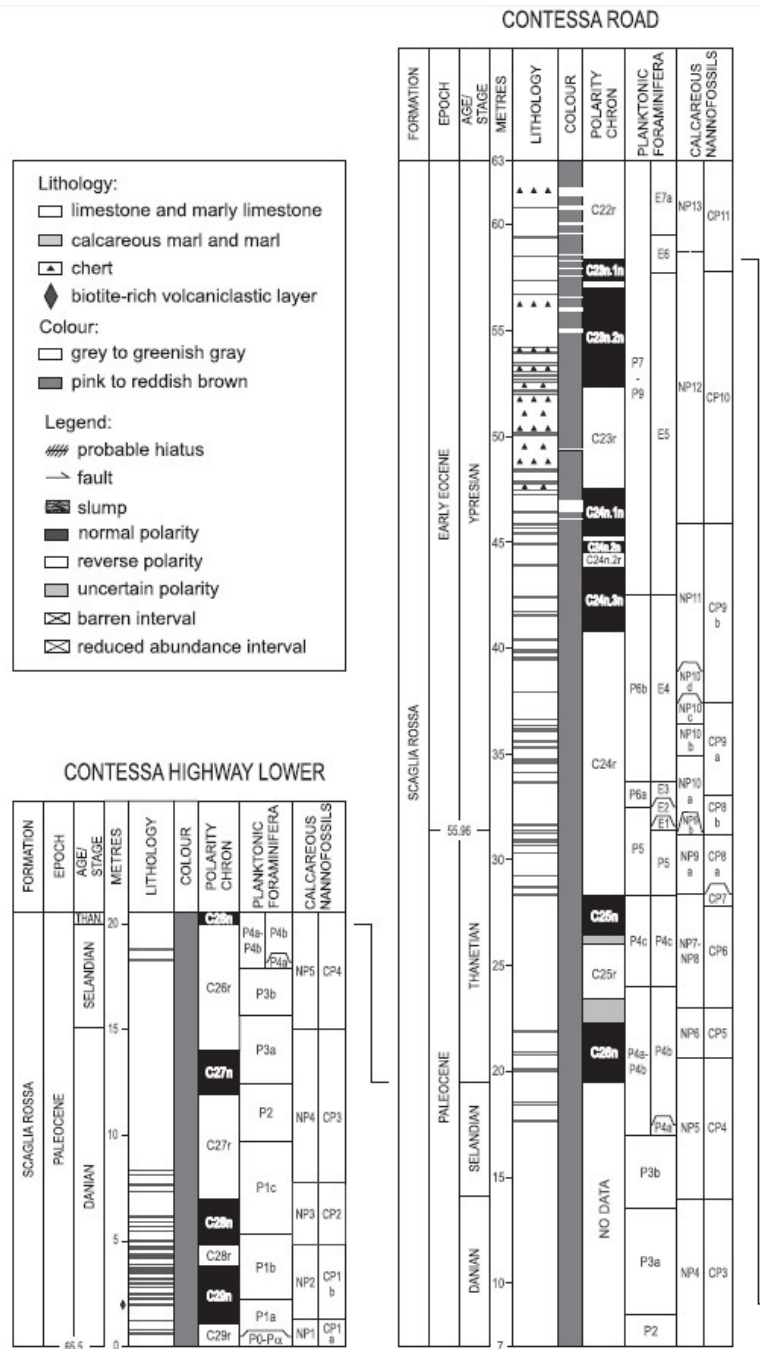
Figure 1.6*. Integrated stratigraphy of the Contessa Highway Lower and Contessa Road sections. Chronostratigraphy is after Ogg et al. (2008). Correlation between these sections is tied to the base of Chron C26n. Planktonic foraminiferal Zones and Subzones are after Berggren et al. (1995), Berggren and Pearson (2005) and Wade et al. (2011) (codified as P). Calcareous nannofossil Zones and Subzones are after Martini (1971) (codified as NP) and Okada and Bukry (1980) (codified as CP).*
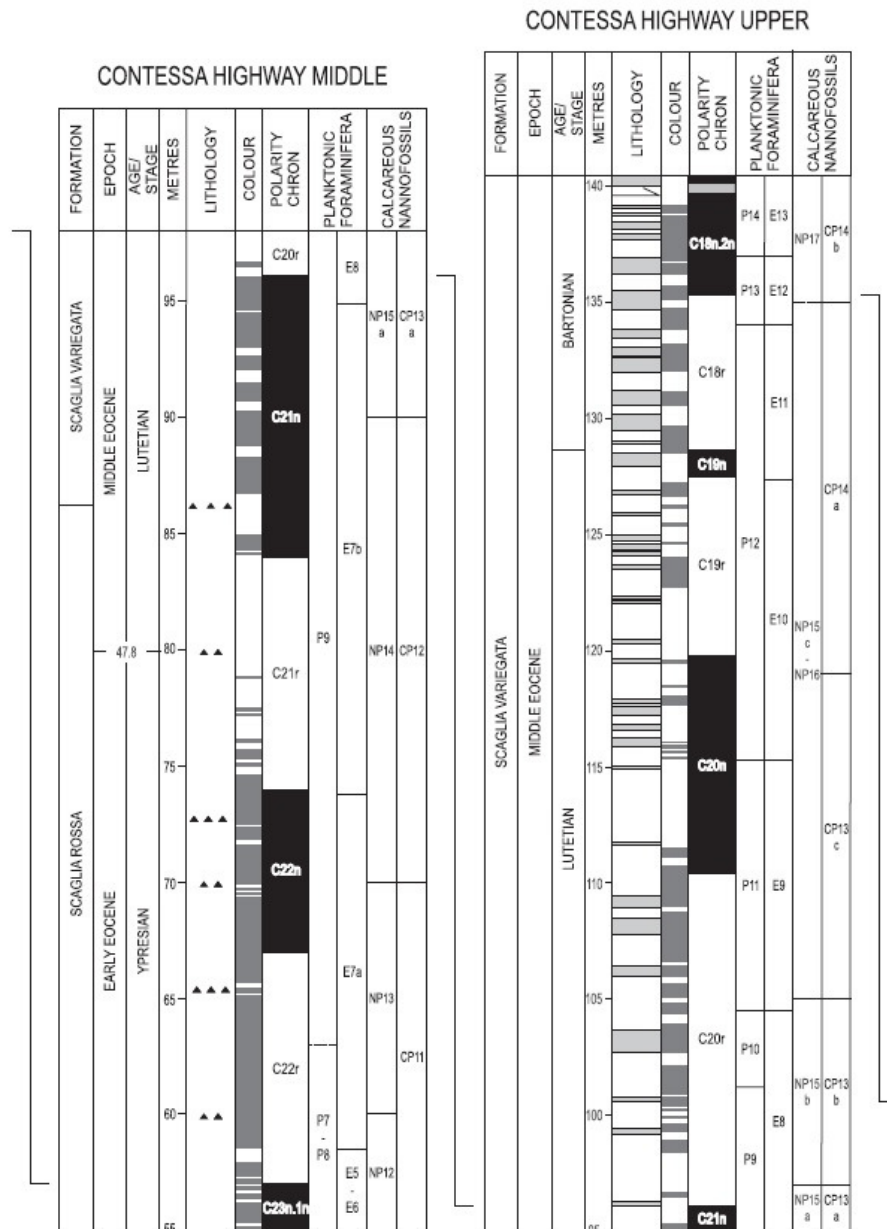
Figure 1.7. *Integrated stratigraphy of the Contessa Highway Middle and Contessa Highway Upper sections. Chronostratigraphy is after Molina et al. (2011), Ogg et al. (2008), Jovane et al. (2010), Ogg et al. (2008) and Molina et al. (2011). Correlation between Contessa Road and Contessa Highway Middle sections is tied to the top of Chron C23n.1n and that between Contessa Highway Middle and Contessa Highway Upper sections to the top of Chron C21n. Planktonic foraminiferal Zones and Subzones are after Berggren et al. (1995) (codified as P) and Berggren and Pearson (2006) and Wade et al. (2011) (codified as E). Calcareous nannofossil Zones and Subzones are after Martini (1971) (codified as NP) and Okada and Bukry (1980) (codified as CP).*

Further to the east, at the Indian Ocean, the Neo-Tethys record is found on oceanic sediments. Ocean Drilling Program (ODP) Leg 115 in the western equatorial Indian Ocean was designated to undertand the Neogene sedimentation and Cenozoic evolution of the Reúnion hotspot. The paleomagnetic study of the sediments recovered on the Leg 115 contributed to these scientific objectives, including the 711A drill site, near the Seychelles Archipelago, Madingley Rise, northern Indian Ocean, for which biostratigraphic data (planktonic foraminifera, diatoms and nannofossils), $CaCO_3$, opal content, magnetic susceptibility and other parameters were already available. This core contains the most complete and least disturbed record from the middle Eocene to Oligocene from the northern Indian Ocean. The sediments consist of brown and white interlayered clays and nannofossil/radiolarian chalks, respectively. Paleomagnetic measurements from late Eocene to late Oligocene (Figure 1.8) have been made (Schneider and Kent, 1990; Touchard et al., 2003), but modern high-resolution methods are needed to develop a good magnetostratigraphic age model.
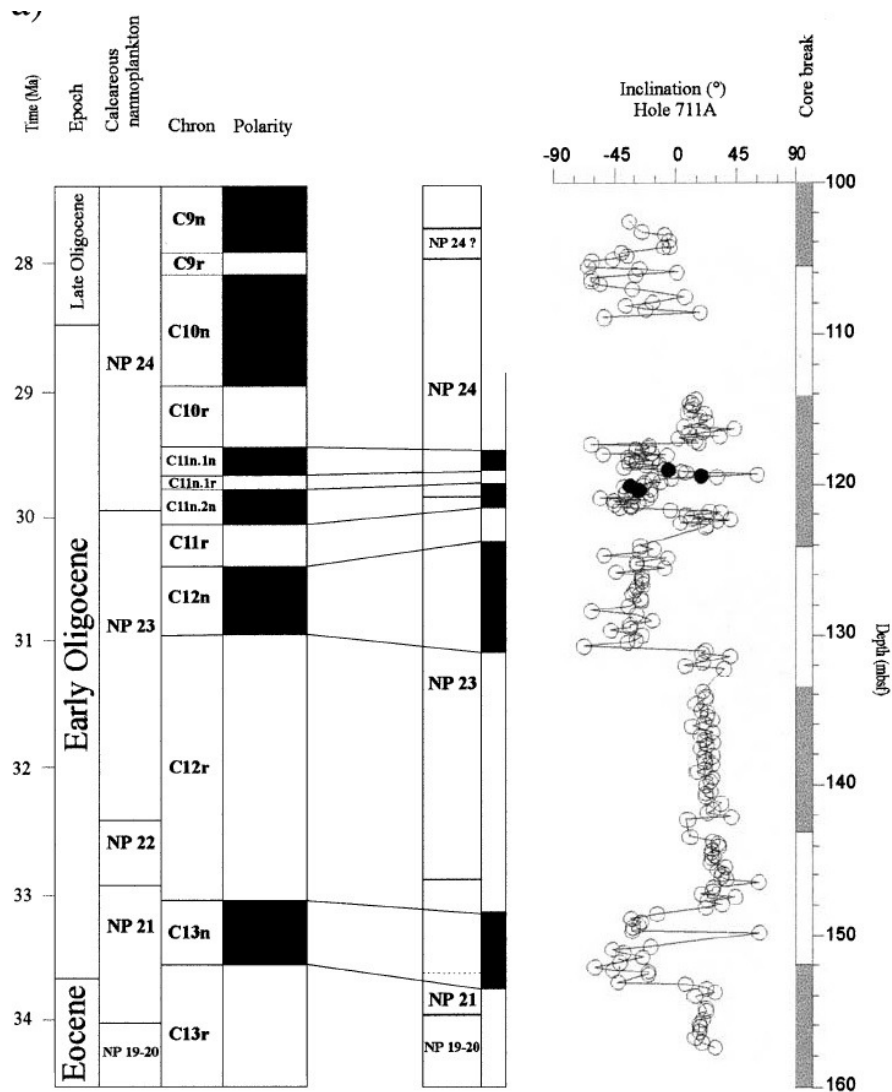
Figure 1.8. *ChRM inclinations versus depth in Hole 711A, together with biostratigraphy, compared to the GPTS and calcareous nannofossil biochronology; dark symbols indicate the tephra layers (Touchard et al., 2003).*

1.3. Main Objectives

The purpose of this study is to better understand the phenomena of abrupt climatic changes in the Paleocene. New paleomagnetic and paleorecords data were then generated for the Neo-Tethys and Indian Oceans in two key areas in order to address the following main objectives:

(i)   Provide an accurate integrated age model based in magneto and biostratigraphy for the Tethyan and Indian Ocean sections; a robust age model forms the framework for future paleoceanographic and paleoclimatic studies at these sites.

(ii)   Provide a high-resolution environmental magnetic, micropaleontological and stable isotopic datasets of the western Tethyan pelagic sections during the Paleogene interval. These results coupled with paleobiological data are then used to derive a paleoenvironmental scenario for the climatic events in the Neotethys realm.

(iii)   Perform a detailed study of the MECO, in which magnetic mineralogical proxies for its recognition in the geological record and the paleoceanographyc mechanisms involved (the iron-fertilization hypothesis) are investigated.

1.4. General Outline

The present Thesis is a composition of scientific papers that I authored or co-authored during the past four years. In order to facilitate the reading through the Thesis, the geological setting of the two studied areas – the Umbria-Marche basin and the Indian Ocean – is described together in Chapter 2. This Chapter consists of a compilation of information available in three different manuscripts that I have participated as leading author or co-author (Coccioni et al., 2012; Jovane et al., 2013; Savian et al., 2013), as well as data from the literature. This information is not repeated in the next Chapters.

Chapter 3 consists of an integrated magnetobiostratigraphic record for the Eocene-Oligocene interval to generate a high-resolution age model for Monte Cagnero section. The original goal of the study was to obtain a reliable chronostratigraphic framework for studying the Eocene–Oligocene paleoceanographic changes during the switch from greenhouse to icehouse conditions, which is the main topic of interest of the senior author. But this work also provides the chronological framework for studying the MECO event, being the basis for

Chapter 4, thus justifying its inclusion in the Thesis. The studied sediments consist of alternating reddish and greenish limestones and marlstones. A new integrated age model for the section is based on high-resolution paleomagnetic analyses, combined with detailed planktonic foraminiferal and calcareous nannofossil biostratigraphic results. Rock magnetic measurements show that the magnetic mineralogy is dominated by a mixture of high- and low-coercivity minerals, likely representing a combination of hematite and magnetite. A robust magnetostratigraphic signal, together with the identification of multiple bioevents, allows the construction of a detailed age model for the section. Based on these results, we infer that the section spans a continuous interval (to magnetochron resolution) from the middle Eocene to the lower Oligocene (~41 to ~27 Ma).

The related manuscript was published as:

Jovane, L., Savian, J., Coccioni, R., Frontalini, F., Bancalà, G., Catanzariti, R., Luciani, L., Bohaty, S., Wilson, P., and Florindo, F. (2013). Integrated magnetobiostratigraphy of the middle Eocene-lower Oligocene interval from the Monte Cagnero section, central Italy. *Geological Society, London, Special Publications*, **373**, first published March 25, 2013; doi 10.1144/SP373.13.

Chapter 4 reports results of high-resolution environmental and rock magnetic investigations at the Neotethyan Monte Cagnero (MCA) section (northeastern Apennines, Italy), where the MECO has been recognized. Earth's climate experienced a warming event known as the Middle Eocene Climatic Optimum (MECO) at ~40.0 Ma, which was an abrupt reversal of a long-term Eocene cooling trend. This event is characterized in the deep Southern, Atlantic, Pacific and Indian Oceans by a distinct negative $\delta^{18}O$ excursion over 500 kyr. We report results of high-resolution paleontological, geochemical, and rock magnetic investigations of the Neo-Tethyan Monte Cagnero (MCA) section (northeastern Apennines, Italy), which can be correlated on the basis of magnetobiostratigraphic results to the MECO event recorded in deep-sea sections. In the MCA section, an interval with significantly increased eutrophic nannofossil taxa (and decreased abundances of oligotrophic taxa) spans the peak MECO warming and its aftermath and coincides with a positive carbon isotope excursion, and a peak in magnetite and hematite contents. The magnetite content peak reflects

the appearance of magnetofossils, while the hematite peak is attributed to an enhanced detrital mineral contribution, likely as aeolian dust transported from the continent adjacent to the Neo-Tethys Ocean during a drier, more seasonal climate during the peak MECO warming. Based on our new geochemical, paleontological and magnetic records, the MECO warming peak and its immediate aftermath are interpreted as a period of high primary productivity. Sea-surface iron fertilization is inferred to have stimulated high phytoplankton productivity, increasing organic carbon export to the seafloor and promoting enhanced biomineralization of magnetotactic bacteria, which are preserved as magnetofossils during the warmest periods of the MECO event in the MCA section. Together with previous studies, our work reinforces the connection between hyperthermal climatic events and the occurrence (or increased abundance) of magnetofossils in the sedimentary record.

The related manuscript was submitted as:

Savian, J.F., Jovane, L., Trindade, R.I.F., Frontalini, F., Coccioni, R., Bohaty, S.M., Wilson, P.A., Florindo, F., Sprovieri, M., Roberts, A.P., Catanzariti, R., and Figueira, R.C.L. (Submitted). Enhanced primary productivity and magnetotactic bacterial production in response to middle Eocene warming in the Neo-Tethys Ocean. *Earth and Planetary Science Letters*.

Chapter 5 presents a high-resolution study at Contessa Valley (Gubbio, central Italy), that integrates stable isotope stratigraphy, calcareous nannofossil and foraminiferal biostratigraphy and geochemistry. I have contributed to the study with the rock magnetic and magnetostratigraphic datasets and participated in the integration of results. This well-preserved succession offers an excellent opportunity to identify and constrain the Palaeocene to early Eocene hyperthermal events and carbon isotope excursions (CIEs). Our dataset provides the first evidence in the Tethys Ocean of several CIEs previously identified in the Pacific, Atlantic and Southern Oceans, highlighting their global significance, but also present other CIEs still not identified elsewhere. Their characteristics are compared with those reported for deep-sea cores and other land-based sections to test whether the signature associated with the documented CIEs in our composite section can be traced over a wider area. The Contessa composite section is here stablished as a reference succession for the the

magnetobiochronostratigraphic framework of the early Paleogene and its hyperthermal events and CIEs. This reference succession is now being studied in terms of its magnetic mineralogy to test the intimate correlation between events of abrupt increase in sea surface temperature and the occurrence (or increase in abundance) of magnetofossils. This correlation is already proven by other authors in Southern Ocean sections for the PETM, and by our own work on the Neo-Thetys for the MECO event.

The manuscript was included in thesis almost in its original form, with a final comment on the perspectives of magnetic mineralogical studies of hyperthermal fingerprinting in this succession. The related paper was published as:

Coccioni, R., Bancalà, G., Catanzariti, R., Fornaciari, E., Frontalini, F., Giusberti, L., Jovane, L., Luciani, V., Savian, J., Sprovieri, M. (2012). An integrated stratigraphic record of the Palaeocene–lower Eocene at Gubbio (Italy): new insights into the early Palaeogene hyperthermals and carbon isotope excursions. *Terra Nova*, **24**, 380-386, doi: 10.1111/j.1365-3121.2012.01076.x.

Chapter 6 presents a high resolution magnetostratigraphic and environmental magnetism record and a new integrated age model for the middle Eocene to-lower Oligocene section of Hole 711A. Correlation of the polarity pattern to the geomagnetic polarity timescale provides a record from Chron C19r (middle Eocene) to C12r (early Oligocene). Our results extend the existing polarity record down into the middle Eocene and confirm published results from the lower Oligocene section of the hole. These new results from Hole 711A have important implications for identifying and dating global climate change events, and for reconstructing calcite compensation depth (CCD) history at this site. In addition, variations of magnetic parameters across the hole show strong similarities to those observed in Monte Cagnero, suggesting that similar mechanisms of primary productivity enhancement have also operated in this pelagic oceanic environment.

The chapter corresponds to a modified version of the following manuscript, with the addition of magnetic mineralogical data (environmental magnetism and FORC diagrams) and specific discussion:

Savian, J., Jovane, L., Bohaty, S., Wilson, P. (2012). Middle Eocene to early Oligocene magnetostratigraphy of ODP Hole 711A (Leg 115), western equatorial Indian Ocean. *Geological Society, London, Special Publications*, **373**, first published March 25, 2013; doi 10.1144/SP373.16.

Chapter 2. Geological Context

2.1. Monte Cagnero and Contessa Sections (Neo-Tethys Ocean)

The U–M Apennines is a foreland fold-and-thrust belt (Chiarabba et al. 2005), which was formed in the latest phase of the Alpine–Himalayan orogenesis. These mountains are entirely made from marine sedimentary rocks of the so-called U–Msuccession, which represent a continuous record of the geotectonic evolution of an epeiric sea from the Late Triassic to the Pleistocene. During the Late Triassic and Early Jurassic, at the time of the opening of the North Atlantic, the rifting between Europe and Africa took place within a formerly continuous continental crust at the southern margin of Europe (Centamore et al. 1980; Bosellini 1989). This rifting formed oceanic ancestral basins, which are now preserved in the present Alpine mountain chains, including the Pennine–Liguride Ocean. This new ocean, perhaps connected to part of the ancient Tethyan Ocean to the east, outlined a northward-pointing promontory of African continental crust, commonly referred to as Adria or the Adriatic Promontory (Channell et al. 1979). The Adriatic Promontory was isolated from inputs of clastic sediments. As a large, and nearly isolated, passive continental margin, Adriatic Promontory underwent extensional faulting. Normal faults defined a complex of subsiding blocks leading to an irregular topography of structural highs (horsts) and adjacent depocentres (grabens and/or halfgrabens). Where shallow water carbonate deposition could keep up with subsidence, and where the faulted blocks were large enough to support productive carbonate platform environments, very thick sequences of shallow water carbonates developed on the Adria's crust. In other regions, subsidence and complex block faulting carried the seafloor down, below the photic zone and out of the zone of shallowwater carbonate production. Areas with this history became pelagic basins, such as the U–M Basin, in which the Palaeogene carbonate succession was deposited recording the geologic, biologic and oceanographic evolution of this region, with remarkable continuity and completeness.

The Palaeogene portion of the U–M pelagic succession is represented by three distinct formations (from bottom to top): Scaglia Rossa (early Turonian to middle Eocene), Scaglia Variegata (Middle to late Eocene) and Scaglia Cinerea (late Eocene to earliest Miocene). The

Italian terms 'Rossa', 'Variegata' and 'Cinerea' refer to the red, variegated and ashy colour, respectively, and 'Scaglia' to the scaly, conchoidal fracture typical of these thinly bedded rocks. The Palaeogene Scaglia Rossa corresponds to the R3 and R4 members of Alvarez and Montanari (1988) and is made up of well-bedded, pink to red limestones with red marly interbeds in the Middle–Lower Danian, at the Selandian–Thanetian transition and from the Upper Thanetian to middle Ypresian. Radiolarian chert occurs from the Middle Ypresian to the Lower Lutetian portion of this formation. The Palaeogene Scaglia Rossa varies in thickness between 80 and 100 m. Beginning in the middle Eocene, terrigenous clay input became increasingly important. The Scaglia Variegata represents a transitional interval between the Scaglia Rossa and Scaglia Cinerea and consists of an alternation of white, greenish-grey and pink to red marly limestones and calcareous marls. Its lower boundary is marked by the last occurrence of nodular chert (Lowrie et al. 1982). The top of the Scaglia Variegata is conventionally placed at the top of the uppermost reddish interval (Monaco et al. 1987; Coccioni et al. 1988: Odin and Montanari 1988). The Scaglia Variegata varies from 30 and 95 m in thickness. The Scaglia Cinerea consists mainly of calcareous marls and marls and subordinate marly limestones greenish-grey and grey in colour. This unit varies from 100 to 200 m in thickness and its top is set at the base of the Raffaello Level (Coccioni et al. 1989, 1994), a volcanoclastic bentonite that represents a regional marker bed easily recognizable in the field, which marks the base of the overlying early to Middle Miocene Bisciaro Formation. Biotite-rich layers emplaced as air-fall volcanic ash are found at different stratigraphic levels in the uppermost Scaglia Variegata and throughout the Scaglia Cinerea.

The Palaeogene pelagic sediments the U–M Basin were deposited well above the CCD at Middle to lower bathyal depths (1000–1500 m; Galeotti et al. 2004; Jovane et al. 2007a; Giusberti et al. 2009; Coccioni et al. 2010) and at c. 308N palaeolatitude (Jovane et al. 2007a).

The Monte Cagnero section (43°38'50"N, 12°28'05"E and 727 m above sea-level) lies within the Umbria-Marche Basin (northeastern Apennines, Chiarabba et al., 2005) near Urbania, Italy. The study section ranges from 58 to 128 msl (70-m thick) and comprises the Priabonian-Rupelian boundary at 114.1 msl, which corresponds to 19 msl in the Massignano Section (Coccioni et al., 2008; Hyland et al., 2009).

The Monte Cagnero section has been proposed as the Rupelian/Chattian GSSP (Coccioni et al., 2008). The lithologies of the entire Eocene and Oligocene section consist of alternating reddish/greenish gray calcareous marl and marly limestones from the Scaglia Variegata and Scaglia Cinerea Formations, which largely represent pelagic carbonate successions (Figure 2.1) (e.g., Jovane et al. 2007a, b; 2009; 2013). The lower part of the study section consists of ~21 m (58.00-79.50 msl) of 0.15 to 1.00-m-thick red-violet limestone and 0.20 to 2.00-m-thick violet marls with intercalations of white marl corresponding to the lower member of Scaglia Variegata Formation. We recognize the middle member of the Scaglia Variegata Formation as ~24 m (79.50–103.50 msl) of alternating 0.15 to 0.35 -m-thick marly limestones and green/gray marls. The upper member of the Scaglia Variegata Formation (103.50–107.50 msl) is represented by a series of 0.15-m-thick beds of red calcareous marls. The Scaglia Variegata Formation comprises a time interval from the end of the early Eocene to the end of the late Eocene (~47-~35 Ma) (e.g., Jovane et al., 2007a). Above 107.50 msl, the Scaglia Variegata Formation grades into gray marl and marly limestone of the mainly Oligocene Scaglia Cinerea Formation (e.g., Jovane et al., 2007a). Benthic foraminiferal data from Guerrera et al. (1988) and Parisi et al. (1988) interpret lower bathyal paleo-depths (1000–2000 m) during the middle Eocene, which gradually shoaled in the early late Eocene to mid-bathyal depths (800–1000 m). In the early Oligocene, upper bathyal paleo-depths (400–600 m) are estimated. Between 103.5 and 103.30 msl lies a 0.2 m layer of slightly deformed marl of the Scaglia Cinerea Formation associated with slumping.

Figure 2.1. *High-resolution lithostratigraphic sequence of the Monte Cagnero section from meter stratigraphic level (msl) 58 to 128 following the legend. Purple diamonds and blue lines indicate samples used for thermomagnetic curves and magnetostratigraphy. At 114.1 msl is marked the Eocene-Oligocene boundary (Coccioni et al, 2008; Hyland et al., 2009; Jovane et al., 2013).*

The Contessa Highway (CHW) (lat. 43°22'47" N; long. 12°33'45" E) and Contessa Road (CR) (lat. 43°22'47" N; long. 12°33'50" E) sections, located a few kilometres northwest of Gubbio (central Italy) (Figure 2.2), are probably among the best studied Cenozoic Tethyan successions. They are characterized by a continuous record of many crucial aspects of the Earth's history from the Cretaceous∕ Palaeogene (K ∕ Pg) boundary through to the Upper Oligocene (e.g., Lowrie et al., 1982; Cresta et al., 1989; Coccioni et al., 2010a,b; Galeotti et

al., 2010; Jovane et al., 2010). As the lower part of the CR section is affected by some tectonic disturbances, we used two distinct portions of the CHW and CR sections to construct a Palaeocene–lower Eocene complete and well-preserved composite stratigraphic succession, 67 m in thickness and 16 Ma in duration, on the basis of biostratigraphic correlation. This succession, which is the focus of this study, was deposited at an average sedimentation rate of ~0.5 cm⁄ka and belongs to the Scaglia Rossa Formation that is made up of well-stratified red to pinkish, pelagic coccolith-foraminiferal limestones with subordinated marls deposited at middle to lower bathyal depths (1000–1500 m) (Galeotti et al., 2004; Jovane et al., 2007; Giusberti et al., 2009; Coccioni et al., 2010a), and at ~30°N palaeolatitude (Jovane et al., 2007). Marls ranging from 1 to 20 cm in thickness are localized within the middle-lower Danian, at the Selandian-Thanetian transition and from the upper Thanetian upwards. Chert beds and nodules are associated with the middle–upper Ypresian limestones.
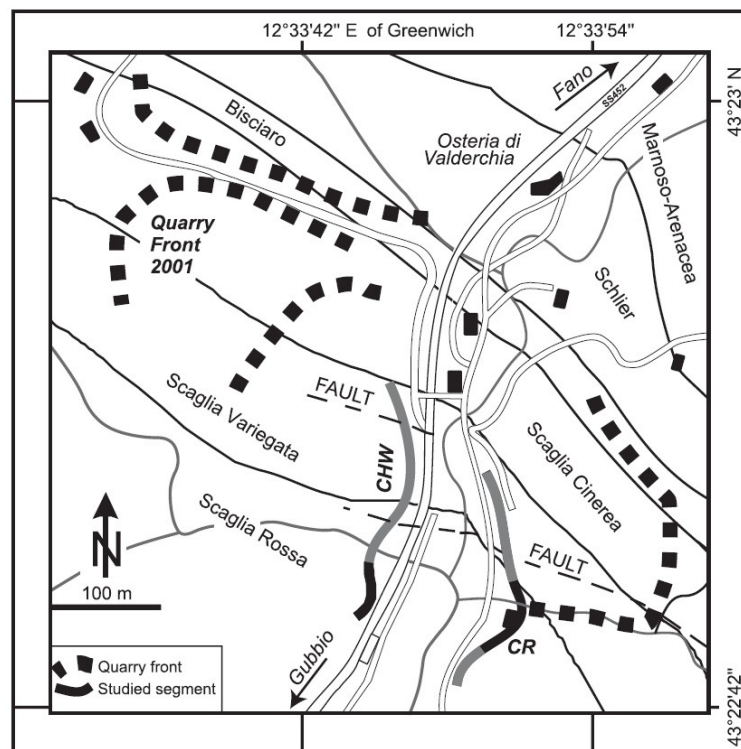
Figure 2.2. *Location map of the Contessa sections (CHW–Contessa Highway and CR–Contessa Road) on a simplified map that gives the formation boundaries in the Contessa Valley.*

Palaeomagnetic data indicate eight chrons interpreted as Chron C29r to C22r based on comparison with calcareous plankton biostratigraphy, which spans from planktonic foraminiferal standard Zones P0–Pa to P9 and E1 to E7a (Berggren et al., 1995; Wade et al., 2011), and from calcareous nannofossil standard Zones and Subzones NP1 to NP13 and CP1a to CP11 (Martini, 1971; Okada and Bukry, 1980). Interestingly, Galeotti et al. (2010) presented an integrated stratigraphic analysis, including biostratigraphy based on calcareous nannofossils, magnetostratigraphy and cyclostratigraphy, and wt.% $CaCO_3$ and bulk carbon isotope records across the upper Palaeocene-lower Eocene interval at CR section comprising the PETM, ETM2 and ETM3. However, in our study, this interval has been investigated at higher resolution also providing a biostratigraphical framework based on foraminifera.

2.2. ODP Hole 711A (Indian Ocean)

ODP Hole 711A (2844.56′S, 61809.78′E) was drilled near the Seychelles Archipelago, between Madingley Rise and Carlsberg Ridge at a water depth of 4430 m, northern Indian Ocean (Figure 2.3). Hole 711A was advanced to 104.5 m below seafloor (mbsf) using the advanced piston corer system, recovering 95.1 m (91%) and advanced to 249.6 mbsf using the extended core barrel system, recovering 108.7 m (80%) (Backman et al., 1988). We studied the depth interval of Cores 711A-14X to -21X, which encompass sediments from the middle Eocene to lower Oligocene interval. The middle Eocene-to-lower Oligocene strata within Hole 711A primarily consist of carbonate-rich sediments characterized as clay-bearing nannofossil oozes/ chalks (68–173 mbsf; Lithostratigraphic Unit III), and clay-bearing nannofossil chalks with interbedded radiolarian oozes and radiolarian-bearing nannofossil chalks with carbonate content comprise about 70–80% (173–249.6 mbsf; Lithostratigraphic Unit IV; Backman et al. 1988; Okada 1990).
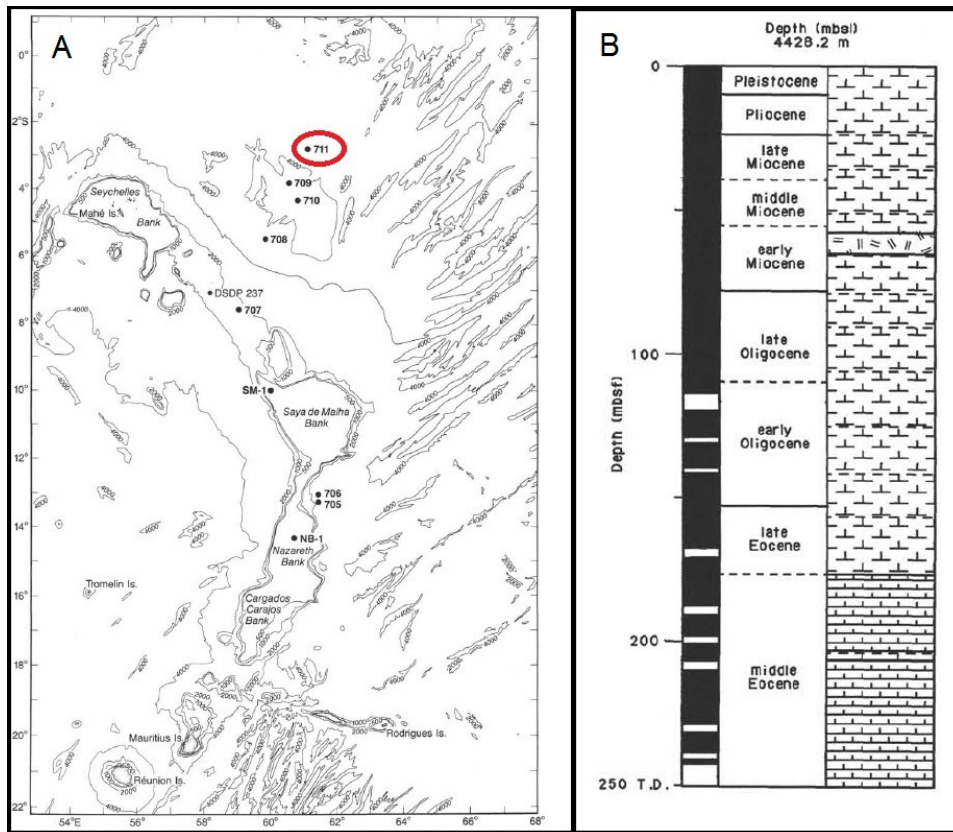
Figure 2.3. (A) *Geological map with bathymetric features around the Mascarene Plateau and the location of Site 711. (B) Stratigraphic summary of Site 711 with recovery section (black column) and division of geologic timescale of the Core (After Backman et al., 1988).*

Previous biostratigraphic work in the Eocene–Oligocene section of Hole 711A includes studies of planktonic foraminifera, diatoms and nannofossil (Fenner and Mikkelsen 1990; Fornaciari et al. 1990; Johnson 1990; Mikkelsen 1990; Okada 1990; Rio et al. 1990). Moreover, $CaCO_3$, opal and magnetic susceptibility parameters have also been measured (Hampel and Bohrmann 1990; Peterson and Backman 1990; Robinson 1990). Palaeomagnetic measurements (progressive alternating-field demagnetization) have been measured in all Leg 115 sites (Schneider & Kent 1990a), and a more detailed palaeomagnetic study was performed by Touchard et al. (2003) in the upper 100–160 mbsf interval of Hole 711A. In this present study, a total of 375 discrete samples were taken by International ODP personnel in Kochi (Japan) pressing 7 cm^3 plastic samples boxes into the working half of the cores at an average c. 20 cm spacing.

Chapter 3. Integrated magnetobiostratigraphy of the middle Eocene-lower Oligocene interval from the Monte Cagnero section, central Italy

3.1. Introduction

The Cenozoic Era represents the last 65 Myr, from the end of the Cretaceous to the present, and is a transformational time in the evolution of Earth's paleoclimate. Planktonic foraminiferal oxygen isotope ($\delta^{18}O$) records from all major ocean sedimentary basins indicate a cooling trend over the past 50 Myr, since the early Eocene climatic optimum (EECO, ~53-51 Ma ago) (e.g. Zachos et al., 2001, 2008). The middle Eocene to early Oligocene was a key interval for Earth`s transition from warmer (greenhouse) to cooler (icehouse) conditions. This interval is characterized by the expansion of Antarctic large ice sheets to ≥50% the size of the present day volume (Zachos et al., 1996; Lear et al., 2000; Coxall et al., 2005; Katz et al., 2008; Coxall and Wilson, 2011), culminating in the Eocene-Oligocene (E-O) climate transition (Oi-1; ~33.5 Ma) (Miller et al., 1991).

The long-term cooling trend through the Eocene did not occur as a single gradual change. There are a series of distinct cooling and warming episodes superimposed on the cooling trend (e.g., Shackleton and Kennett, 1975; Miller et al., 1991; Zachos et al., 1996, 2001, 2008; Bohaty and Zachos, 2003; Edgar et al., 2007, 2010; Jovane et al., 2007a,b, 2009; Ivany et al., 2008; Merico et al., 2008; Bohaty et al., 2009; Luciani et al., 2010, Spofforth et al., 2010). The most important climatic warming event in this interval is the Middle Eocene Climatic Optimum (MECO) that is characterized by a large negative $\delta^{18}O$ excursion at ~40 Ma (Bohaty and Zachos, 2003; Bohaty et al., 2009; Edgar et al., 2010). The causes of this event, which has been identified at multiple deep-sea drill sites around the globe and in outcrop sections in the Tethys region (Jovane et al., 2007b; Bohaty et al., 2009; Edgar et al., 2010; Luciani et al., 2010; Spofforth et al., 2010; Dawber and Tripati, 2011), are still unknown. The main hypothesized causes for the Oi-1 abrupt cooling at the E-O transition include the opening of Southern Ocean gateways (e.g. Livermore et al., 2005), decreasing concentrations of greenhouse gases in the atmosphere, orbital forcing (e.g., DeConto and

Pollard, 2003; Coxall et al., 2005; Lyle et al., 2005; Pagani et al., 2005; Pearson et al., 2009), and closure of the Neo-Tethys gateway (e.g. Jovane et al., 2007a, 2009). Concerning the last hypothesis, new data from the Tethys Ocean are needed to better assess the effects of the gradual closure of the Neo-Tethys gateway, which was driven by collision between Arabia and Eurasia (Jovane et al., 2007a, 2009; Allen and Armstrong, 2008). The gradual nature of the closure resulted in paleoceanographic oscillations, particularly clear evidence in environmental magnetic properties, in the Neo-Tethys region prior to the Oi-1 event (Jovane et al., 2007a), perhaps as a result of variations in the subtropical Eocene Neo-Tethys (STENT) current (Jovane et al., 2009).

The Monte Cagnero section (Figure 3.1), near Urbania (central Italy), is an important sedimentary sequence for study of paleoclimate events from the middle Eocene to upper Oligocene. Biostratigraphic studies of several microfossil groups have been carried out for this section, including dinoflagellates (Brinkhuis and Biffi, 1993), calcareous nannofossils (Baumann and Roth, 1969; Baumann, 1970; Maiorano and Monechi, 2006) and foraminifera (Baumann and Roth, 1969; Baumann, 1970; Parisi et al., 1988; Verducci and Nocchi, 2004). An integrated stratigraphy of the Oligocene pelagic sequence at Monte Cagnero has been constructed by Coccioni et al. (2008). The integrated stratigraphy indicates a stratigraphic equivalence between meter stratigraphic level (msl) 114.1 at Monte Cagnero and msl 19 at the section at Massignano, which represents the Global boundary Stratotype Section and Point (GSSP) for the Eocene-Oligocene boundary (Premoli Silva and Jenkins, 1993; Coccioni et al., 2008; Hyland et al., 2009). A previous magnetostratigraphic interpretation (Hyland et al., 2009) covers mainly the Oligocene part of the section, from 100 to 146.5 msl, and in the lower part the Priabonian–Rupelian boundary. The Monte Cagnero section is a unique and representative section for the Eocene and Oligocene epochs in the Umbria-Marche Basin, and offers the possibility of correlation with the Contessa Highway section (e.g. Jovane et al., 2007b) ~40 km south, and with the Massignano stratotype section (e.g. Jovane et al. 2009) ~ 100 km east (Figure 3.1).

In this study, we present a high-resolution magneto-, bio-, and chronostratigraphic study of the Monte Cagnero section spanning the middle Eocene to lower Oligocene interval. We extend the stratigraphic study of the section from 128 msl down to 58 msl. The main objectives of this work were (1) to obtain an accurate magnetostratigraphy for the middle

Eocene–lower Oligocene interval, and (2) to refine the age calibration of biostratigraphic events in the same interval. This work has resulted in better documentation of the relationship between the gradual closure of the Neo-Tethys gateway and the resulting variation of the Sub-Tropical Eocene Neo-Tethys (STENT) (Jovane et al., 2009). A robust age model forms the framework for future paleoceanographic studies at this site, which will be used in studies of important climatic events, such as the MECO and the Oi-1 events.

Figure 3.1. *(A) Location map of the Monte Cagnero Section. (B) Representative picture from Scaglia Cinerea, which is part of the Monte Cagnero section (photo taken in March 2008).*

3.2. Methods

3.2.1. Paleomagnetism

A total of seven hundred samples were collected at ~0.1 m intervals from the Monte Cagnero section and used for all analyses reported here. Paleomagnetic sampling consisted of 241 oriented block samples for magnetostratigraphic analysis at ~0.3 m resolution. The oriented block samples were cut into 2 or 3 paired cubes (named A and B), in order to apply both alternating field (AF) (A samples) and thermal demagnetization (B samples) methods. Before analysis, each dry sample was weighed with a high precision balance, and, due to the irregular volume of the samples, all data were normalized relative to mass.

Because of the low intensity of the natural remanent magnetization (NRM) observed in a pilot study, samples were collected between 78 to 102 msl from two parallel transects at a distance of 20 m from the central main transect. The purpose of this sampling strategy was to increase the number of samples in this key interval. We designated these two sections as Y and Z, in addition to the central section called X. All the materials studied are archived in the laboratory of the Dipartimento di Scienze della Terra, della Vita e dell'Ambiente, Università di Urbino, Italy.

All paleomagnetic measurements were carried out at the University of Southampton's paleomagnetic laboratory of the National Oceanography Centre Southampton, UK. We measured the low-field mass-specific bulk magnetic susceptibility (χ) in all samples using a KLY-4 Kappabridge (AGICO) instrument. Measurements were performed using a three-axis 2-G Enterprises cryogenic magnetometer (model 755R), housed in a magnetically shielded room. Progressive AF demagnetization steps (5, 10, 15, 20, 25, 30, 35, 40, 45, 50, 60, 70, and 80 mT) were applied to all "A" specimens, and stepwise heating to the "B" specimens (25, 100, 150, 200, 250, 300, 350, 400, 450, 500, 520, 540, 560, 580, 600, 620, 640, 660, 680, and 700 °C). The 241 discrete "A" samples from the Monte Cagnero section were subjected to progressive AF demagnetization to remove possible magnetic overprints due to secondary magnetization and to discern characteristic remanent magnetization (ChRM) directions.

Magnetic components were identified using stereographic projections, orthogonal and demagnetizing intensity plots. The characteristic remanent magnetization (ChRM) directions

were calculated using principal component analysis (Kirschvink, 1980) using the paleomagnetic data software package REMASOFT 3.0. The paleomagnetic results were rectified removing the tectonic tilt of Monte Cagnero section, which dips between 20° to 22° to the WNW (mean strike N30°E).

To obtain information on the magnetic mineralogy of the study samples, thermomagnetic analyses were performed using a CS-3 Kappabridge at the paleomagnetic laboratory of the IAG - University of São Paulo, São Paulo (Brazil). Thermomagnetic analyses are produced by heating samples and then measuring susceptibility as a function of temperature, revealing features typical of individual magnetic minerals or groups of minerals (e.g., Hrouda, 1994; Dunlop and Özdemir, 1997; Hrouda, 2003). The temperature dependence of magnetic susceptibility was measured up to 700°C (high-temperature) on selected samples (22). The thermomagnetic curves were measured in argon atmosphere in order to eliminate oxidation and alteration of magnetic minerals during heating. For the same set of samples, low temperature thermomagnetic curves also were performed down to -192°C for the same samples. These measurements were performed under air atmosphere. The thermomagnetic curves were interpreted and evaluated using the software package CUREVAL (AGICO).

3.2.2. Biostratigraphy

3.2.2.1. Planktonic foraminifera

Marly and soft marly-limestone samples for planktonic foraminiferal analysis were disaggregated using dilute hydrogen peroxide and Desogen (a surfactant). Hard marly limestone and limestone samples were prepared using the cold acetolyse technique of Lirer (2000), sieving through a 63 μm mesh, and drying at 50°C. This method enabled extraction of identifiable foraminifera even from indurated limestones. The combined preparation techniques allowed accurate taxonomic determination and detailed analysis of foraminiferal assemblages through the entire Monte Cagnero section. The residues were studied with a binocular microscope to characterize assemblages and identify biostratigraphic marker species, following the taxonomic criteria of Pearson et al. (2006). The two planktonic foraminiferal zonations of Berggren et al. (1995) and Wade et al. (2011) were followed.

3.2.2.2. Calcareous nannofossil

Samples for calcareous nannofossil analysis were prepared from unprocessed material as simple smear slides using standard preparation methods (Bown and Young, 1998). Smear slides were studied using a Leitz Laborlux 12 Pol light microscope both under crossed polarized and transmitted light at a magnification of 1250×. Nannofossil taxa were identified according to the taxonomic concepts summarized by Perch-Nielsen (1985). The standard calcareous nannofossil zonations of Martini (1971) and Okada and Bukry (1980) are widely used for low- and mid- latitude biostratigraphic studies in the Paleogene, and these were adopted in this paper.

3.3. Results

3.3.1. Paleomagnetic behavior and polarity zonation

The natural remanent magnetization (NRM) of the Monte Cagnero sample set varies from 4.27×10^{-10} Am^2/kg to 4.71×10^{-7} Am^2/kg, with mean values of 3.49×10^{-8} Am^2/kg (Figure 3.2). The NRM intensities are significantly lower in the interval between 78 to 104 msl and the magnetic behavior during demagnetization is not completely resolvable.

AF demagnetization was more effective in removing the secondary magnetization than thermal demagnetization at Monte Cagnero section. In most samples, a low-coercivity component was removed after AF demagnetization between 10–80 mT and after thermal demagnetization at 200–540°C. Stable paleomagnetic behavior (with maximum angular deviation (MAD) values below 15°) was obtained for 105 samples (44% of the total analyzed samples). Thermal treatment performed on all 241 "B" samples showed stable behavior for 65 samples (27%). For a total of 170 samples (70%), based on the observed demagnetization behavior (Figure 3.3), we isolated the ChRM component recognizing both normal and reverse polarity directions (Figure 3.4).

The magnetic polarity record from the Monte Cagnero section was divided into thirteen magnetozones (Figure 3.4). A high-resolution record was obtained between 58 and 79 msl and between 102 and 124 msl (Figure 3.4). Between these intervals (79-102 msl), a much lower resolution record was obtained due to the complex behavior of the samples during demagnetization. Many of these samples with poor demagnetization behavior have MAD values >15° and were not used to define the magnetic polarity record. The magnetozones were defined using multiple and consecutive samples with the same polarities along the section.
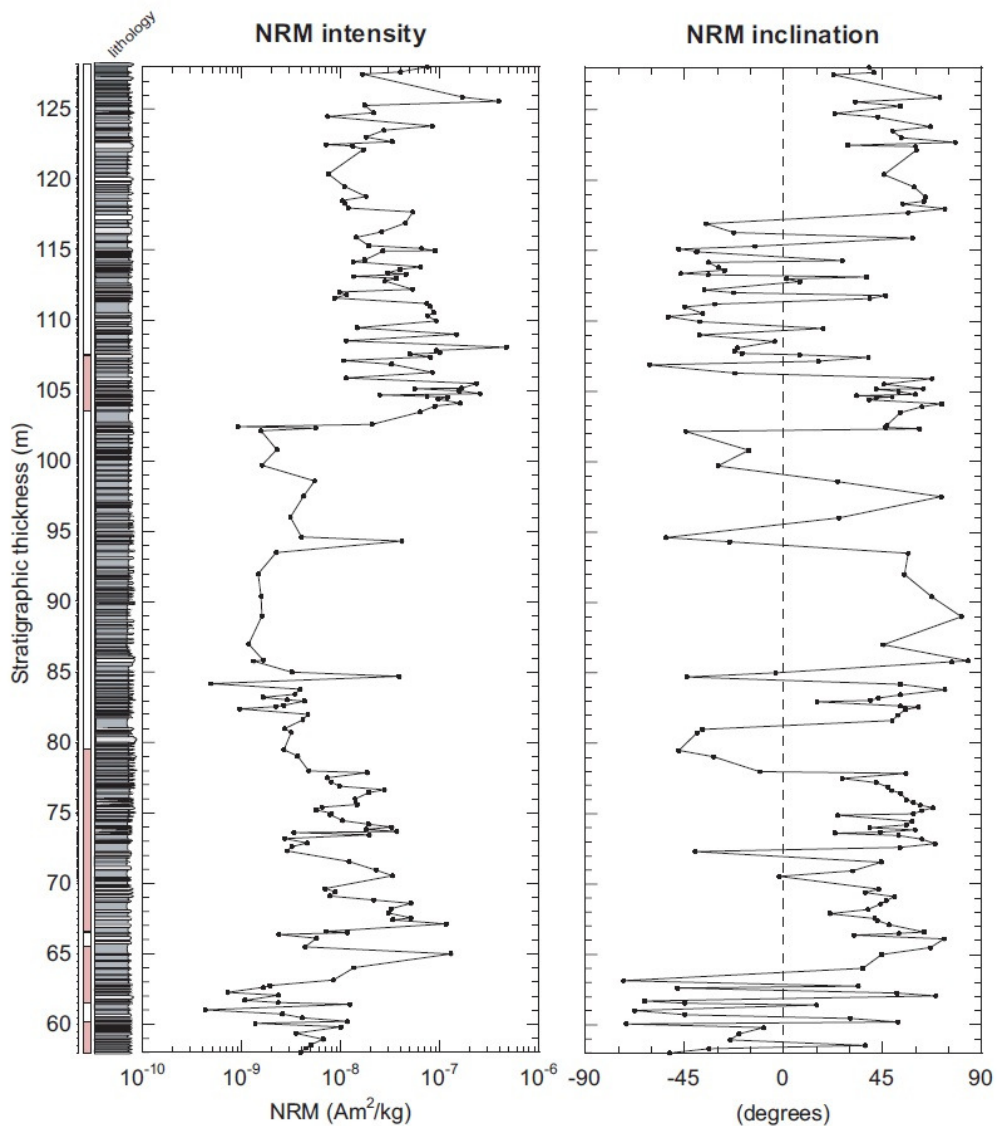
Figure 3.2. *Intensity and inclination of the natural remanent magnetization (NRM) along the Monte Cagnero section from 58 to 128 msl compared with lithostratigraphic column.*
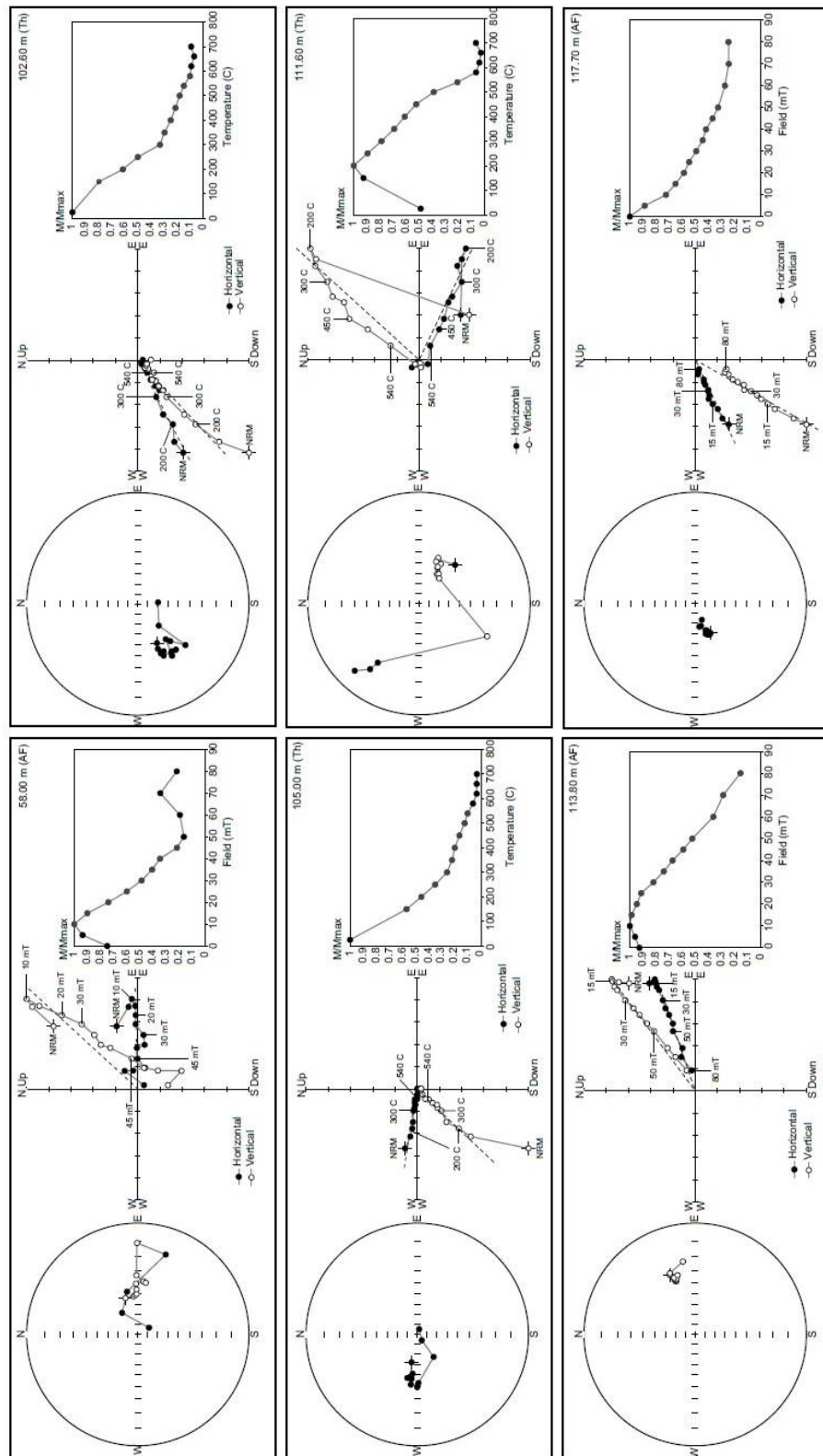
Figure 3.3. *Selected representative orthogonal plots, stereograms and intensity decay plots. Solid (open) squares represent the projection on the horizontal (vertical) plane. The demagnetization levels are represented in mT.*

49
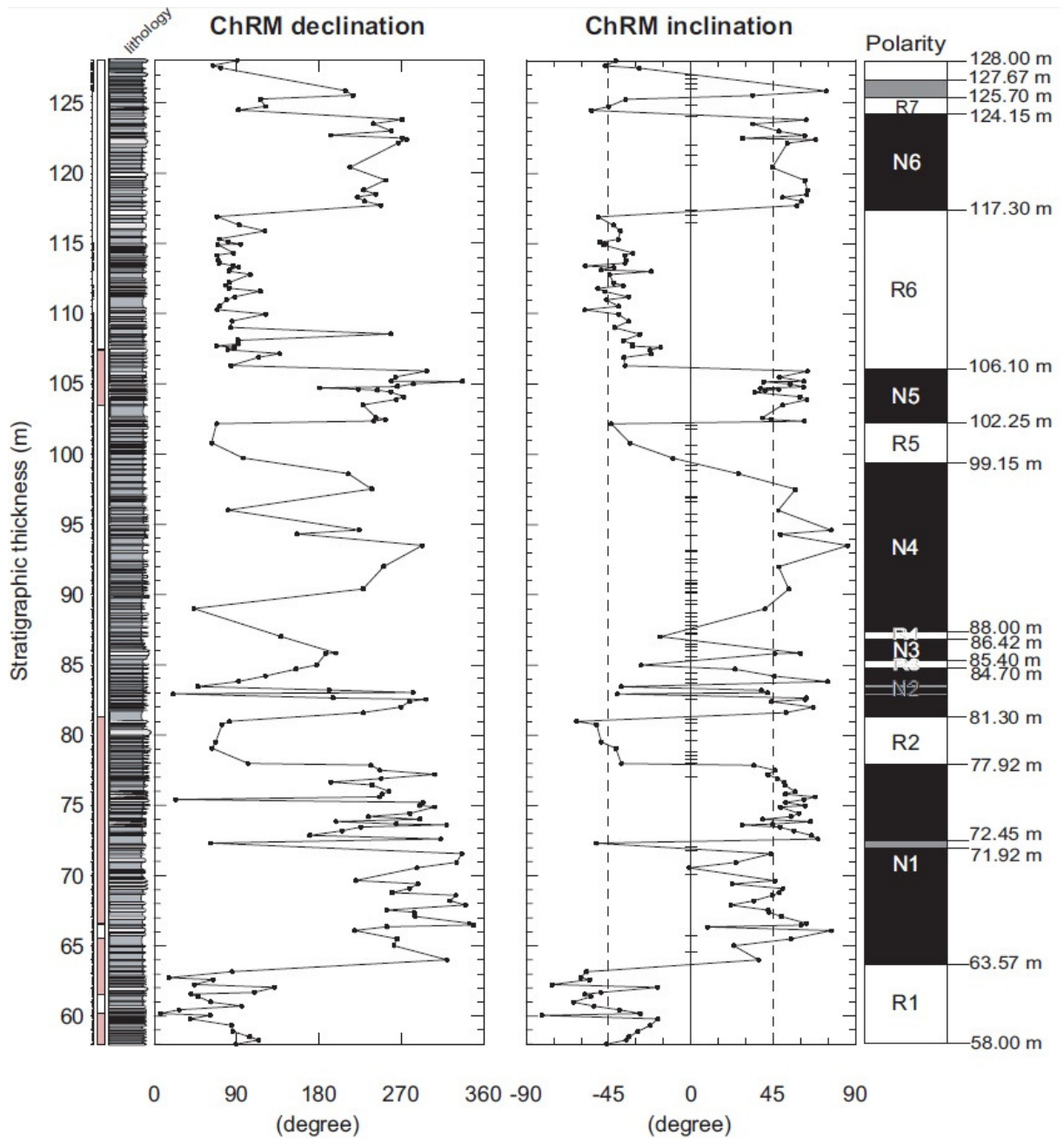
Figure 3.4. *Intensity and inclination of the characteristic remanent magnetization (ChRM) along the Monte Cagnero section from 58 to 128 msl compared with lithostratigraphic column. On the right site, we also included the magnetozones and the boundary between them in msl. Black horizontal lines at 0 degrees in the inclination of ChRM represent samples for which we have not been able to calculate the ChRM because of high MAD values. The dashed line represents the GAD based on the reconstruction of Besse and Courtillot (1998).*

The arithmetic mean inclination and declination for the normal polarity samples used for in the magnetozones are 50.8° and 245.8° (colatitudes=48.8°; N=94; α_{95}= 3.40), respectively. For the reverse polarity samples, the means are -42.8° and 83.2° (colatitudes= -48.9°; N=69; α_{95}= 3.52), respectively. Samples with ChRM inclinations below 20° were not considered when calculating the means. At this location, the expected average values are 56° for inclination and 6° for declination (Besse and Courtillot, 1991). Thus, published values of inclination and declination are close to the cone of confidence determined here. For the samples that retained a weak magnetization (in several cases we were not able to remove the secondary components), we believe the reversal test and results to be acceptable.

The thermomagnetic heating and cooling curves for selected samples from Monte Cagnero section are shown in Figure 3.5. For all samples, we observe magnetic mineralogical transformations during thermal treatment detected by the variation of magnetic susceptibility versus temperature changes. Samples at 58.60 and 68.65 msl (Figures 3.5A and D) show initially low values of magnetic susceptibility corresponding to a presence of dia- and/or paramagnetic minerals. Samples at 63.35 msl (Figure 3.5B) and 64.70 msl (Figure 3.5C) show an increase of the magnetic susceptibility at around 300–400∘C, and then a major fall after 580°C indicating the presence of magnetite with minimal presence of hematite. The sample at 64.70 msl shows the reversible behavior after heating; however, after heating at 700°C under open-air conditions, the samples at 58.60, 68.65, and 63.35 msl suffered an irreversible mineralogical transformation indicated by the higher susceptibility of the cooling curve. For samples at 58.60 and 68.65 msl, the susceptibility increases rapidly during cooling between 600–500°C indicating that magnetite is product of clays during thermal treatment. In samples from 63.35 and 64.70 msl, the increase begins at approximately 650°C suggesting that new hematite was also produced. These mixtures of different magnetic phases are often found in carbonate samples, and the formation of secondary (authigenic) iron oxides is thought to result from the presence of pre-existing iron-bearing minerals (Channell et al., 1982; Channell and McCabe, 1994, Jovane et al., 2007a,b).
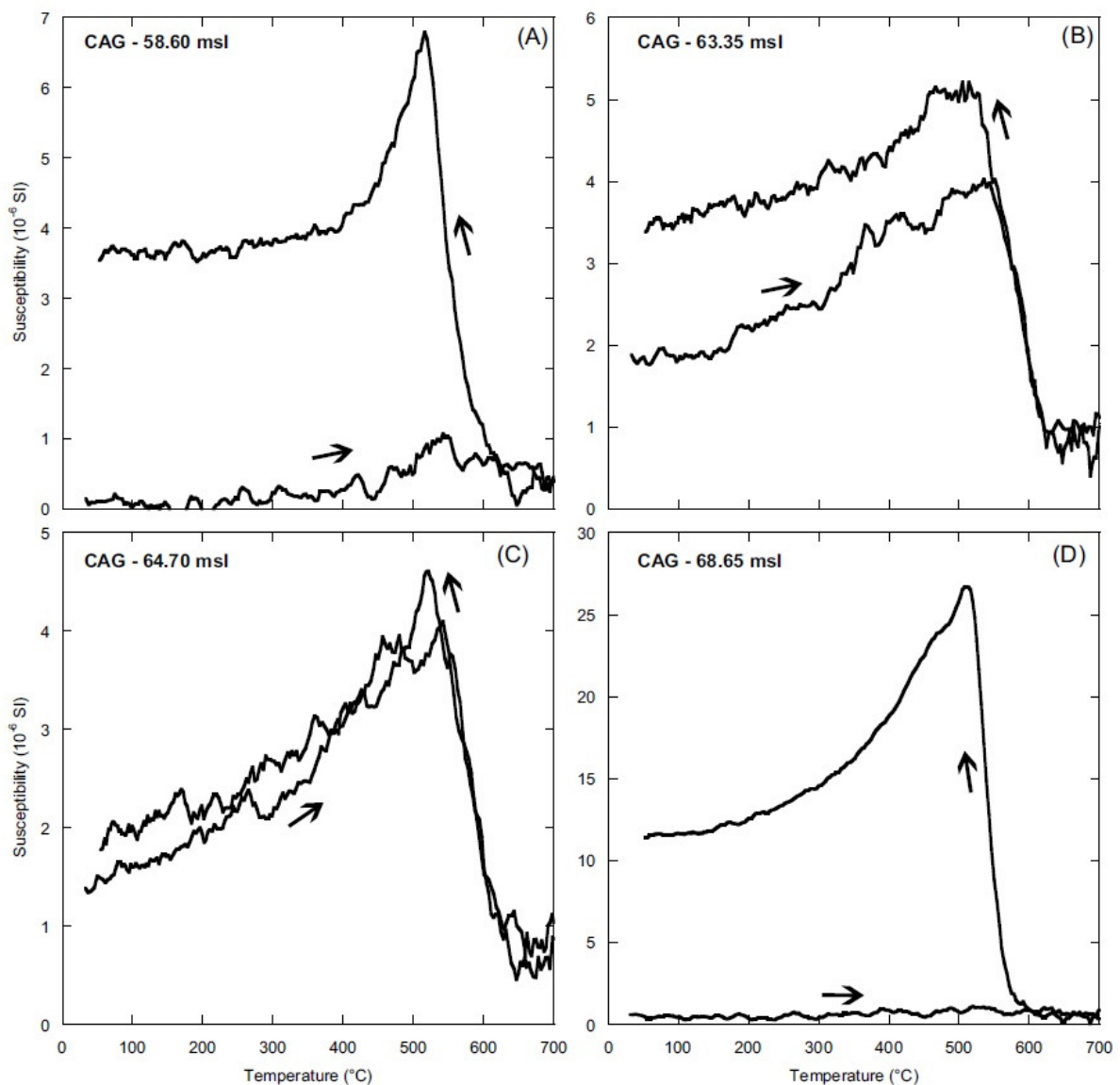
Figure 3.5. Temperature versus magnetic susceptibility for four samples from the Monte Cagnero section. Details on the significance for magnetic mineral associations from heating progression and the cooling return are in the text. The furnace diamagnetism has been subtracted.

3.3.2. Biostratigraphy

The biostratigraphy of the Monte Cagnero section was initially documented by Baumann and Roth (1969). They established a correlation between planktonic foraminiferal

and calcareous nannofossil biozonations from the Eocene-Oligocene boundary interval to the uppermost Oligocene and identified seven nannofossil biozones corresponding to Zones NP19/20–NP24 of Martini (1971). Compared with several other sections of the Umbria-Marche Scaglia succession, the Monte Cagnero section is the most expanded and continuous section straddling the E-O boundary (Baumann, 1970). Further biostratigraphic refinement of the Monte Cagnero section, encompassing ~55 m of the Eocene (Scaglia Variegata Formation) and ~30 m of the overlying Oligocene section (Scaglia Cinerea Formation), was completed by Guerrera et al. (1988) and Parisi et al. (1988). A further refinement of the middle–late Eocene planktonic foraminiferal biostratigraphy at the Monte Cagnero section was performed by Verducci and Nocchi (2004), who also attempted to identify significant paleoclimatic and paleoceanographic events across this time interval. More recently, Coccioni et al. (2008) proposed the Monte Cagnero section as a potential candidate for the Chattian GSSP, and Hyland et al. (2009) nominated this section as a parastratotype for the Eocene-Oligocene GSSP at Massignano.

3.3.3. Planktonic foraminifera

Planktonic foraminifera are abundant and diverse throughout the study interval of the Monte Cagnero section, with high species richness and assemblages typical of late Eocene–early Oligocene low-latitude pelagic environments. Preservation is mostly moderate to good therefore offering the possibility of accurate taxonomic.

The following main biostratigraphic events (bioevents) were identified and correlated with the planktonic foraminiferal biozones (from bottom to top): (l) Lowest Occurrence (LO) of *Orbulinoides beckmanni* at 63.2 msl; (2) Highest Occurrence (HO) of *O. beckmanni* at 65.5 msl; (3) HO of *Morozovelloides crassatus* at 85.0 msl; (4) LO of *Globigerinatheka semiinvoluta* at 86.5 msl; (5) HO of *Globigerinatheka semiinvoluta* at 101.1 msl; (6) LO of *Turborotalia cunialensis* at 102.50 msl; (7) HO of *Globigerinatheka index* 107.52 msl; (8) HO of *Cirbrohantkenina inflata* 112.90 msl; (9) HO of *Turborotalia cerroazulensis* 113.6 msl; (10) HO of *Hantkenina alabamensis* at 114.1 msl. The lower part of the study section is assigned to Zones P12 of Berggren et al. (1995) and E11 of Wade et al. (2011), based on the

absence of *O. beckmanni*, which defines the lower and the upper boundaries of Zone P13 (*Globigerapsis beckmanni* Total Range Zone) of Berggren et al. (1995) and Zone E12 (*O. beckmanni* Taxon-range Zone) of Wade et al. (2011), respectively (Figure 3.6). Following Berggren et al. (1995), the LOs of *G. semiinvoluta* and *T. cunialensis* and the HOs of *C. inflata* and *T. cerroazulensis* are used to mark the P14/P15, P15/P16, P16/P17 and P17/P18 zonal boundaries, respectively (Figure 3.6). According to Wade et al. (2011), the HOs of *M. crassatus*, *G. semiinvoluta* and *G. index* and the LO of *H. alabamensis* define the E13/E14, E14/E15, E15/E16 and El6/O1 zonal boundaries, respectively (Figure 3.6). Following Coccioni et al. (1988), Nocchi et al. (1988) and Premoli Silva and Jenkins (1993), the E-O boundary is placed at 114.1 msl, at the extinction level of the planktonic foraminiferal Family *Hantkeninidae* (Figure 3.6).

3.3.4. Calcareous nannofossil

In all study samples from the Monte Cagnero section, calcareous nannofossils are abundant, and preservation varies from moderate to poor. The following primary bioevents were identified in the Monte Cagnero section (from bottom to top) (Figure 3.6): (1) HO of *Chiasmolithus solitus* at 70.0 msl; (2) LO of *Chiasmolithus oamaruensis* at 84.0 msl; (3) HO of *Chiasmolithus grandis* at 85.50 msl; (4) HO of *Chiasmolithus oamaruensis* at 98.5 msl; (5) HO of *Discoaster saipanensis* at 108.5 msl; and (6) Acme Base (AB) of *Clausicoccus obrutus* >5.7μm at 114.5 msl. The lower part of the section is assigned to zones NP16 and CP14a of Martini (1971) and Okada and Bukry (1980), respectively, based on the presence of *Reticulofenestra umbilica* and the absence of *Blackites gladius* (Figure 3.6). The HO of *C. solitus* marks the NP16/NP17 and CP14a/CP14b zonal boundaries of Martini (1971) and Okada and Bukry (1980), respectively. Following the biostratigraphical scheme of Martini (1971), we used the LO of *C. oamaruensis* to define the base of NP17/NP18-NP19 zonal boundary, the HOs of *C. oamaruensis* and *D. saipanensis* to mark NP18-19/NP20 and NP20/NP21 zonal boundaries, respectively (Figure 3.6). Since the LO of *Isthmolithus recurvus*, which defines both NP18/NP19 and CP15a/CP15b zonal boundaries of Martini (1971) and Okada and Bukry (1980), respectively, was not identified, zones NP18 and NP19 have been combined, as well as subzone CP15a (Figure 3.6). According to the

biostratigraphical biozonations of Okada and Bukry (1980), the HOs of *C. grandis* and *D. saipanensis* were used to define the CP14b/CP15, and CP15/CP16a zonal boundaries, respectively (Figure 3.6). The AB of *C. obrutus* >5.7μm was proposed by Hyland et al. (2009) to define the CP16a/CP16b zonal boundary instead of the AE of *Clausicoccus* as suggested by Backman (1987). This event is placed immediately above the E-O boundary and falls in the middle-upper part of chron C13r (Figure 3.6).
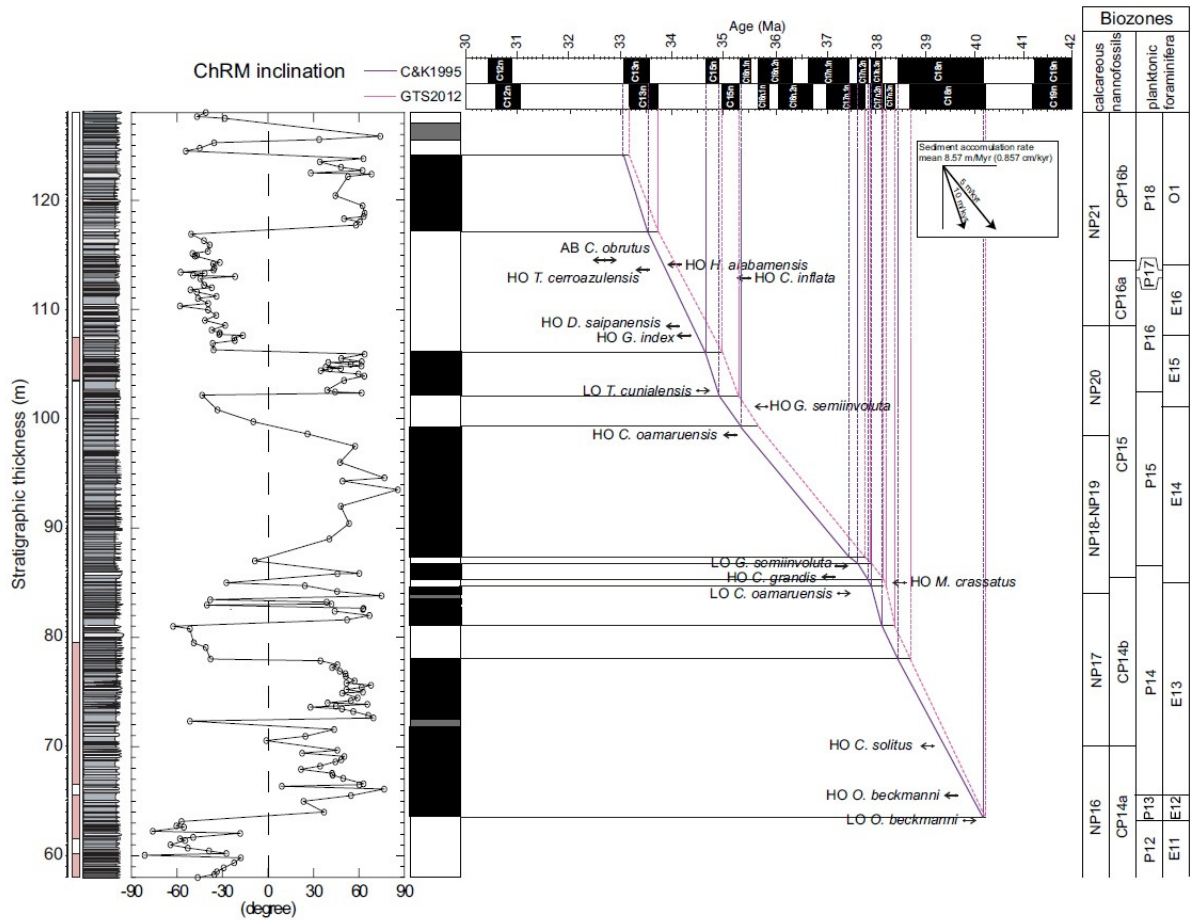
Figure 3.6. *Correlation between age of the geomagnetic polarity time scale (C&K1995, Cande and Kent, 1995; and Gee and Kent, 2007; GTS2012, Vandenberghe et al., 2012) and ChRM inclination of the Monte Cagnero section polarity zonations (purple solid line). Calcareous nannofossil and planktonic foraminiferal data were used to constrain the interpretation. Planktonic foraminiferal zones are after (P) Berggren et al. (1995) and (E) Wade et al. (2011); calcareous nannofossil zones are after (NP) Martini (1971) and (CP) Okada and Bukry (1980). Correlation between chron ages at Monte Cagnero and the Geologic Time Scale (GTS2012; Vandenberghe et al., 2012) and magnetozones is also shown*

(pink dashed line). LO—Lowest Occurrence; HO—Highest Occurrence; AB—Acme Base. Sedimentation rates are tabulated for each chron interval. The Eocene-Oligocene boundary is at 114.1 msl (Coccioni et al, 2008; Hyland et al., 2009).

3.4. Discussion

3.4.1. Correlation to the geomagnetic polarity time scale (GPTS)

A series of thirteen magnetozones are recognized within the Monte Cagnero section in a sequence of six normal polarity intervals and seven reversal polarity intervals (Figure 3.4). We interpreted the magnetic polarity record based on the Geomagnetic Polarity Time Scale (GPTS) calibrations of Cande and Kent (1995; C&K1995) and Vandenberghe et al. (2012; GTS2012). Magnetozones R1 (58.00–63.57 msl), N1 (63.57–77.92 msl), R2 (77.92–81.30 msl), N2 (81.30–84.70 msl), R3 (84.70–85.40 msl), N3 (85.40–86.42 msl), N3 (86.42–88.00 msl), N4 (88.00–99.15 msl), R5 (99.15–102.25 msl), N5 (102.25–106.10 msl), R6 (106.10-117.30 msl), N6 (117.30–124.15) and R7 (124.15–128.00 msl) are interpreted to correspond respectively to chrons C18r, C18n, C17r, C17n.3n, C17n.2r, C17n.2n, C17n.1r/C17n.1n/C16n, C15r, C15n, C13r, C13n and C12r (Figures 3.4 and 3.6). Our magnetostratigraphy is based on a straightforward interpretation for most of the section, with some uncertainties in the depth interval between ~90 and 95 msl - an interval which is characterized by low concentration of magnetic minerals. Through linear interpolation between chron boundary ages (Cande and Kent, 1995; Vandenberghe et al., 2012), we have constructed a detailed age–depth model for the Monte Cagnero study section (Figure 3.6). The age–depth model for the interval between ~90 and 95 msl is mainly based on the biostratigraphic results because the magnetostratigraphy in this interval is less reliable than the rest of the section (Figure 3.6).

The top of the study section has an interpreted age of ~ 32.6 Ma within chron 12r (C&K95, 30.939–33.058 Ma; GTS2012, 31.034–33.157), while the bottom has an age of ~ 40.8 Ma within Chron 18r (40.130–41.257 Ma) (Figure 3.6). No faults, condensed layers or hiatuses have been recognized along the section that might indicate a time discontinuity in the section. Consequently, the entire Monte Cagnero section spans a time interval of at least 13

Myr (8 Myr in our segment and the 5 Myr through the Oligocene section documented by Hyland et al. (2009) and Coccioni et al. (2008)) in one continuous and undisturbed sedimentary sequence. The chron 12r interval was identified in previous work on this section (Hyland et al., 2009), which is in agreement with our polarity and age interpretations.

3.4.2. Eocene-Oligocene sedimentation rates at Monte Cagnero

Based on the GPTS calibrations of Cande and Kent (1995) (confirmed in Gee and Kent, 2007), sedimentation rates throughout the Monte Cagnero section vary from 14.07 m/Myr (chron 13n) to 5.34 m/Myr (Chron 17n.1r). The average sedimentation rate, which is calculated by linear interpolation between consecutive chron boundaries, is 8.57 m/Myr (0.857 cm/kyr) (Figure 3.7A).

Appling the most recent GTS chron ages from Vandenberghe et al. (2012), the calculated sedimentation rates for the Monte Cagnero section are very similar to those obtained using the GPTS of Cande and Kent (1995) (Figure 3.7B) with an average sedimentation rate of 8.68 m/Myr. These values confirm the duration of the chrons for this period from Cande and Kent (1995), Gee and Kent (2007), and Jovane et al. (2010) and GTS 2012 (Vandenberghe et al., 2012). Furthermore, the calculated sedimentation rates for the Monte Cagnero section are comparable with sedimentation rates of coeval sections at Massignano (upper Eocene to lower Oligocene) and Contessa Highway (middle Eocene), which have average rates of 7.3 and 6.4 m/Myr, respectively (Jovane et al., 2007a,b).
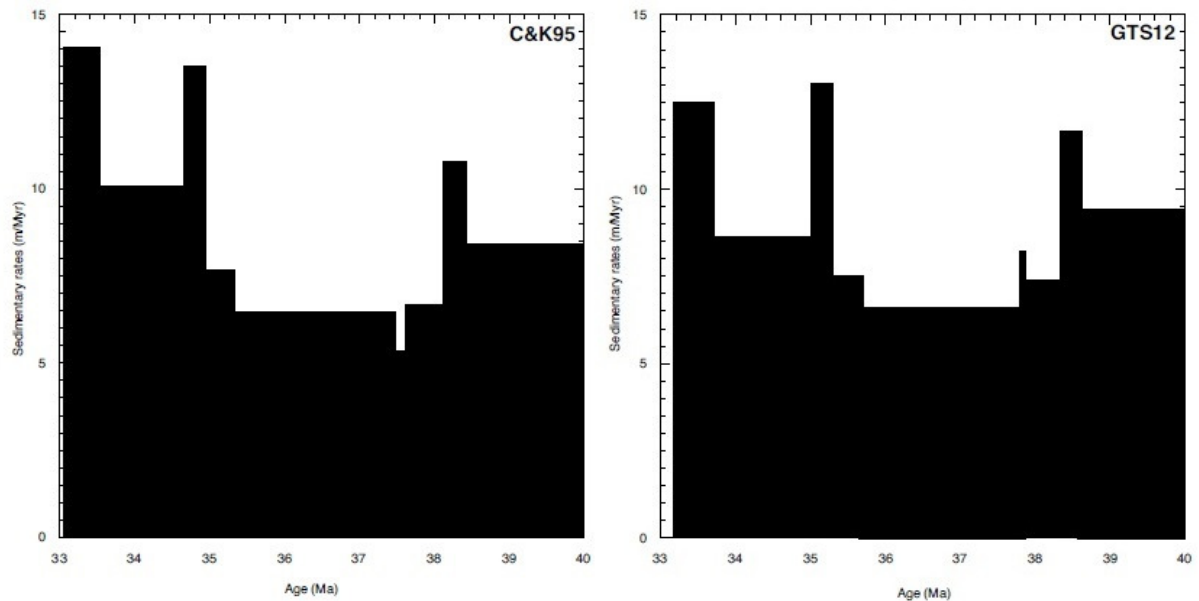
Figure 3.7. *Variation of sedimentation rates at Monte Cagnero versus age for the middle Eocene-early Oligocene interval. The average sedimentation rate is 8.57 m/Myr using Cande and Kent (1995), Gee and Kent (2007) and Jovane et al. (2010). The average sedimentation rate is 8.68 m/Myr using the GTS from Vandenberghe et al. (2012). Depths units are in meters stratigraphic level (msl).*

3.4.3. Refinement of age calibrations for biostratigraphic events

All of the biostratigraphic marker taxa that define the standard planktonic foraminiferal zones of Berggren et al. (1995) and Wade et al. (2011), through the middle–late Eocene and early Oligocene, occur in the analyzed material from the Monte Cagnero section. Additionally, most of the key markers used to define the standard calcareous nannofossil zonations of Martini (1971) and Okada and Bukry (1980) occur together with several additional marker species. Our integrated biostratigraphic study provides evidence that the 58–127 msl interval at the Monte Cagnero section is continuous, within biostratigraphic and magnetostratigraphic resolution, between planktonic foraminiferal Zones P12 and P18 of Berggren et al. (1995) and between Zones E11 and O1 of Wade et al. (2011). Also, a complete record of calcareous nannofossil Zones NP16 to NP21 of Martini et al. (1971) and CP14a to CP16b of Okada and Bukry (1980) is present (Figure 3.6).

At Monte Cagnero, however, some bioevents that mark the zonal boundaries are placed at different stratigraphic levels compared to the current standard magneto-biochronological timescale (Luterbacher et al., 2004, with updates from Ogg et al., 2008). The main discrepancies, from bottom to top, are as follows:

1) the HO of *C. solitus* (NP16/NP17 and CP14a/CP14b zonal boundaries) occurs higher in the upper part of Chron C18n.2n;

2) the LO of *C. oamaruensis* (NP17/NP18-NP19 zonal boundary) is found lower in Chron C17n.3n;

3) the HO of *C. grandis* (CP14b/CP15 zonal boundary) occurs lower at the base of Chron C17n.2n;

4) the HO of *G. semiinvoluta* (E14/E15 zonal boundary) is identified higher in the middle part of Chron C15r;

5) the HO of *D. saipanensis* (NP20/NP21 and CP15/CP16a zonal boundaries) is recognized higher in the lower part of Chron C13r.

These discrepancies are likely due to the fact that the markers adopted in standard calcareous nannofossil zonations of Martini (1971) and Okada and Bukry (1980) for the Paleogene Period might be latitudinally restricted and facies dependent (Fornaciari et al., 2010). Moreover, the biostratigraphic resolution of the calcareous nannofossil and planktonic foraminiferal schemes for the middle Eocene–early Oligocene is low and some bioevents have been rarely calibrated to high-resolution magnetostratigraphic records. Accordingly, correlations of the standard calcareous nannofossil and planktic foraminiferal biohorizons, to the geomagnetic polarity time scale (GPTS; Cande and Kent 1995; CK95) remain disputed for Paleogene times. The data presented above and summarized in Table 3.1 expand the existing database of calcareous nannofossil and planktonic foraminiferal biochronology during the middle–late Eocene and early Oligocene.

Planktonic foraminiferal and calcareous nannofossil events and Chron boundaries	Depth (msl)	Age (Ma)	Astronomical Age (Ma)
LO *Orbulinoides beckmanni*	63.20	40.50[1]	40.330[6]
C18r/C18n.2n	63.57	40.130[3]	40.120[6]
HO *Orbulinoides beckmanni*	65.50	40.00[1]	39.860[6]
HO *Chiasmolithus solitus*	70.00	40.40[2]	
C18n.2n/C18n.1r	71.92	39.756[4]-39.631[3]	
C18n.1r/C18n.1n	72.45	39.686[4]-39.552[3]	
C18n.1n/C17r	77.92	38.668[4]-38.426[3]	
C17r/C17n.3n	81.30	38.380[4]-38.113[3]	
C17n.3n/ C17n.2r	83.50	38.202[4]-37.920[3]	
LO *Chiasmolithus oamaruensis*	84.00	37.00[2]	
C17n.2r/C17n.2n	84.00	38.135[4]-37.848[3]	
C17n.2n/C17n.1r	84.70	37.908[4]-37.604[3]	
HO *Morozovelloides crassatus*	85.00	38.00[1]	
C17n.1r/C17n.1n	85.40	37.785[4]-37.473[3]	
HO *Chiasmolithus grandis*	85.50	37.10[2]	
LO *Globigerinatheka semiinvoluta*	86.50	38.00[1]	
C17n.1n/C16r?	92.00	36.969[4]-36.618[3]	
C16r?/C16n	93.40	36.700[4]-36.341[3]	
HO *Chiasmolithus oamaruensis*	98.50	35.40[2]	35.404[5]
C16n/C15r	99.15	35.706[4]-35.343[3]	35.340[5]
HO *Globigerinatheka semiinvoluta*	101.10	35.80[1]	35.520[5]
C15r/C15n	102.25	35.294[4]-34.940[3]	34.960[5]
LO *Turborotalia cunialensis*	102.50	35.30[1]	35.185[5]
C15n/C13r	106.10	34.999[4]-34.655[3]	34.728[5]
HO *Globigerinatheka index*	107.52	34.30[1]	34.400[5]
HO *Discoaster saipanensis*	108.50	34.20[2]	
HO *Cribrohantkenina inflata*	112.90	34.00[2]	34.221[5]
HO *Turborotalia cerroazulensis*	113.60	33.80[1]	
HO *Hantkenina alabamensis*	114.10	33.70[1]	33.703[5]
AB *Clausicoccus obrutus*	114.50	n.a.	
C13r/C13n	117.30	33.705-33.545[3]	33.545[5]
C13n/C12r?	126.67	33.157-33.058[3]	

Table 3.1. *Planktonic foraminiferal and calcareous nannofossil events and interpretation of Chrons boundaries for the Monte Cagnero section. Bioevent ages of Wade et al. (2011) (1), and Berggren et al. (1995) (2). Magnetochron ages from Cande and Kent (1995) (3) and Vandenberghe et al., 2012 (4). Astronomical ages from Jovane et al., (2006) (5) and Jovane et al., (2010) (6).*

3.5. Conclusions

The Monte Cagnero section located in the northeastern Apennines near Urbania in the Umbria-Marche Basin (Italy), provides the most complete and continuous stratigraphic sequence representing the middle Eocene to lower Oligocene interval (~55 to 28 Ma) currently identified in central Italy, spanning a time interval of at least ~13 Myr. In this study, we have obtained new insight on the nature and age of these strata based on high-resolution magnetostratigraphic analyses and detailed calcareous nannofossil and planktonic foraminiferal analyses. These data form the basis of a new, robust age-depth model for the middle Eocene–lower Oligocene interval.

The Monte Cagnero section consists of limestone and marlstone of reddish and greenish color. The magnetic mineralogy of these rocks is represented mainly by low-coercivity minerals (most likely magnetite or maghemite) in a mixture in some intervals of high coercivity minerals (most likely hematite). The high-resolution definition of the occurrence of those intervals along the section has important implications for climate studies and paleoceanographic events in the Neo-Tethys Realm during from the middle to the late Eocene. Our new magneto-biostratigraphy for the Monte Cagnero section also provides a precise age model across several crucial climate events. The refined age information for this section, in addition to multi-disciplinary climatic proxy studies, that are currently ongoing, will allow reconstruction of environmental change across the greenhouse-icehouse transition. The Monte Cagnero section likely records important middle Eocene–early Oligocene climate events, such as the E-O climate transition at ~34 Ma and MECO event at ~40 Ma. New insights into these events and related regional climate changes in the Tethys region will be gained through future paleoclimatic studies of the Monte Cagnero section and application of the high-resolution integrated age-model presented here.

Chapter 4. Enhanced primary productivity and magnetotactic bacterial production in response to middle Eocene warming in the Neo-Tethys Ocean

4.1. Introduction

The early part of the Cenozoic Era was characterized by greenhouse conditions through the early Eocene, followed by a ~17 Myr-long cooling trend (e.g. Zachos et al., 2008). This long-term cooling trend was interrupted by the Middle Eocene Climatic Optimum (MECO) – a warming event that peaked at ~40.0 Ma (base of Chron C18n.2n) (Bohaty and Zachos, 2003; Bohaty et al., 2009). The MECO event has been recognized from multiple sites in the Southern, Atlantic, Pacific, Indian, and Tethyan Oceans (Figure 4.1a). It was first identified in foraminiferal stable isotope records from the Atlantic and Indian sectors of the Southern Ocean (Barrera and Huber, 1993; Bohaty and Zachos, 2003) and the hallmark of the event is a distinct negative δ^{18}O excursion that spanned 500 kyr (Bohaty et al., 2009). The end of the event was marked by a prominent negative shift in benthic foraminiferal δ^{13}C of up to ~1.0‰ (e.g. Bohaty et al., 2009; Edgar et al., 2010). The long-lasting δ^{18}O excursion, with a <100 kyr warming peak (MECO warming), has been interpreted to indicate a ~4-6°C temperature increase of both surface and intermediate deep waters (Bohaty et al., 2009; Edgar et al., 2010). Organic molecular paleothermometry in the southwest Pacific revealed absolute sea surface temperatures of 24°C to 26°C just below the onset of MECO, and MECO peak temperatures exceeding 28°C (Bijl et al., 2010). The temperature increase corresponded to a concomitant pCO$_2$ increase by a factor of 2 to 3 (Bijl et al., 2010). An atmospheric pCO$_2$ rise has also been inferred at other sites by changes in deep ocean chemistry as revealed by the net decline in carbonate accumulation that reflects widespread calcite compensation depth (CCD) shoaling (Bohaty et al., 2009). The abrupt pCO$_2$ increase during the MECO event has been tentatively ascribed to massive decarbonation during subduction of Tethyan Ocean pelagic carbonates under Asia as India drifted northward (Bohaty and Zachos, 2003; Bijl et al., 2010).
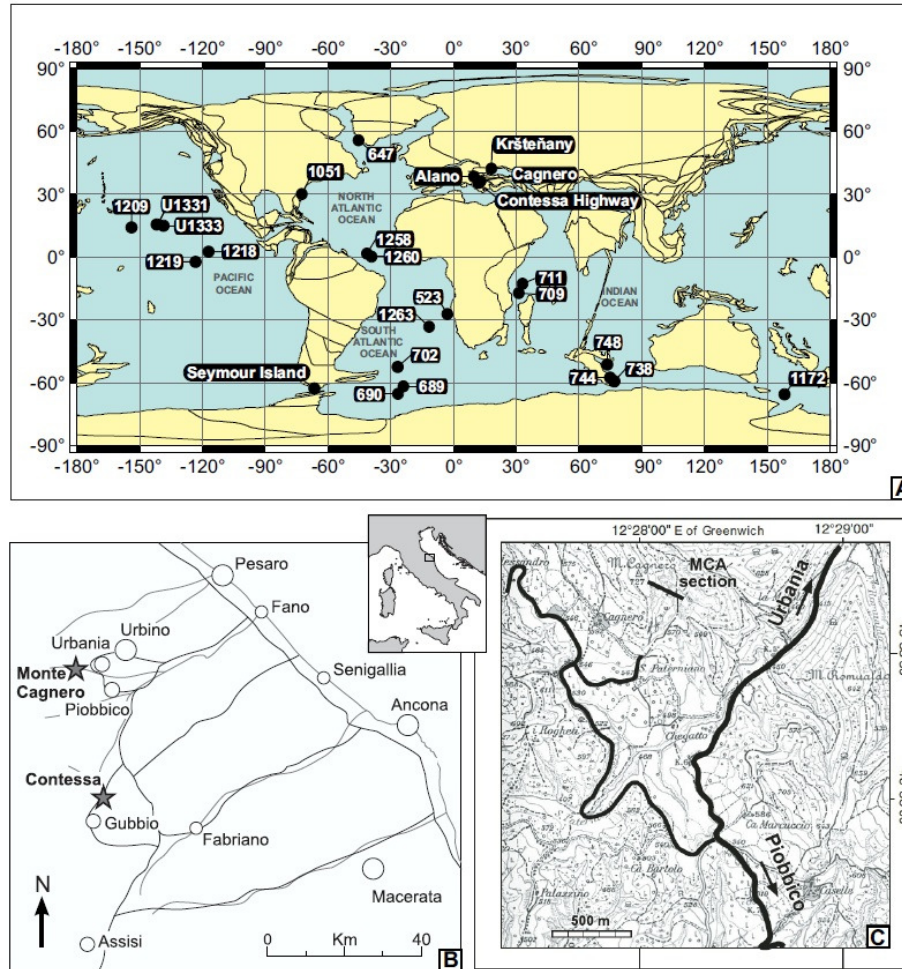
Figure 4.1. *(a) Palaeogeographic reconstruction at 40 Ma and location of the Prydz Bay (ODP Leg 119, Sites 738, 744), south Kerguelen Plateau (ODP Leg 120, Site 748), Weddell Sea (ODP Leg 113, Sites 689, 690), Angola Basin (DSDP Leg 73, Site 523), Islas Orcadas Rise (ODP Leg 114, Site 702), Black Nose (ODP Leg 171, Site 1051), Shatsky Rise (ODP Leg 198, Site 1209), "Paleogene Equatorial Transect" (ODP Leg 199, Sites 1218, 1219), Mascarene Plateau (ODP Leg 115, Sites 709, 711), Walvis Ridge (ODP Leg 208, Site 1263), Demerara Rise (ODP Leg 207, Sites 1258, 1260), East Tasmanian Plateau (ODP Leg 189, Site 1172), Pacific Equatorial Age Transect (IODP Legs 320-321, Sites U1331-U1333), Labrador Sea (ODP Leg 105, Site 647) and Monte Cagnero, Contessa Highway, Alano, Kršteňany, and Seymour Island on-land sections. Reconstruction made using the web-based software at http://www.odsn.de/odsn/services/paleomap/paleomap.html. (b) Location of the Monte Cagnero (MCA) and Contessa Highway sections. (c) Location of the Monte Cagnero (MCA) section (Lat. 43°38'50"N, Long. 12°28'05"E, 727 m above sea level) near the town of Urbania, Italy.*

The Contessa Highway (CHW) section in Central Italy was the first land-based section where MECO was documented (Figures 4.1a, b; Jovane et al., 2007a). More recently, the MECO event was also recognized at the Alano di Piave section, northeast Italy (Figure 4.1a; Luciani et al., 2010). In the Alano section the MECO event is followed by deposition of two organic-rich intervals (ORG1 and ORG2; Spofforth et al., 2010), which are thought to represent rapid organic carbon burial contemporaneous with the global pCO$_2$ drawdown during the post-MECO recovery interval. Significant paleoredox, foraminifera and calcareous nannofossil assemblage changes have been documented in the same section that point to a shift toward more eutrophic waters and a lowering of oxygen availability at the end of MECO during deposition of sapropel-like beds (Spofforth et al., 2010; Luciani et al., 2010; Toffanin et al., 2011). Deposition of organic-rich sediments after the transient warming event has been associated with enhanced delivery of terrestrial material that would have both increased nutrient availability to the sea surface and stimulated primary productivity (Spofforth et al., 2010).

In marine environments, changes in primary productivity are directly related to the distribution and availability of nutrients and can be tracked by several proxies. One proxy is the relative abundance of magnetofossils in pelagic sediments (e.g. Hesse, 1994; Tarduno, 1994; Tarduno and Wilkison, 1996; Lean and McCave, 1998; Yamazaki and Kawahata, 1998; Kopp and Kirschvink, 2008; Yamazaki, 2008, 2009; Roberts et al., 2011; Chang et al., 2012; Larrasoaña et al., 2012; Yamazaki, 2012). Magnetofossils are the inorganic remains of magnetotactic bacteria, which intracellularly biomineralize magnetically non-interacting single domain (SD) crystals of magnetite (Fe$_3$O$_4$) or greigite (Fe$_3$S$_4$), or both, that are arranged in chains within the cell (Bazylinski and Frankel, 2003; Faivre and Schüler, 2008; Kopp and Kirschvink, 2008; Moskowitz et al., 2008). These chains of nanocrystals (40-120 nm) are used by the magnetotactic bacteria to orientate themselves relative to the Earth's magnetic field (Blackmore, 1975) in order to find optimal living conditions in strongly chemically stratified aquatic environments (Bazylinski and Frankel, 2004). Magnetosomes can be preserved in sediments and in some cases may account for 20–60% of their bulk magnetization (Egli, 2004; Housen and Moskowitz, 2006; Roberts et al., 2011). Although magnetotactic bacteria are found in various marine environments (e.g. Petersen et al., 1986;

Vali et al., 1987; McNeill, 1990; Petermann and Bleil, 1993; Hesse, 1994; Housen and Moskowitz, 2006; Jovane et al., 2012), detection of fossil magnetosomes can be complicated by their mixture with other magnetic minerals, or with magnetic particles with different magnetic domain structures. Nevertheless, magnetofossils have been reported from pelagic marine environments of different ages, such as the Cretaceous-Paleogene boundary (e.g. Abrajevitch and Kodama, 2009), the Paleocene-Eocene boundary (e.g. Chang et al., 2012; Larrasoaña et al., 2012), the Eocene (e.g. Roberts et al., 2011, 2012), and the Miocene (Florindo et al., in press). Magnetosome abundance in sediments is strongly controlled by the availability of particulate iron and organic carbon flux to the seafloor (Roberts et al., 2011), which can be related to climate, including hyperthermal conditions (e.g. Schumann et al., 2008; Chang et al., 2012; Larrasoaña et al., 2012).

Here we present a high-resolution environmental magnetic, micropaleontological and stable isotopic investigation of the western Tethyan pelagic marine section at Monte Cagnero (MCA), Italy, which spans the late middle Eocene interval. Environmental magnetic data are used to detect magnetofossils and paleoproductivity variations across the MECO event and just after the warming event. These results, combined with paleoecological data from nannofossils and foraminifera, are used to assess paleoenvironmental scenarios associated with the MECO event in the Neo-Tethys realm.

4.2. Geological Setting and Magnetobiostratigraphical framework

A continuous Paleogene sedimentary record is preserved in the Scaglia Formation, which includes pelagic limestones and marly limestones of the Umbria–Marche succession, central Italy. The MCA section is exposed on the southeastern slope of Monte Cagnero (Lat. 43°38'50"N, Long. 12°28'05"E, 727 m above sea level) near the town of Urbania, northeastern Apennines, Italy (Figure 4.1). Because of its completeness and stratigraphic continuity, the MCA section is an important pelagic sedimentary succession for studying Eocene and Oligocene climatic events (Coccioni et al., 2008; Hyland et al., 2009; Jovane et al., 2013). The 100 m stratigraphic level at the MCA section is equivalent to meter level 0 of the GSSP for the Eocene/Oligocene boundary at Massignano (e.g. Premoli Silva and Jenkins,

1993; Coccioni et al., 2008; Hyland et al., 2009; Jovane et al., 2004, 2006, 2007b, 2013). We focus on the lower part of the section, from 58 to 72 meters stratigraphic level (msl) (Figure 4.2). This 14-m-thick interval of the MCA section belongs to the Scaglia Variegata Formation that consists of bundles of limestone-marl couplets. A lower bathyal (1000-2000 m) water depth was inferred for the depositional environment of the MCA section during the middle Eocene (Guerrera et al., 1988; Parisi et al., 1988), which gradually shoaled to mid-bathyal (800-1000 m) and upper bathyal (400-600 m) water depths in the late Eocene and early Oligocene, respectively.

High-resolution magnetobiostratigraphic calibration of the MCA section was carried out by Coccioni et al. (2008), Hyland et al. (2009), and Jovane et al. (2013). The studied interval spans from the middle-upper part of Chron C18r to the lowermost part of C18r.1r with an average sedimentation rate of ~8.57 m/myr following the geomagnetic polarity timescale (GPTS) of Cande and Kent (1995) (confirmed by Ogg, 2012). The primary nannofossil and foraminiferal biostratigraphic events identified are (from bottom to top) the: (l) lowest occurrence (LO) of *Orbulinoides beckmanni* at 63.2 msl; (2) highest occurrence (HO) of *O. beckmanni* at 65.5 msl; and (3) HO of *Chiasmolithus solitus* at 70.0 msl (Jovane et al., 2013). It is worth noting, however, that recognition of the LO of *O. beckmanni* can be subjective because this taxon originates from *Globigerinatheka euganea*, and some transitional forms of problematic taxonomic assignment occur from 62.8 to 63.2 msl. Additionally, identification of the HO of *O. beckmanni* is hampered by its scarce abundance, moderate preservation of planktic (P) and benthic (B) foraminifera and some problematic specimen identifications up to 66.60 msl. Nevertheless, the MCA biostratigraphic record in the 58-72 msl interval is likely continuous and is interpreted to span planktonic foraminiferal Zones P12 to P14 of Berggren et al. (1995) and Zones E11 to E13 of Wade et al. (2011), and calcareous nannofossil Zones NP16 to NP17 of Martini et al. (1971) and CP14a to CP14b of Okada and Bukry (1980).
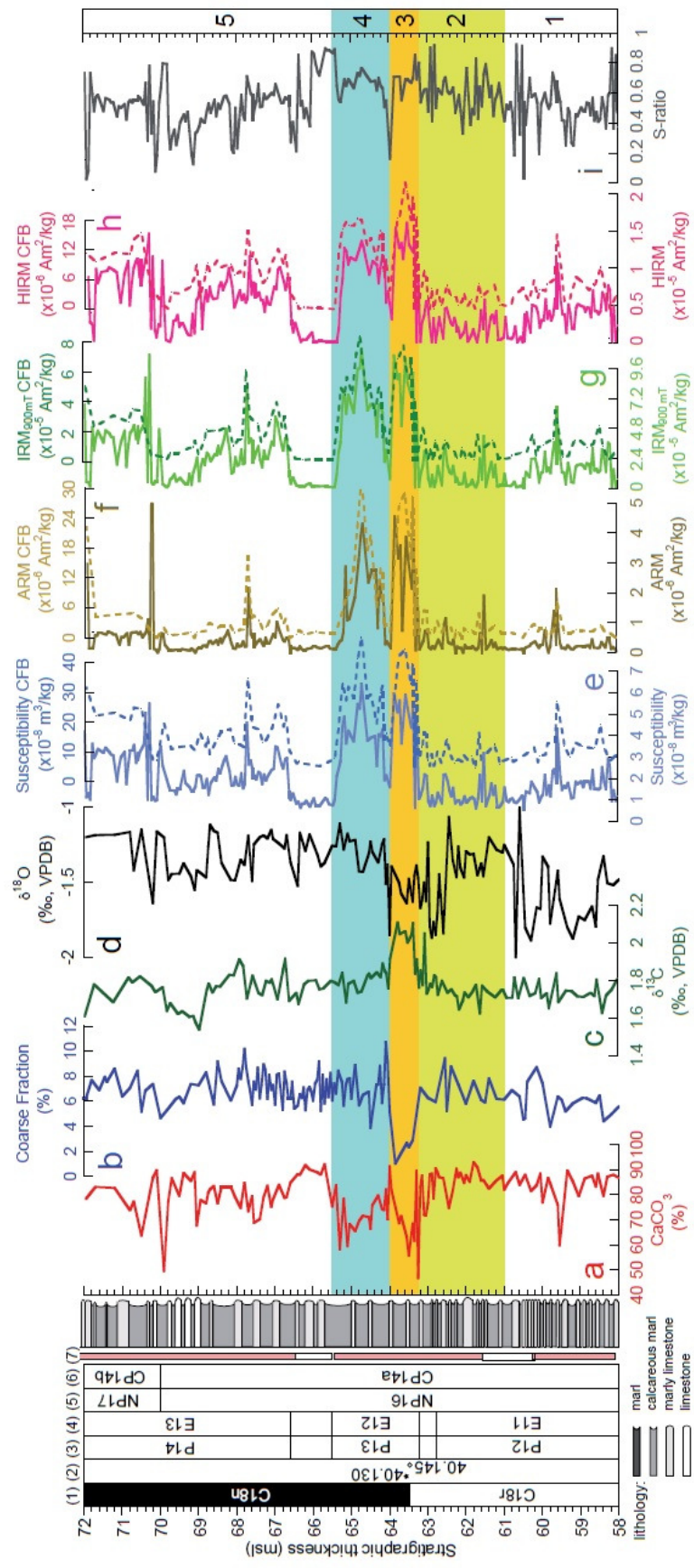
Figure 4.2. *Changes in CaCO₃ content, coarse fraction, δ¹³C and δ¹⁸O in bulk sediments, low-field magnetic susceptibility (χ), and rock magnetic properties (anhysteretic remanent magnetization, ARM; isothermal remanent magnetization, IRM at 900mT; hard isothermal remanent magnetization, HIRM; S-ratio300) across the 14-m-thick studied MCA section. χ, ARM, IRM900mT, and HIRM300mT were also calculated on a carbonate-free basis (CFB, dashed lines). The magnetobiostratigraphy is from Jovane et al. (2013). Numerical ages (1) are from Cande and Kent (1995) (stars) and Ogg (2012) (diamonds). Biostratigraphy is based on the planktonic foraminiferal Zones of Berggren et al. (1995) (2) and Wade et al. (2011) (3) and calcareous nannoplankton Zones of Martini (1971) (4) and Okada and Bukry (1980) (5). The areas shaded in yellow, orange and green highlight the Intervals (2-4) that represent the MECO, MECO warming peak and the post-MECO periods.*

4.3. Material and methods

Two-hundred-sixty-five bulk rock samples were collected at ~5 cm stratigraphic intervals from the MCA section, corresponding to a temporal spacing of ~6 kyr between samples. High-resolution calcium carbonate, stable isotopic, rock magnetic and micropaleontological analyses were performed. Carbonate contents were measured at the National Oceanography Centre, Southampton (NOCS). One hundred-twenty-five bulk rock samples were reduced to fine powder in an agate mortar and their CaCO₃ content was obtained using a Dietrich-Frühling calcimeter that measures the CO_2 volume produced by complete dissolution of pre-weighed samples (300±1 mg each) in 10% vol. HCl. Total carbonate contents (wt.% CaCO₃) were computed with a precision of 1% taking into account pressure and temperature of the laboratory environment, the amount of bulk sample used, and the volume of CO_2 in the calcimeter. Standards of pure calcium carbonate (e.g. Carrara Marble) were measured every ten samples to ensure proper calibration. For coarse-fraction analyses, weighed freeze-dried samples were soaked in deionized distilled water, and were washed through 63 μm sieves. The >63 μm fraction residue was collected, dried, and weighed. The coarse fraction is defined as the weight percent ratio of the >63 μm size fraction to the weight of the bulk sample (~100 g for each sample) (Broecker and Clark, 1999, 2001). This index has been largely used as an indicator of carbonate dissolution (e.g. Hancock and

Dickens, 2005; Colosimo et al., 2006; Leon-Rodriguez and Dickens, 2010; Luciani et al., 2010).

Oxygen and carbon isotope analyses were conducted using VG Optima and VG Prism dual-inlet isotope ratio mass spectrometers at NOCS. One-hundred-twenty-five samples were reacted in a common acid bath at 90°C using an automated carbonate preparation system with a carousel device. NBS-19, Atlantis II, and an in-house Carrara Marble standard were included in all sample runs. All values are reported in standard delta notation (δ) in parts per mil (‰) relative to VPDB (Vienna Pee Dee Belemnite), and analytical precision is estimated at 0.06‰ (1σ) for $\delta^{13}C$ and 0.08‰ (1σ) for $\delta^{18}O$.

Paleomagnetic and environmental magnetism measurements were carried out at NOCS and at the University of São Paulo (USP). The magnetic remanence of 253 unoriented block samples (5-cm resolution) was measured using a three-axis 2-G Enterprises cryogenic magnetometer (model 755R), housed in a magnetically shielded room at NOCS. Low-field magnetic susceptibility (χ) was measured with a Kappabridge KLY-3 (AGICO) magnetic susceptibility meter. All data were normalized by mass, due to the irregular sample volumes. An anhysteretic remanent magnetization (ARM) was imparted in a 100 mT alternating field (AF) with a direct current bias field of 0.05 mT. An isothermal remanent magnetization (IRM) was imparted in a direct field of 900 mT (IRM_{900mT}) and was demagnetized in backfields of 100 mT ($-IRM_{100mT}$) and 300 mT ($-IRM_{300mT}$). From these measurements, we calculated the S-ratio ($S_{300mT} = [-IRM_{300mT}/IRM_{900mT}]$) and "hard" isothermal remanent magnetization ($HIRM_{300mT} = [IRM_{900mT}+IRM_{300mT}]/2$), in order to investigate the coercivity of magnetic minerals. Hysteresis loops and first-order reversal curve (FORC) diagrams were analysed for eight samples from the MCA section spanning the MECO interval and from immediately before and after the warming event. Measurements were performed in a Princeton Measurements Corporation vibrating sample magnetometer (MicroMag) at NOCS. FORCs were measured with an averaging time of 200 ms, a smoothing factor (SF) of 4, and using the input parameters of Egli et al. (2010) (H_{c1} = 0 mT, H_{c2} = 110 mT; H_{u1} = -15 mT, H_{u2} = +15 mT; δH = 0.63 mT). FORC diagrams were produced using the MATLAB routine of Egli et al. (2010). Magnetic mineralogy was further investigated at USP for selected samples through acquisition of an IRM and measurement of thermomagnetic curves. IRM acquisition curves were obtained for six samples with a 2-G Enterprises pulse magnetizer and a cryogenic

magnetometer (model 755UC). IRM acquisition curves were analyzed with cumulative log-Gaussian functions (CLG) using the software of Kruiver et al. (2001). The CLG function is described by three parameters (SIRM, $B_{1/2}$ and dispersion parameter, DP) that characterize magnetic minerals (Robertson and France, 1994; Kruiver et al., 2001). Thermomagnetic curves up to 700 °C were obtained using a KLY-4S AGICO magnetic susceptibility meter with high-temperature attachment at USP to determine the Curie or Néel temperatures of magnetic minerals.

Al, Ba, Cr, Co, Fe, Mo, Ni and V contents were determined for twenty-two samples along the MCA section. Around 30 mg of sample powder was weighed and digested in a Teflon pump adding initially 5 mL of HNO3, and then 2 mL of HF and 2 mL of H_2O_2. The procedure was carried out in a microwave oven. Samples were then heated to evaporate HF. After HF evaporation, 10 mL of 5% HNO_3 was added. Finally, the sample was diluted to reach 30 mL and Al, Ba, Cr, Co, Fe, Mo, Ni and V were analysed with inductively coupled plasma optical emission spectrometry (ICP-OES) at USP.

For calcareous nannofossil analyses, samples were prepared from unprocessed material as simple smear slides using standard preparation methods (Bown and Young, 1998) at the Istituto di Geoscienze e Georisorse CNR di Pisa, Italy. Smear slides were studied under a Leitz Laborlux 12 Pol light microscope both under crossed nicols and transmitted light at a magnification of 1250x. Most nannoplankton species were identified according to the taxonomy of Perch-Nielsen (1985) except for sphenoliths and Dictyococcites that were classified following Fornaciari et al. (2010) and *Reticulofenestra umbilicus* that was defined following the taxonomic criteria adopted in Backman and Hermelin (1986), ascribing to this species all specimens >14 mm and lumping as *Reticulofenestra spp*. all the specimens <14 mm. Assemblages were studied following quantitative counting methods based on at least 300 specimens. Following Toffanin et al. (2011), the relative abundances of species belonging to the *genus Sphenolithus* were determined by counting 100 specimens. Rare taxa, such as the *genus Helicosphaera* and species belonging to the *genus Chiasmolithus* were counted in a prefixed area of 10 mm^2 (three-four transects). The standard calcareous nannofossil zonations of Martini (1971) and Okada and Bukry (1980) are widely used for low- and middle latitude Eocene-Oligocene (E-O) biostratigraphic studies, and were adopted in this paper. In order to infer probable temperature and trophic variations of surface waters, most calcareous

nannofossils were, whenever possible, allocated into groups of environmental affinities, largely following Haq and Lohman (1976), Aubry (1992), Gardin and Monechi (1998), Bralower (2002), Tremolada and Bralower (2004), Persico and Villa (2004), Gibbs et al. (2006), Villa et al. (2008), Raffi et al. (2009) and Agnini et al. (2011). Thus, according to this literature, the following environmental groups have been used: eutrophic taxa (*Dictyococcites bisectus*, *D. scrippsae*, *Reticulofenestra daviesi*), and oligotrophic taxa (*Cribrocentrum reticulatum*, *Ericsonia spp.*, *Sphenolithus spp.*, *Zygrablithus bijugatus*).

For foraminiferal analyses, samples were treated at the Università degli Studi di Urbino, following the cold acetolyse technique of Lirer (2000) by sieving through a 63 μm mesh and drying at 50 °C. The cold acetolysis method enabled extraction of generally easily identifiable foraminifera even from indurated limestones. This technique offered the possibility of accurate taxonomic determination and detailed foraminiferal assemblage analysis. For planktonic foraminifera, all samples were studied for biostratigraphy and quantitative analysis was performed on a subset of 101 samples. The residues were studied with a binocular microscope to characterize assemblages and to identify biostratigraphic marker species. A representative split of at least 300 specimens was picked from the >63 μm fraction, mounted on micro-slides for permanent record and identification purposes, and classified following the taxonomic criteria of Berggren and Pearson (2005). The planktonic foraminiferal zonations of Berggren et al. (1995) and Wade et al. (2011) were followed. Following Hancock and Dickens (2005), the fragmentation index (FI) was calculated using at least 300 specimens and including the whole test, fragments and dissolved tests to estimate carbonate dissolution effects. For benthic fornaminifera, a quantitative study of sixty-four selected samples was performed. A representative split of the >90 μm fraction was used to pick approximately 300 specimens. The sample–split weight used to pick benthic foraminifera was determined so that the foraminiferal density (FD), expressed as the number of foraminifera per gram of dry sediment, could be calculated. The planktonic to planktonic and benthic (P/P+B) ratio, expressed as a percentage, and the percentages of agglutinants were also calculated.

4.4. Results

4.4.1. Micropaleontology

Benthic foraminiferal assemblages are generally diverse and well preserved throughout the studied MCA section, except at 63.2-64.0 msl where evidence of partial dissolution is observed (Figure 4.3). The assemblages are dominated by calcareous-hyaline forms with variable percentages of agglutinants that are more abundant at the base of the section and at 63.2-64 msl (Figure 4.3). The P/(P+B) ratio fluctuates throughout the sequence, with the lowest values at 63.2-64 msl where both the highest FD value of and percentage fragmentation are documented (Figure 4.3). The 63.2-65.5 msl interval is therefore characterized by pronounced paleoecological and paleoenvironmental changes. The increase of benthic to planktonic foraminifera and of agglutinated forms that are less prone to dissolution might reflect shallowing of the lysocline. In addition, increased FD values might suggest greater nutrient availability at the seafloor probably related to increased detrital mineral influx associated to with intensified hydrological and weathering cycles.
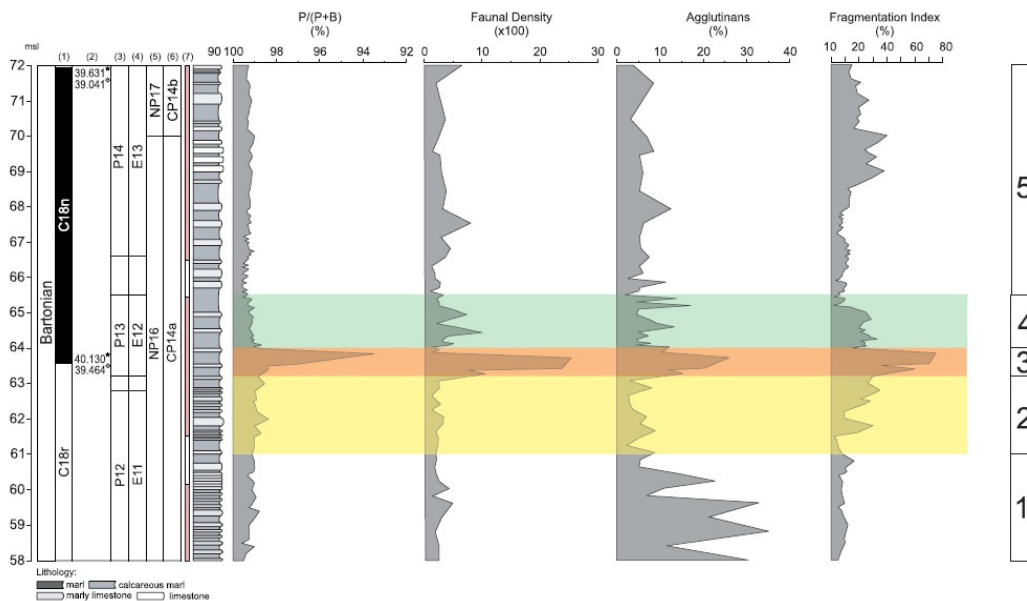
Figure 4.3. *Changes in selected benthic and planktonic foraminiferal parameters [P/(P+B) ratio, foraminiferal density (FD), agglutinans vs. calcareous ratio, and fragmentation index across the studied segment at MCA. Magnetobiochronostratigraphy and shaded areas as in Figure 4.2.*

4.4.2. Stable isotopes

Bulk $\delta^{13}C$ and $\delta^{18}O$ values average 1.8‰ and -1.4‰, respectively, through the studied MCA (Figures 4.2c, d). $\delta^{13}C$ has background values of ~1.8‰ and is characterized by an increase from ~1.6 to 2.1‰ at 63.2-65.5 msl (~40.20-40.06 Ma), with a peak value of 2.1‰ at 63.35 msl (~40.1 Ma) (Figure 4.2c). The peak value is followed by a smoothly decreasing trend up to 66.34 msl (~39.8 Ma). Bulk $\delta^{18}O$ varies from -0.2‰ to -3.3‰ and is noisy (Figure 4.2d). Similarly noisy $\delta^{18}O$ in the correlative Contessa Highway section (CHW) was interpreted as resulting from burial diagenesis and/or meteoric water diagenesis (Jovane et al., 2007a). It is well known that bulk carbonate $\delta^{13}C$ is more robust to diagenesis than $\delta^{18}O$ because the carbon content of fluids and fluid/rock ratios is often too low compared to that of carbonate rocks to modify significantly their carbon isotopic composition (e.g. Veizer and Hoefs, 1976).

4.4.3. Environmental magnetism

Low-field magnetic susceptibility (χ) along the studied MCA section varies between 0.57×10^{-8} and 6.42×10^{-8} m^3/kg (Figure 4.2e), whereas CaCO$_3$ contents vary between 47% and 93% (Figure 4.2a). Two narrow intervals (63.30-63.90 msl and 64.15-65.30 msl) have lower CaCO$_3$ contents and higher χ values (Figures 4.2a, e). CaCO$_3$ and χ have a significant negative correlation (r = -0.72; i.e. lower CaCO$_3$ is related to higher χ values, which correspond to peak abundances of paramagnetic (e.g. clays) and ferrimagnetic minerals). To account for dilution effects by the carbonate matrix, we calculated magnetic parameters (χ, ARM, IRM$_{900mT}$ and HIRM$_{300mT}$) on a carbonate-free basis (CFB, dashed lines in Figures 4.2e-h). To achieve this, we normalized the magnetic parameters by (100 wt.% CaCO$_3$). All magnetic parameters that depend on the concentration of ferrimagnetic minerals are well correlated before and after this normalization (Figures 4.2e-h). For example, the ARM and ARM CFB, IRM$_{900mT}$ and IRM$_{900mT}$ CFB, and HIRM$_{300mT}$ and HIRM$_{300mT}$ CFB have pronounced peaks at 63.30-63.90 msl and 64.15-65.30 msl, as mentioned above.

The relative concentration of different magnetic minerals across the studied interval can be inferred from the S-ratio$_{300mT}$ and HIRM$_{300mT}$ (Bloemendal et al., 1992; Liu et al., 2007). The large IRM$_{300mT}$ and S-ratio$_{300mT}$ fluctuations indicate variable proportions of low and high-coercivity magnetic minerals, i.e. magnetite (predominant when S-ratio is near 1) and hematite (present in significant concentrations when HIRM is high and S-ratio is close to 0). The presence of mixtures of magnetic minerals with contrasting coercivities is corroborated by stepwise IRM acquisition curves. IRM acquisition curves were measured at fields up to 1 T for six representative samples along the MCA section (Figure 4.4a; Table 4.1) and components due to different magnetic minerals were fitted using CLG functions (Figures 4.4b-d) (Kruiver et al., 2001; Heslop et al., 2002). Three magnetic components were identified (Table 1). They correspond to a low-coercivity component (B$_{1/2}$ = 16 mT, DP = 0.40-0.45), a medium-coercivity component (B$_{1/2}$ = 50-70 mT, DP = 0.30-0.40) and a high-coercivity component (B$_{1/2}$ = 250-479 mT, DP = 0.24-0.30), similar to those found by Roberts et al. (2011, 2012) for pelagic sediments. The low-coercivity component varies from 5% to 17% for samples collected inside the magnetic mineral concentration peaks. These samples also have a predominant medium-coercivity component. Outside the peaks (samples 67.55 and 68.60 msl), IRM acquisition curves can be fitted without the low-coercivity component, which suggests that this component has negligible concentrations at these stratigraphic levels. In these samples, the high-coercivity component can reach up to 82% of the total IRM. χ-T curves indicate that magnetite is the dominant magnetic mineral (Figure 4.5).
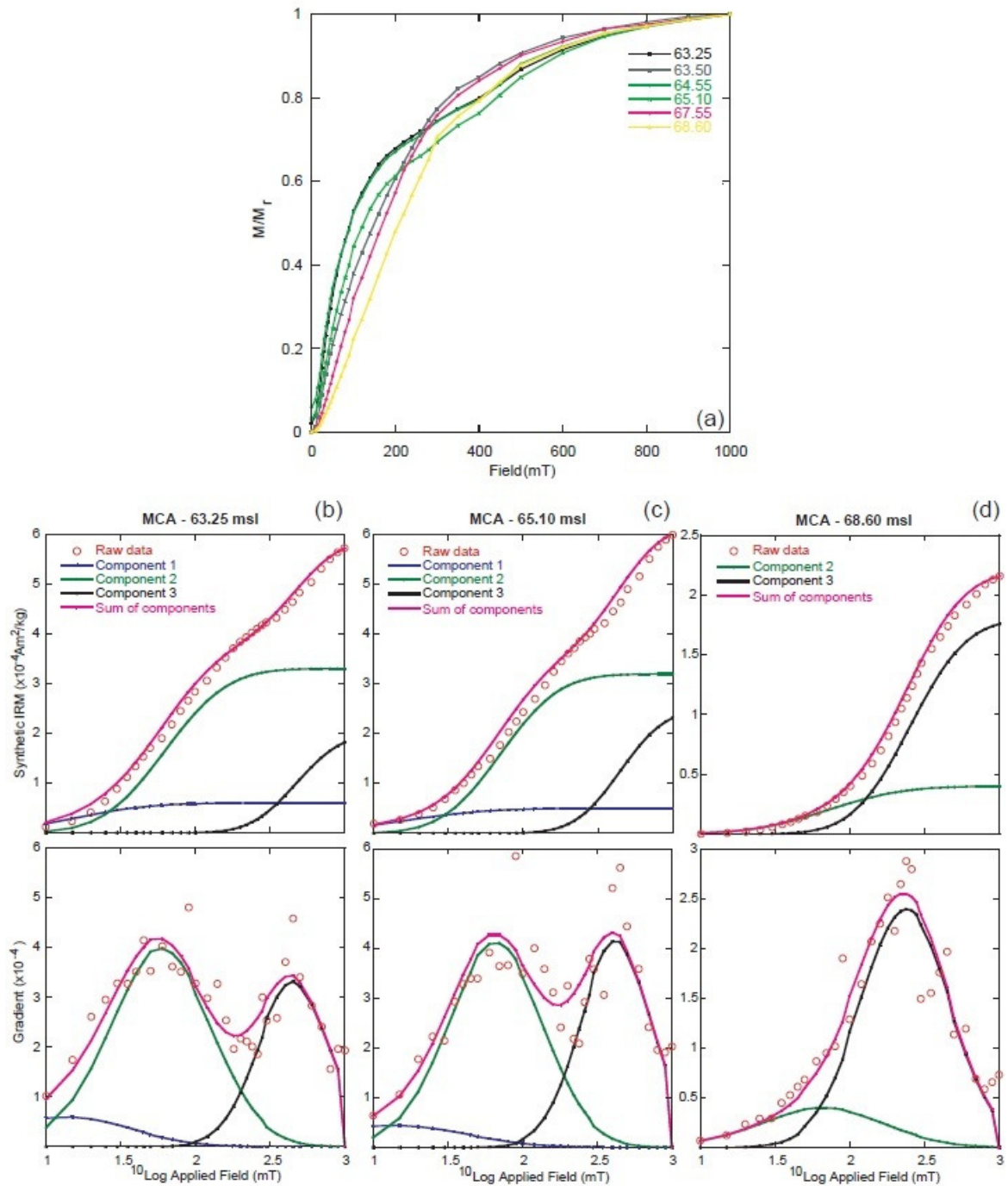
Figure 4.4*. (a) IRM acquisition curves for six representative samples from the MCA section. (b-d) IRM unmixing analyses (Kruiver et al., 2001; Heslop et al., 2002) for three representative samples; (b) and (c) represent samples collected inside the magnetic mineral concentration peaks and (d) from outside the peaks. Raw data (circles) and calculated IRM acquisition curves are shown for two and three fitted components after fitting of a spline function.*

Sample	Component 1	Component 2	Component 3	Component 1	Component 2	Component 3
	SIRM (Am^2/kg)	SIRM (Am^2/kg)	SIRM (Am^2/kg)	Contribution (%)	Contribution (%)	Contribution (%)
MCA-63.25	6.00E-05	3.30E-04	2.00E-04	10	56	34
MCA-63.50	3.00E-05	2.00E-04	4.20E-04	5	31	65
MCA-64.55	1.20E-04	3.20E-04	2.50E-04	17	46	36
MCA-65.10	5.00E-05	3.20E-04	2.50E-04	8	52	40
MCA-67.55	NA	1.40E-04	2.40E-04	NA	37	63
MCA-68.60	NA	4.00E-05	1.80E-04	NA	18	82
	$B_{1/2}$ (mT)	$B_{1/2}$ (mT)	$B_{1/2}$ (mT)	Contribution (%)	Contribution (%)	Contribution (%)
MCA-63.25	15.8	63.1	478.6	10	56	34
MCA-63.50	15.8	50.1	251.2	5	31	65
MCA-64.55	15.8	63.1	446.7	17	46	36
MCA-65.10	15.8	70.8	446.7	8	52	40
MCA-67.55	NA	70.8	239.9	NA	37	63
MCA-68.60	NA	70.8	251.12	NA	18	82
	DP $(\log_{10} mT)$	DP $(\log_{10} mT)$	DP $(\log_{10} mT)$	Contribution (%)	Contribution (%)	Contribution (%)
MCA-63.25	0.40	0.33	0.24	10	56	34
MCA-63.50	0.40	0.30	0.30	5	31	65
MCA-64.55	0.45	0.34	0.24	17	46	36
MCA-65.10	0.45	0.31	0.24	8	52	40
MCA-67.55	NA	0.40	0.30	NA	37	63
MCA-68.60	NA	0.40	0.30	NA	18	82

Table 4.1. *Parameters associated with components identified from IRM analysis of the six representative samples from Monte Cagnero section.*
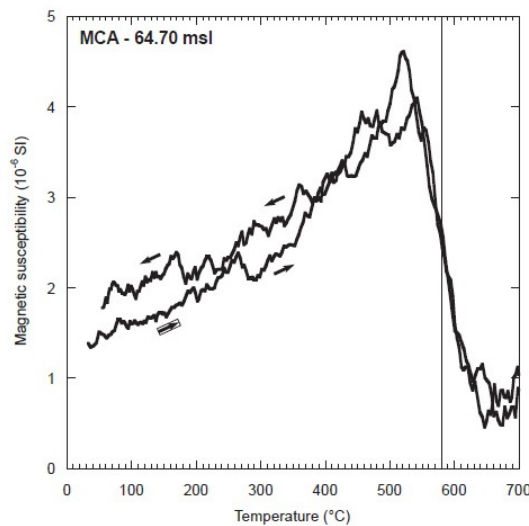
Figure 4.5. *Thermomagnetic curve for a representative sample from 64.70 msl. This sample contains magnetite as dominant magnetic carrier (sharp decline in susceptibility to approximately 580 °C). The susceptibility during the cooling cycle was not thermal altered during heating.*

Hysteresis data (Figure 4.6; Table 4.2), including the ratio of saturation remanence to saturation magnetization (Mr/Ms) and the coercivity of remanence to coercive force (Hcr/Hc), from MCA samples lie within the pseudo-single domain (PSD) field of Day et al. (1977). The presence of high-coercivity hematite mixed with lower coercivity fine-grained magnetite does not affect significantly the Day plot because SD hematite has similar hysteresis ratios to those of SD magnetite (Dunlop, 2002). The significant departure of bulk hysteresis parameters from values expected for uniaxial SD magnetite for both the MCA and CHW samples (Figure 4.6) can be related to significant admixtures of non-SD detrital magnetite grains (superparamagnetic, PSD and multi-domain grains) in the studied samples (Dunlop, 2002; Roberts et al., 2012) as suggested by the IRM acquisition curves.
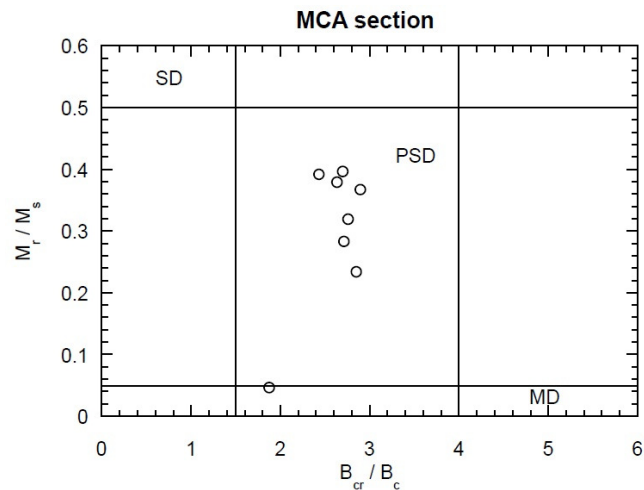
Figure 4.6. Day plot diagram (Day et al., 1977) for nine representative samples from MCA section. The data fields represented in the diagram Mr/Ms versus Bcr/Bc is subdivided in single domain (SD), pseudo-single domain (PSD) and multi domain (MD) titanomagnetite particles.

Sample ID	Depth (msl)	M_r (Am²/kg)	M_s (Am²/kg)	M_r/M_s	B_c (mT)	B_{cr} (mT)	B_{cr}/B_c
MCA-58.15	58.15	18.61E-09	44.89E-09	0.41	28.65E-03	287.27E-03	10.00
MCA-64.55	64.55	394.32E-09	1.03E-06	0.37	27.47E-03	72.34E-03	2.63
MCA-63.25	63.25	428.86E-09	1.83E-06	0.23	20.02E-03	57.05E-03	2.85
MCA-64.90	64.90	497.47E-09	1.26E-06	0.39	30.42E-03	73.96E-03	2.43
MCA-63.50	63.50	741.31E-09	2.01E-06	0.36	29.24E-03	84.64E-03	2.89
MCA-65.10	65.10	545.76E-09	1.70E-06	0.31	28.79E-03	79.39E-03	2.76
MCA-63.85	63.85	768.56E-09	2.70E-06	0.28	22.17E-03	60.15E-03	2.71
MCA-66.30	66.30	46.93E-09	997.2E-09	0.04	5.04E-03	9.45E-03	1.87
MCA-64.50	64.50	429.7E-09	1.08E-06	0.39	33.79E-03	91.15E-03	2.70

Table 4.2. Measured hysteresis parameters for the studied sediments from MCA and CHW sections.

FORC diagrams provide detailed information about magnetic interactions and microcoercivity distributions (Roberts et al., 2000). High-resolution FORC measurements following the specifications of Egli et al. (2010) can be used to detect the presence of biogenic magnetite (e.g. Egli et al., 2010, Roberts et al., 2011, 2012; Jovane et al., 2012; Larrasoaña et al., 2012). FORC distributions are nearly identical in the high-magnetization intervals between 63.2 and 65.5 msl (Figures 4.2, 4.7). These FORC diagrams have a sharp horizontal ridge (Figure 4.7) that indicate negligible magnetic interactions and a dominance of non-interacting SD particles (Roberts et al., 2000) that is characteristic of intact magnetosome chains (Egli et al., 2010; Roberts et al., 2011, 2012; Jovane et al., 2012; Larrasoaña et al., 2012). The coercivity distribution has a broad peak between 3 and 21 mT, with a maximum at 10 mT (Figure 4.7) that falls within the range expected for magnetite magnetosomes (Egli, 2004; Egli et al., 2010; Kopp and Kirschvink, 2008). The weaker signal in the outer parts of the FORC diagrams is indicative of minor but variable contributions from coarser-grained magnetic particles (Roberts et al., 2000). FORC diagrams from samples below 61 msl and above 65.5 msl have contrasting behaviour, with weak magnetizations and no measurable FORC distributions (Figures 4.7a, h).

To compare our results to those from a nearby section, we also performed FORC analyses on samples from the MECO interval at the Contessa Highway (CHW) section between 135 and 139 msl as defined by Jovane et al. (2007a). This interval is characterized a peak in magnetic concentration dependent parameters (e.g. χ, ARM, IRM). A horizontal ridge

due to non-interacting SD magnetite with coercivities between 10 and 50 mT is also evident in these samples (Figure 4.7i).
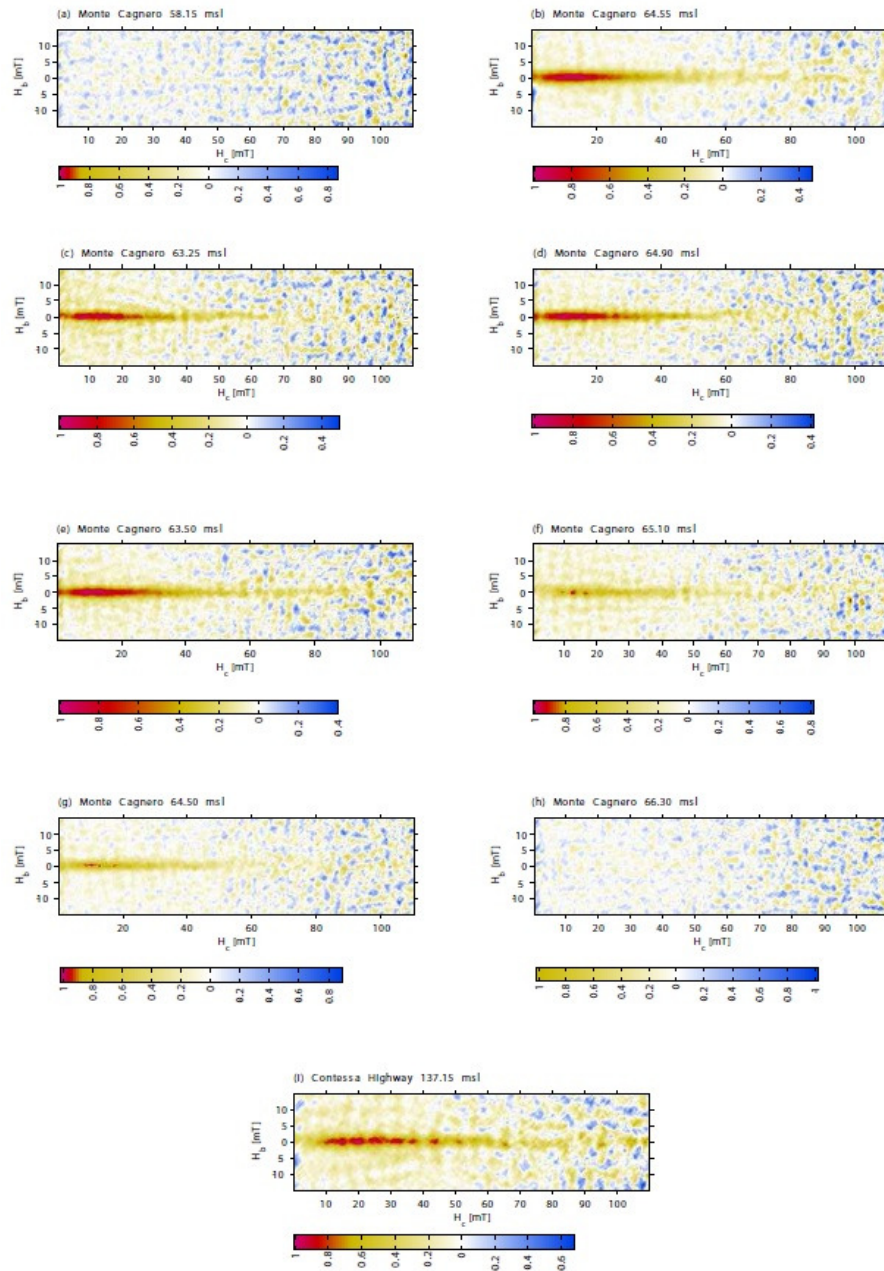
Figure 4.7. *FORC diagrams for nine MCA samples ("inside" and "outside" the MECO event) and one sample from Contessa Highway (during the MECO event). The FORC diagrams shows sharp ridge which indicative of non-interacting SD particles (Roberts et al., 2000) during the MECO climax event in Monte Cagnero and Contessa Highway. Samples 58.15 and 66.30 did not show the same behavior. The sharpness of the ridges during the MECO event indicates the presence of magnetofossils (Egli et al., 2010).*

4.4.4. Geochemistry

Elemental abundances of Al, Ba, Fe, Co, Ni, Cr, Mo, and V were measured to assess paleoredox/paleoxygenation conditions, source variations of terrigenous materials, paleoproductivity patterns and possible anomalies related to biotite-rich volcanic ashes in the studied pelagic carbonates. Elemental ratios, including Ba/Al, Fe/Al, Co/Al, Ni/Al, V/Cr, Ni/Co, Mo/Cr, Cr/Al, V/Al, and V/(V+Ni), are shown in Figure 4.8. Ba, Cd, Mo, Sr, Ba/Al and Al/Ti have been proposed as proxies for oceanic primary productivity (Moreno et al., 2002; Pattan et al., 2003; Wei et al., 2003). Trace element indices such as Ni/Co, V/Cr and V/(V+Ni) are widely used to evaluate paleoredox/ paleoxygenation conditions (Rimmer et al., 2004). Jones and Manning (1994) suggested that Ni/Co ratios <5 are indicative of oxic conditions, while values of 5–7 indicate dysoxic conditions, and values >7 are indicative of suboxic to anoxic conditions. Hatch and Leventhal (1992) compared V/(V + Ni) ratios to other geochemical redox indicators, including degree of pyritization, and suggested that ratios greater than 0.84 are indicative of euxinic conditions, while values of 0.54-0.82 are representative of anoxic waters, and values of 0.46-0.60 indicate dysoxic conditions. In the MCA section, these indices point to dysoxic conditions between 61 and 65.5 msl (Figure 4.8).
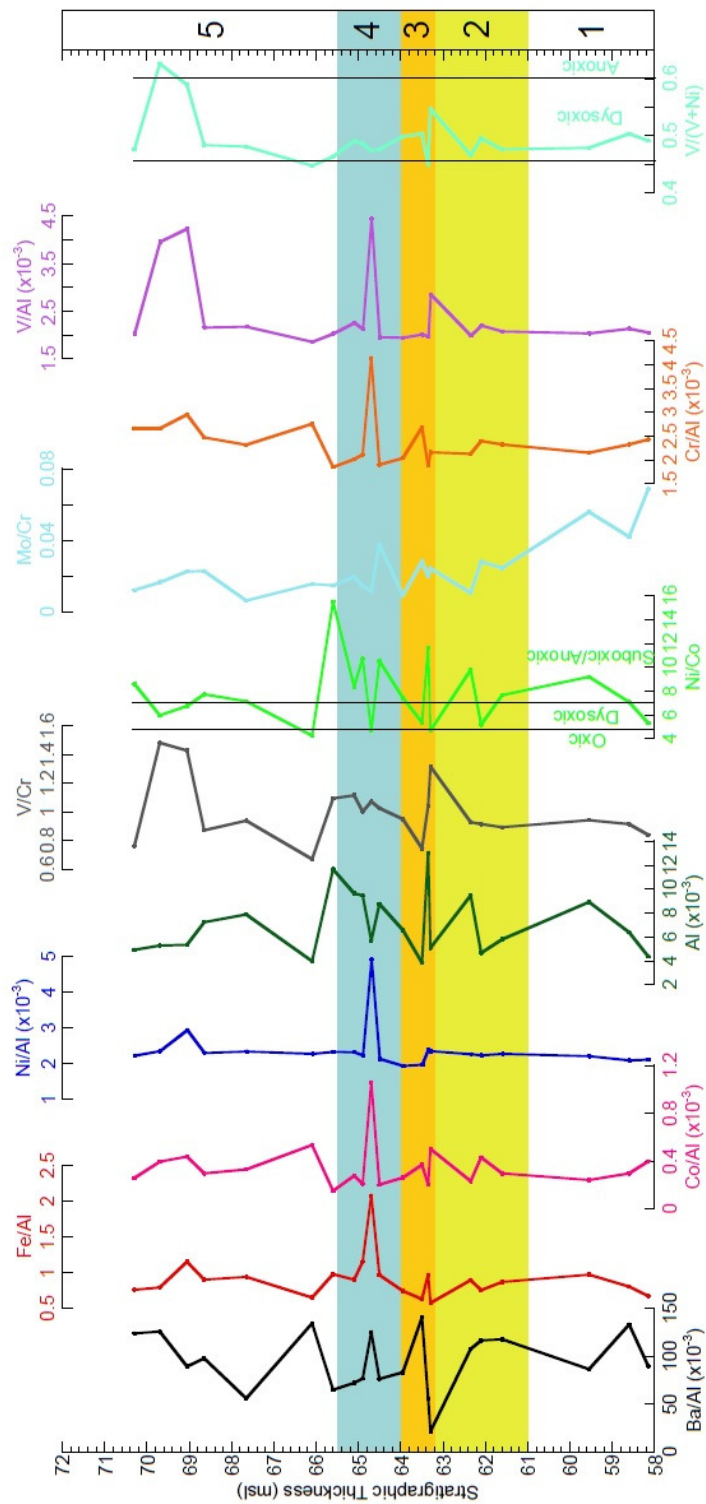
Figure 4.8. *Stratigraphical log plotted against selected trace elements and ratios. Magnetobiochronostratigraphy and shaded areas as in Figure 4.2.*

81

4.5. Discussion

4.5.1. The MECO event in the Neo-tethys

Benthic and planktonic foraminiferal and calcareous nannofossil assemblages in the MCA section across the Chron C18r/C18n boundary are affected by important faunal turnovers. Together with rock magnetic, geochemical and stable isotope data, they enable subdivision of the studied 14-m-thick section into five discrete intervals (Figures 4.2, 4.3, 4.8, 4.9): Interval 1 (58-61 m, ~370 kyr), Interval 2 (61-63.2 m, ~250 kyr), Interval 3 (63.2-64 m, ~70 kyr), Interval 4 (64-65.5 m, ~200 kyr) and Interval 5 (65.5-72 m, ~780 kyr). Following Bohaty et al. (2009), the total duration of the MECO event is estimated to be ~500 kyr with a peak warming at the end of the event. During the warming peak, a shoaling of the CCD by up to 500-1500 m has been reported in the Pacific, Atlantic and Indian oceans where a total loss of carbonate is reported at sites with paleodepths below ~3000 m (Bohaty et al., 2009; Pälike et al., 2012). Interval 3 of the MCA section is characterized by the lowest $CaCO_3$ contents in the studied section and the highest bulk carbonate $\delta^{13}C$ values. It also has the lowest concentrations of the coarsest foraminiferal fraction, which is used as a proxy for carbonate dissolution (e.g. Hancock and Dickens, 2005; Colosimo et al., 2006; Leon-Rodriguez and Dickens, 2010; Luciani et al., 2010). Dissolution during this interval is also supported by increased values of the planktonic foraminiferal fragmentation index, greater relative abundances of agglutinated foraminifera that are less prone to dissolution, and a clear decrease of the P/P+B ratio (Figure 4.3). In contrast, there is no evidence for carbonate dissolution upsection in Intervals 4 and 5. Interval 3 falls within the lowermost part of Chron C18n, therefore it can be magnetostratigraphically correlated with peak MECO warming in marine sediment cores (Bohaty et al., 2009), and in the Tethyan CHW (Jovane et al., 2007a) and Alano sections (Luciani et al., 2010; Spofforth et al., 2010; Toffanin et al., 2011). Thus, observed changes in paleoenvironmental proxies provide clues that point to seafloor $CaCO_3$ dissolution and lysocline shallowing at the MCA site during the MECO warming. Interval 3 is immediately followed by an interval with lower $CaCO_3$ contents associated with higher magnetic susceptibility values. On the basis of available magnetobiostratigraphic results, Interval 4 correlates well with the organic-rich ORG1 unit identified at the Alano section (Spofforth et al., 2010; Luciani et al., 2010). These organic-rich layers are thought to

represent rapid organic carbon burial events at the end of the MECO event, probably induced by enhanced delivery of terrestrial material to the ocean (Spofforth et al., 2010).
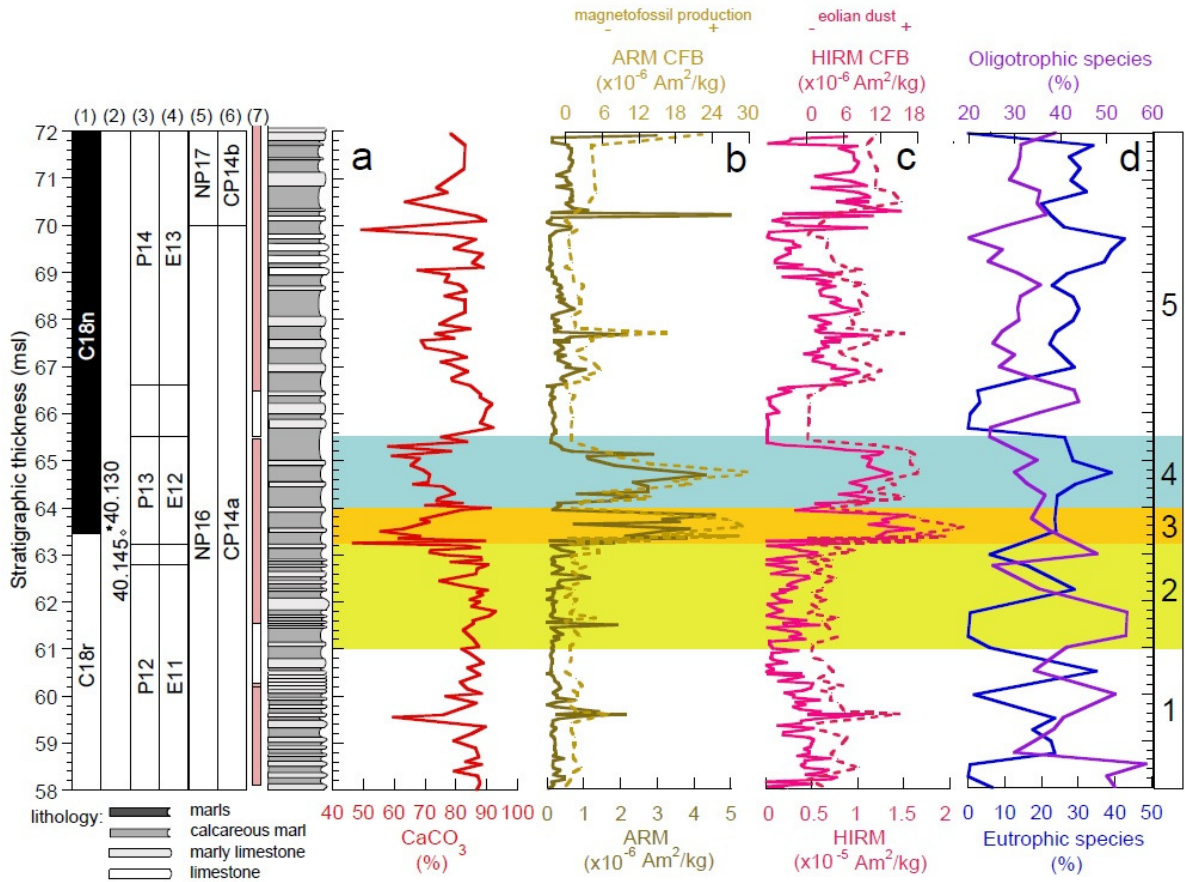
Figure 4.9. *Productivity proxies based on selected calcareous nannofossil genera and magnetic parameters from the MCA section. (a) CaCO₃, (b) ARM, and ARM CFB, (c) HIRM and HIRM CFB, and (d) eutrophic and oligotrophic nannofossil taxa. The increase in eutrophic taxa coincides with an increase in ARM and HIRM during the MECO interval. These results suggest an increase in iron fertilization and high primary productivity during MECO. Magnetobiochronostratigraphy and shaded areas are as in Figure 4.2.*

4.5.2. Ocean iron fertilization and magnetotactic bacterial abundance during the MECO event

Detrital magnetic minerals can be delivered to the deep sea through different transportation pathways, including ice-rafting, mass flows, hemipelagic sediment plumes or wind (e.g. Evans and Heller, 2003). Fine-grained terrigenous inputs that reached the deep, carbonate-dominated MCA site were most likely transported by suspended plumes or wind. Both processes result in similar grain-size distributions and mineralogy (Rea, 1994). Hemipelagic sediment has been reported in modern environments as far as 500 km from the coast, with values in excess of 900 km suspected (Rea, 1994 and references therein). Such distances are within the expected range of the MCA section from the paleoshoreline of the Neo-Tethys. Nevertheless, processes that control hemipelagic and aeolian inputs to the deep sea tend to be out of phase; wet conditions (and enhanced runoff) in the source region would favor hemipelagic fluxes, whereas drier source region climates would enhance aeolian dust fluxes. Enhanced aeolian supply relative to detrital fluxes into the Neo-Tethys has been reported on the southern Tethyan margin (central Egypt) as a result of drier, likely more seasonal, climatic conditions during the Paleocene-Eocene Thermal Maximum (PETM) (Schulte et al., 2011). Similar observations have been made for the PETM in the Bighorn Basin, Wyoming (Wing et al., 2005; Kraus and Riggins, 2007; Smith et al., 2009), East Africa (Handley et al., 2012) and the southern Kerguelen Plateau, Indian Ocean, on the Antarctic margin (Larrasoaña et al., 2012).

Environmental magnetic parameters can serve as sensitive aeolian dust proxies, given the high abundance of hematite that forms in oxidizing, dehydrating desert environments (Larrasoaña et al., 2003; Liu et al., 2012 and references therein). Hematite concentrations can be easily tracked using the "hard" IRM on a carbonate free basis ($HIRM_{900mT}$ CFB). In the MCA section, $HIRM_{900mT}$ CFB has two pronounced peaks in Intervals 3 and 4 (Figure 4.9c), which coincide with the MECO peak warming and the post-MECO recovery. We interpret the increased hematite concentrations in Intervals 3 and 4 to be related to the presence of an enhanced aeolian dust component similar to scenarios proposed for other Eocene sites (Roberts et al., 2011; Larrasoaña et al., 2012).

Aeolian dust is a potential source for iron fertilization of the ocean (Maher et al., 2010; Roberts et al., 2011; Larrasoaña et al., 2012; Liu et al., 2012). Roberts et al. (2011) reported enhanced iron supply by aeolian dust in Eocene sediments (ODP Hole 738B) of the southern Kerguelen Plateau (Indian Ocean), where a marked increase in hematite concentrations

coincided with a switch from oligotrophic to eutrophic conditions. The interval with higher hematite concentrations is also coincident with increased magnetofossil abundances. Roberts et al. (2011) argued that iron input and increased organic carbon delivery to the seafloor were the main factors that controlled the abundance of magnetotactic bacterial populations. Likewise, in the MCA section the magnetic proxies classically used to trace low-coercivity magnetite (ARM CFB) and high-coercivity hematite ($HIRM_{900mT}$ CFB) co-vary, which indicates a concomitant increase in concentration of both magnetic minerals in Intervals 3 and 4 (Figs. 4.2 and 4.9b, c). A significant fraction of the magnetite in these intervals is due to magnetofossils as recorded by FORC signatures that are typical of non-interacting SD magnetite (Figure 4.7). The same intervals are characterized by a marked increase in eutrophic calcareous nannofossil taxa (Figure 4.9d). Thus, in the pelagic setting of the MCA section, phytoplankton productivity was likely stimulated by sea surface iron fertilization produced by addition of iron-rich aeolian dust to surface waters. This promoted enhanced organic carbon export to deeper waters and burial on the seafloor, which stimulated increased magnetotactic biomineralization. The iron needed for biomineralization by magnetotactic bacteria is likely to have been provided by suboxic diagenetic iron reduction that released Fe^{2+} from the most reactive iron-bearing minerals. Thus, simultaneous delivery of enhanced organic carbon, reactive iron-bearing aeolian dust particles and non-reactive aeolian hematite particles to the seafloor would have released the existing limitation on key nutrients (carbon and iron) for an existing, but small, population of magnetotactic bacteria to produce the observed magnetic signatures. In the MCA section, we find no sign of magnetofossils outside Intervals 3 and 4 (Figures 4.7a-h), which suggests that accumulation of magnetite magnetofossils was strongly controlled by delivery of iron and carbon to the seafloor, as suggested by Roberts et al. (2011), in association with the MECO event.

4.6. Conclusion

An integrated high-resolution stable isotope, geochemical, micropaleontological and environmental magnetic analysis has been carried out over a 14-m-thick interval of the Monte Cagnero section (Umbria-Marche Basin), Italy, which corresponds to the 40.79-39.12 Ma period around the Middle Eocene Climatic Optimum (MECO). Magnetic parameters indicate

a concomitant increase of aeolian iron supply in the form of hematite, and a higher abundance of magnetite magnetofossils produced by magnetotactic bacteria as indicated by FORC diagrams that are typical of non-interacting SD magnetite between 63.2 and 65.5 msl. This interval corresponds to peak MECO warming and its aftermath. Intervals with enhanced magnetofossil concentrations correspond to those for which other proxies systematically point to an increase in primary productivity, which was probably stimulated by increased aeolian supply of detrital iron to surface ocean waters. Such a scenario has been recently envisaged for the PETM event (e.g. Chang et al., 2012; Larrasoaña et al., 2012), and we now confirm a similar connection between magnetofossil abundance and paleoproductivity through the MECO event. It reinforces the connection between hyperthermal climatic events and the occurrence (or increased abundance) of magnetofossils. Further work is needed to assess whether the preserved inorganic remains of magnetotactic bacteria can provide a useful paleoproductivity proxy in ancient carbonate sediments.

Chapter 5. An integrated stratigraphic record of the Paleocene-lower Eocene at Gubbio (Italy): new insights into the early Palaeogene hyperthermals and carbon isotope excursions

5.1. Introduction

The long-term warming trend from the Palaeocene through the early Eocene, most likely driven by a multimillion year rise in atmospheric pCO_2 (Zachos et al., 2008), was punctuated by a series of abrupt, but short-lived (<300 ka) episodes of widespread warming. These transient events, termed ''hyperthermals'' (Thomas et al., 2000), are associated with major perturbations in the Earth's carbon cycle, major ecologically controlled biotic turnovers, temporary shoaling of the lysocline and carbonate compensation depth (CCD) inducing carbonate dissolution, and accelerated hydrological cycle (e.g., Kennett and Stott, 1991; Zachos et al., 2001; Bralower et al., 2002; Cramer et al., 2003; Bowen et al., 2006; Sluijs et al., 2007; Quillévéré et al., 2008; Westerhold et al., 2008; and references therein). So far, at least four short episodes of global warming have been recognized in the early Eocene: the largest of hyperthermals, the Palaeocene-Eocene Thermal Maximum (PETM, or ETM1, ~ 55.5 Ma) and three smaller warming events known as the Eocene Thermal Maximum 2 (ETM2 or H1 or Elmo, ~53.7 Ma), the H2 (~53.6 Ma) and the Eocene Thermal Maximum 3 (ETM3 or K or X, ~52.5 Ma) (Kennett and Stott, 1991; Thomas and Zachos, 2000; Bralower et al., 2002; Zachos et al., 2004, 2005, 2010; Lourens et al., 2005; Nicolo et al., 2007; Röhl et al., 2005, 2007; Agnini et al., 2009; Stap et al., 2010a,b; Lunt et al., 2011). Available information, albeit somewhat tentative, suggests that other brief episodes in the early Palaeogene may also be characterized by elevated sea surface temperatures and negative carbon isotope excursions (CIEs), and may be therefore considered suspected hyperthermals (i.e., Thomas and Zachos, 2000; Thomas et al., 2000, 2006; Cramer et al., 2003; Zachos et al., 2004; Röhl et al., 2005; Nicolo et al., 2007; Quillévéré et al., 2008; Coccioni et al., 2010a; Westerhold et al., 2011).

Accordingly, documentation of the early Palaeogene hyperthermals is, as yet, insufficient to assess their exact number, timing, duration and magnitude of warming. In

addition, although previous analysis and astronomical tuning provide compelling evidence of the timing of the hyperthermal series and their relation to orbital changes (e.g., Cramer et al., 2003; Lourens et al., 2005; Westerhold et al., 2007; Zachos et al., 2010), it is not obvious whether they share a common origin. The accurate characterization of the stratigraphic record and chronological framework encompassing the entire series of documented and suspected Palaeocene-early Eocene hyperthermals as well as any CIE, which may be proved to be an hyperthermal, placing them in a proper temporal context of short- and longer-term variations in climate and the carbon cycle is a fundamental prerequisite to ascertain their global distribution and to resolve their origin and causal relationships.

We present a high-resolution, integrated stratigraphic analysis, including biostratigraphy based on calcareous nannofossils and foraminifera, magnetostratigraphy and environmental magnetism, wt.% $CaCO_3$ and bulk carbonate isotope records for the Palaeocene–lower Eocene interval of the reference pelagic succession in Contessa Valley (Gubbio, Italy). With its complete and wellpreserved record, this sedimentary succession of the subtropical–tropical western Tethys Ocean may provide key data to: (1) establish a complete and integrated stratigraphic framework at middle-low latitudes encompassing the Danian–latest Ypresian interval from 6~5.5 to ~49.5 Ma, (2) identify and well constrain the signatures of the Palaeocene–early Eocene documented and suspected hyperthermals, as well as of the CIEs from a magnetobiochronostratigraphic point of view and (3) characterize their features and compare them with those reported for deep-sea cores and other land-based sections to test whether the signature associated with the CIEs documented in Contessa Valley may give evidence for tracing them over wider areas.

5.2. Material and methods

A total of 907 bulk rock samples were collected at ~7 cm intervals corresponding to ~16 ka from the Contessa Highway (CHW) – Contessa Road (CR) composite section.

5.2.1. Mineralogy, geochemistry and environmental magnetism

5.2.1.1. Calcium carbonate

Calcium carbonate analyses were performed on six hundred and ten samples. The bulk rock samples were reduced to fine powder in an agate mortar. Calcium carbonate content measurements were obtained using a Dietrich–Frühling calcimeter. The method is based on the measurement of CO_2 volume produced by the complete dissolution of pre-weighted samples (300 ± 1 mg each) in 10% vol. HCl. Total carbonate contents (wt.% $CaCO_3$) were computed with a precision of 1% using formulae that take into account pressure and temperature of the lab environment, amount of bulk sample used, and the volume of CO_2 developed in the calcimeter. Standards of pure calcium carbonate (i.e., Carrara Marble) were measured every ten samples to ensure proper calibration.

5.2.1.2. Stable isotopes

Stable isotope analyses were conducted on eight hundred and eight bulk samples using an automated continuous−flow carbonate preparation GasBenchII device (Spötl and Vennemann, 2003) and a ThermoElectron Delta Plus XP mass spectrometer in the geochemistry laboratories at the IAMC–CNR Institute of Naples. The acidification of samples was performed at 50 °C. An internal standard (Carrara Marble with $\delta^{18}O=-2.43$ versus Vienna Pee Dee Belemnite [VPDB] and $\delta^{13}C=2.43$ versus VPDB) was run for every six samples and for every thirty samples the NBS19 international standard was measured. Standard deviations of carbon and oxygen isotope measurements were estimated at 0.1‰ and 0.08‰, respectively, on the basis of replicate measurements of 20% of the analyzed samples. All of the stable isotope data are reported in per mil (‰) relative to the VPDB standard. Following Corfield et al. (1991), the Paleogene Scaglia sediments at CHW−CR composite section might be affected by diagenesis, and oxygen isotope values have, therefore, been disregarded.

5.2.1.3. Magnetic susceptibility

A total of eight hundred and thirty-nine samples was used for paleomagnetic analyses in the magnetically shielded laboratory at the Istituto Nazionale di Geofisica e Vulcanologia (INGV), Rome. A range of rock magnetic measurements was used to investigate the magnetic mineralogy throughout the studied section. The low field mass–specific magnetic susceptibility (MS) was measured with a Kappabridge KLY–2 magnetic susceptibility meter.

5.2.1.4. Environmental magnetism

Environmental magnetism was analyzed in eight hundred and twenty-three samples. These analyses were carried out at the National Oceanography Centre Southampton (NOCS), University of Southampton, UK. Artificial remanences were also measured, including the anhysteretic remanent magnetization (ARM) imparted in a 100 mT AF, with a superimposed 0.05 mT direct current (DC) bias field, the isothermal remanent magnetization (IRM) imparted in a field of 0.9 T, and back–field demagnetization of the IRM at 0.1 T and 0.3 T. These data were used to determine the S–ratio ($IRM_{-0.3T}/IRM_{0.9T}$) and the hard isothermal remanent magnetization (HIRM = $[IRM_{0.9T} + IRM_{-0.3T}]/2$). Natural and artificial remanences were measured using a 2G Enterprises automated pass–through cryogenic magnetometer (Model 755) with in–line AF demagnetization capability. Environmental magnetic properties (concentration, composition, and dimension of magnetic grains) were defined by investigating ARM, IRM and, from them, other indirect parameters. ARM magnetically excites only finer magnetic minerals, while IRM excites all of them (concentration). Back–field magnetizations allow us to define HIRM and S–ratio300, which give information about coercivities (composition) of the magnetic minerals.

5.2.1.5. Degree of dissolution

We evaluated the degree of dissolution as follows: 1) low degree: generally good preservation of calcareous plankton and benthic foraminifera; planktonic foraminiferal fragments or partially dissolved tests (including specimens showing notable deterioration, missing chambers and substantial breakage) <10%; low abundance of benthic foraminifera (in particular of agglutinans) or high values of planktonic to benthic (P/B) ratio; negligible coccolith fragmentation and overgrowth 2) medium degree: generally moderate preservation of calcareous plankton and benthic foraminifera; planktonic foraminiferal fragments or partially dissolved tests (including specimens showing notable deterioration, missing chambers and substantial breakage) >10% to 50%; moderate abundance of benthic foraminifera (in particular of agglutinans) or medium values of the P/B ratio; moderate coccolith fragmentation and overgrowth; 3) high degree: generally poor to very poor preservation of calcareous plankton and benthic foraminifera; planktonic foraminiferal fragments or partially dissolved tests (including specimens showing notable deterioration, missing chambers and substantial breakage) >50%; high abundance of benthic foraminifera (in particular of agglutinans) or high values of the P/B ratio; high percentages of coccolith fragments and marked overgrowth and recrystallization.

5.2.2. Biostratigraphy

5.2.2.1. Calcareous nannoplankton

Samples were prepared from unprocessed material as smear slides and were examined using a light microscope at 1250x magnification. The calcareous nannofossil standard zonations of Martini (1971) and Okada and Bukry (1980) were applied making additional reference to the zonations of Romein (1979) and Perch−Nielsen (1985) for the Danian.

5.2.2.2. Foraminifera

Samples were treated following the cold acetolyse technique of Lirer (2000) by sieving through a 32 μm mesh and drying at 50 °C.

5.2.2.3. Planktonic foraminifera

The tropical to subtropical planktonic foraminiferal standard zonations of Berggren and Pearson (2005, 2006) and Wade et al. (2011) were followed with additional reference to the earlier zonation of Berggren et al. (1995).

5.2.2.4. Benthic foraminifera

The benthic foraminiferal zonation of Berggren and Miller (1989) was applied.

5.2.3. Magnetostratigraphy

Magnetostratigraphic data are after Lowrie et al. (1982), Galeotti et al. (2000, 2010). For this work, a highly resolved magnetostratigraphic record was constructed on 16 closely spaced (ca. 35 cm, on average) samples from the lower part of CHW section in order to refine the base of Chron C29n and to identify for the first time Chron C28r in the Contessa Highway section.

Paleomagnetic analyses were carried out within a magnetically shielded laboratory at the Istituto Nazionale di Geofisica e Vulcanologia (INGV), Rome. Natural and artificial magnetic remanences were measured using a narrow access pass-through cryogenic magnetometer (2-G Enterprises model 750R) with in-line AF demagnetization capability. One sample from each stratigraphic level was AF demagnetized at successive peak fields of 5, 10, 15, 20, 25, 30, 40, 50, 60, 80, and 100 millitesla (mT). Next, sister samples were thermally demagnetized using a magnetically shielded Pyrex furnace at 100, 200, 300, 330, 360, 400, 450, 500, 550, 600, 650, and 700 °C. The MS was measured after each heating step to monitor for thermal alteration of the magnetic minerals. Thermal and AF demagnetization data were examined using orthogonal vector component diagrams (Zijderveld, 1967); best-fit

lines for the progressive demagnetization data were evaluated by principal component analysis (Kirschvink, 1980). Magnetic polarity was interpreted after calculation of the virtual geomagnetic polarity latitude following Cande and Kent (1995).

5.3. Magnetobiochronologic remarks

All of the biostratigraphic markers that define the standard zones and subzones through the Paleocene−early Eocene occur in the analyzed material (see also Coccioni et al., 2010a). Our integrated biostratigraphic study provides evidence that the CHW-CR composite section is continuous and spans from planktonic foraminiferal Zones P0−Pα to P9 and E1 to E7a, and from calcareous nannofossil Zones and Subzones NP1 to NP13 and CP1a to CP11. However, most likey due to stratigraphic condensation, the biostratigraphic interval corresponding to Zone P0 (*Guembelitria cretacea* Zone) and characterized by the partial range of the nominate taxon between the last occurrence of Cretaceous taxa and the first occurrence of *Parvulorugoglobigerina eugubina*, which defines the base of the next Zone Pα (*P. eugubina* Zone), cannot recognized in the CHW section because this species is already present at the base of the studied section (Coccioni et al., 2010a). Accordingly, in our biostratigraphy it is not possible to separate Zones P0 and Pα, which, consequently, have been combined. Moreover, specimens with ambiguous taxonomic features have prevented the confident identification of the lowest and the highest occurrences of *Heliolithus riedeli* and *Tribrachiatus orthostylus* that define the bases of Zones NP8 and NP13, respectively. Consequently, it was not possible to differentiate Zones NP7 and NP8 but, following Agnini et al. (2006), we were able to confidently place the NP12/NP13 zonal boundary at the lowest occurrence (LO) of *Dictyococcites*.

Our high−resolution stratigraphic framework enables a refinement of the previous calibration of the lower Paleogene geomagnetic reversals in Contessa Valley (Lowrie et al., 1982; Galeotti et al., 2000, 2010) and of the Paleocene−early Eocene magnetobiochronostratigraphy in relation to the current standard Geologic Polarity Time Scale (GPTS04, Gradstein et al., 2004; and GTPS08, Ogg et al., 2008). Some significant mismatches among the GPTSs, the Cenozoic tropical planktonic foraminiferal biostratigraphy

by Wade et al. (2011) and our calcareous plankton biostratigraphic framework are recognized, which show the need to reassess the magnetobiochronostratigraphic scheme of the current standard GPTSs for the Paleocene–early Eocene interval, as has already been done for the middle Eocene CHW section (Jovane et al., 2010). In particular, according to this time–scale and Wade et al. (2011), the LO of *Morozovella aragonensis* (P6b/P7 or E4/E5 zonal boundary) lies in the lower Chron C23r. In the CR section this event is recognized in the middle part of Chron C24n.3n. This remarkable mismatch, leading to the LO of M. aragonensis ~0.8 Myr younger than previously estimated, agrees well with previous findings in the CHW and Bottaccione sections (Cresta et al., 1989).

5.4. A new complete survey of the spatio–temporal distribution of the Palaeocene to early Eocene hyperthermals and CIEs

Our high-resolution magnetobiochronostratigraphic framework, along with the magnetic and geochemical records provide an effective tool for comparison with analogue data from deep-sea cores and other land-based sections. This has allowed us to identify and well constrain hyperthermal events as well as CIEs in the CHW–CR composite section previously documented for the Palaeocene–early Eocene, including Dan–C2, Lower C29n, Top C27n (equivalent to CIE–DS1 and LDE), CIE–DS2, the Early Late Palaeocene Event (ELPE, equivalent to the Mid–Palaeocene Biotic Event, MPBE), A, B1, B2, C1, C2, D1, D2, PETM, E1, E2, F, G, H1, H2, I1, I2, J, K, L and Early Eocene Climatic Optimum (EECO) (e.g., Kennett and Stott, 1991; Zachos et al., 2001; Bralower et al., 2002; Cramer et al., 2003; Bernaola et al., 2007; Arenillas et al., 2008; Quillévéré et al., 2008; Westerhold et al., 2008, 2011; Youssef, 2009; Coccioni et al., 2010a; Sexton et al., 2011; with references therein) (Figure 5.1).
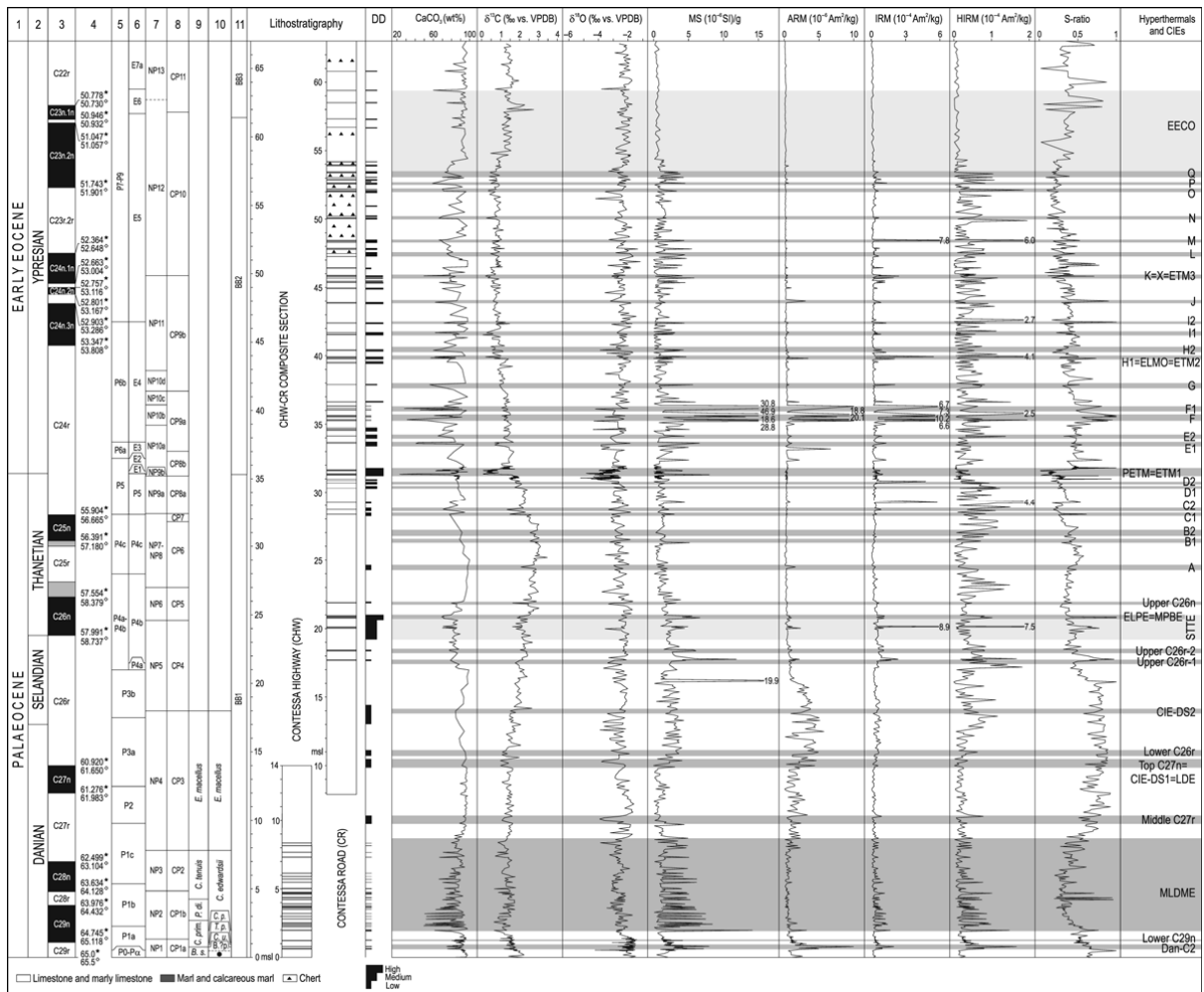
Figure 5.1. *Integrated high-resolution stratigraphic framework of the Palaeocene–early Eocene CHW–CR composite section plotted against dissolution degree (DD), CaCO₃ content, δ¹³C and δ¹⁸O of bulk carbonate, magnetic susceptibility (MS) and environmental magnetism (anhysteretic remanent magnetization, ARM; isothermal remanent magnetization, IRM; hard isothermal remanent magnetization, HIRM; S-ratio). The correlation between the two sections is based on biostratigraphic correlation. More precisely, it is tied to the lowest occurrence of the planktonic foraminifera Morozovella angulata. The CHW−CR composite section starts at the Cretaceous/Palaeogene boundary. Lithostratigraphy is from Galeotti et al. (2000, 2010), Coccioni et al. (2010a) and this study. Chronostratigraphy (1,2) is according to Aubry et al. (2007) and Ogg et al. (2008). Magnetostratigraphy (3) is from Lowrie et al. (1982), Galeotti et al. (2000, 2010) and this study. Numerical ages (4) are from Cande and Kent (1995) (stars) and Gradstein et al. (2004) (diamonds). Biostratigraphy is based on planktonic foraminiferal Zones of Berggren et al. (1995) (5) and Wade et al. (2011)*

(6), calcareous nannofossil Zones of Martini (1971) (7), Okada and Bukry (1980) (8), Romein (1979) (9) and Perch-Nielsen (1985) with the black dot marking the "B.? romeinii-barren interval" Zone (10), and benthic foraminiferal Zones of Berggren and Miller (1989) (11). The grey shaded areas mark the documented and suspected hyperthermals, CIEs as well the inferred Early Eocene Climatic Optimum (EECO).

In addition, we provide the first direct evidence of a number of negative CIEs, on the order of 0.3‰ to 0.8‰, associated with significant decreases in carbonate content and peaks in magnetic susceptibility and magnetic parameters generally linked to marly layers (Figure 5.1). We confidently interpret these abiotic variations as the result of environmental perturbations, which we termed the ''Middle–Lower Danian Multiple Event'' (''MLDME''), ''Middle C27n'' (middle Danian), ''Lower C26r'' (late Danian), ''Upper C26r-1'' and ''Upper C26r–2'' (late Selandian), ''Selandian–Thanetian transition event'' (''STTE''), ''Upper C26n'' (early Thanetian), ''F1'' (early Ypresian) and ''M'', ''N'', ''O'', ''P'' and ''Q'' (middle Ypresian) (Figure 5.1).

The ''MLDME'' is in fact a discrete interval, ~2 Ma long according to Cande and Kent (1995) and Gradstein et al. (2004), which includes 25 thin marly layers and spans part of Chron C29n to Chron C27r. In terms of calcareous plankton biostratigraphy, the ''MLDME'' spans planktonic foraminiferal Zones P1a to P1c and calcareous nannofossil Zones NP2 to NP4 and CP1b to CP3 (Figure 5.1). The ''MLDME'' might be regarded as a series of CIEs comparable to those of the early Danian suspected hyperthermals Dan-C2 and Lower C29n (Quillévéré et al., 2008; Coccioni et al., 2010a).

The ''Middle C27r'' CIE falls in the middle part of Chron C27r, at the planktonic foraminiferal P1c/P2 zonal boundary and within the lower part of calcareous nannofossil Zones NP4 and CP3. The ''Lower C26r'' CIE is found in the lower part of Chron C26r, and within the middle part of planktonic foraminiferal Zone P3a and the middle part of calcareous nannofossil Zones NP4 and CP3. The ''Upper C26r–1'' and ''Upper C26r–2'' CIEs occur in the upper part of Chron C26r and within the lower part of planktonic foraminiferal Zone P4b and the middle part of calcareous nannofossil Zones NP5 and CP4 (Figure 5.1).

The ''STTE'' is an abrupt environmental disruption event documented by pronounced and complex changes in abundance and composition of the foraminiferal and calcareous nannofossil assemblages, intense carbonate dissolution, drop in δ^{13}C bulk carbonate and in carbonate content accompanied by prominent peaks in magnetic susceptibility recognized in three discrete marly beds (Coccioni et al., 2010b) (Figure 5.1), which according to Cande and Kent (1995) and Gradstein et al. (2004) lasted ~250 ka and is centred at ~58.3 Ma (Selandian–Thanetian transition). This relatively long-lasting event falls within the middle–lower part of the planktonic foraminiferal Zone P4b and spans the calcareous nannofossils Zones NP5 to NP6 and CP4 to CP5 and Chrons C26r to C26n (Figure 5.1). The uppermost part of the ''STTE'' would include the ELPE (Bralower et al., 2002; Petrizzo, 2005) or the MPBE (Bernaola et al., 2007), which would therefore become part of a more complex scenario (Coccioni et al., 2010b) (Figure 5.1).

The ''Upper C26n'' CIE lies in the upper part of Chron C26n and within the upper part of planktonic foraminiferal Zone P4b and the middle part of calcareous nannofossil Zones NP6 and CP5. The ''F1'' CIE, which comes just after the F event of Cramer et al. (2003), falls in the middle part of C24r and within the lower part of planktonic foraminiferal Zone P6b, and the upper part of calcareous nannofossil Zones NP10b and CP9a. The ''M'', ''N'', ''O'', ''P'' and ''Q'' CIEs are found from the lower part of Chron C23r.2r to the lower part of Chron C23n.2n and within the middle part of planktonic foraminiferal Zones P7-P9 and E5, and the middle-lower part of calcareous nannofossil Zones NP12 and CP10 (Figure 5.1).

Moreover, we are able to infer the stratigraphic position and timing of the EECO in the CHW–CR composite section by recognizing the distinctive sequence of calcareous nannofossil events as that provided by Agnini et al. (2006). A progressive decrease in the abundance of *Prinsiales* (namely *Toweius*) and low percentages of *Discoaster*, which are correlative to the δ^{18}O decreasing trend leading to the EECO, are first observed at ~55 metre stratigraphic level (msl) (Figure 5.1). Next, the *Discoaster Acme* and the virtual absence of *Prinsiales* (*Toweius*), which are correlative to the EECO δ^{18}O minima as recognized by Zachos et al. (2001), occur between ~57.5 and 63.5 msl together with an increase in the abundance of the warm-water taxa *Coccolithus pelagicus* and *Ericsonia formosa*. Just before the end of the *Discoaster Acme*, the early entry of the *Dictyococcites / Reticulofenestra* group

(*Noelaerhabdaceae*), which is broadly correlative to the onset of the δ^{18}O increasing trend as recognized by Zachos et al. (2001), is found. Finally, an increasing abundance of *Dictyococcites / Reticulofenestra* and low percentages of *Discoaster* are recognized. The EECO, confidently placed in correspondence to the *Discoaster Acme*, spans the upper part of planktonic foraminiferal Zones E5 to the top of E6 and the calcareous nannofossil Zones NP12 to NP13 and CP10 to CP11 (Figure 5.2). In agreement with Westerhold and Röhl (2009), this event spans from the lower part of Chron C23n.2n to the lowermost part of Chron C22r (Figure 5.1). Following the age calibration and the duration of geomagnetic reversal of Cande and Kent (1995) and Gradstein et al. (2004), the EECO in our composite section would have a duration estimated at ~0.90 Ma or ~1.08 Ma respectively.
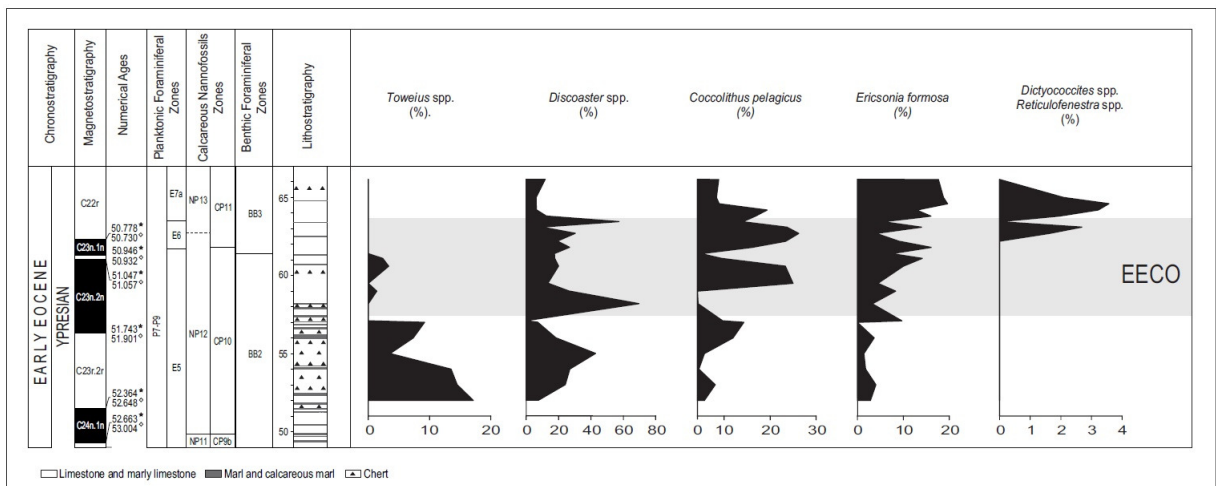
Figure 5.2. *Quantitative nannofossil distribution of key taxa plotted against the integrated high−resolution stratigraphy of the CHW–CR composite section. The gray shaded area marks the inferred stratigraphic position of the Early Eocene Climatic Optimum (EECO).*

We also provide the first direct evidence in the Tethys Ocean of CIEs A, B1, B2, C1, C2, D1, D2, E1, E2, F, G and L (Figure 5.1), previously identified in the Pacific, Atlantic and Southern Oceans (Cramer et al., 2003; Zachos et al., 2010), highlighting the global significance thereof. In addition, we confirm the regional nature of CIE–DS2 (Figure 5.1), previously recognized in the Tethyan area by Arenillas et al. (2008) and Youssef (2009).

However, given the sampling resolution, it is likely that the carbon isotope record is a highly aliased record of orbital scale cyclicity in the δ^{13}C. Accordingly, the identification of the CIEs is here presented as a model rather than as a firmly established isotope stratigraphy.

Our data confirm that carbonate dissolution in the western Tethys during the Palaeocene–early Eocene was extremely severe at the PETM. An enhanced dissolution, which is probably linked to prominent shoaling of the lysocline and CCD, is also documented here through the ''STTE'' and the stratigraphic interval from hyperthermals H1 to K (early Ypresian) when, interestingly, the atmospheric CO_2 reached its highest levels (Zachos et al., 2008) (Figure 5.1).

5.5. Conclusion and perspectives on magnetic mineralogy studies

This study shows that the CHW–CR composite section offers a unique, complete and integrated record for the Palaeocene to early Eocene interval, thus providing a reference succession also for insight into the magnetobiochronostratigraphy and the magnitude of early Palaeogene hyperthermals and CIEs.

Some of these hyperthermal events have been associated to the presence of magnetofossils, identified directly from microscopic observations (TEM) (Schumann et al., 2008; Chang et al., 2012) or indirectly by their magnetic properties (Larassoaña et al., 2012). These findings calls for a common origin for the increase in magnetotactic bacteria activity and the rapid increase in global temperatures either in typical hyperthermals, like the PETM, or in other high-temperature 'anomalous' events, such as the MECO. We have now started a systematic work on the magnetic properties of the CHW-CR to test this hypothesis.

Chapter 6. Middle Eocene to early Oligocene magnetostratigraphy of ODP Hole 711A (Leg 115), western equatorial Indian Ocean

6.1. Introduction

Ocean Drilling Program (ODP) Leg 115 in the western equatorial Indian Ocean was designed to study the Cenozoic evolution of the Réunion hotspot and Neogene sedimentation and dissolution history in the Indian Ocean Basin (Duncan et al., 1990). The main objective for coring at Site 711 was to obtain a complete Neogene sediment sequence to study time dependent vertical changes in the position of the calcite compensation depth (CCD) and variability of carbonate preservation within the sublysocline transition zone (Backman et al., 1988). Moreover, development of accurate age models were to be provided by a combination of bio and magnetostratigraphy (Backman et al., 1988). Hole 711A is located at a water depth at 4430 m on Madingley Rise (Figure 6.1A); a 250-m-thick sedimentary section was recovered. Sediments from Hole 711A span the time period between the Pleistocene and middle Eocene. Paleodepth estimates for the site during the middle Eocene and early Oligocene interval (50-30 Ma) is approximately 3450 m at 42 Ma and 3750 at 30 Ma (Peterson and Backman, 1990).

Previous paleomagnetic studies from the Oligocene interval of Hole 711A (Schneider and Kent, 1990a; Touchard et al., 2003) indicated that the sediments retain a good record of the Earth's past magnetic field; however, the inclination data appear scattered because of magnetic overprints associated with the coring processes (e.g., Roberts et al., 1996; Fuller et al., 1998; Acton et al., 2002). Schneider and Kent (1990) studied the magnetostratigraphy of Hole 711A down to the top of Chron C9n, recognizing the magnetostratigraphic Chrons C18 and C19 based on nannofossil Zone CP19. Touchard et al. (2003) obtained a implemented magnetostratigraphy from 214 samples that spanned the section between 98.8 and 157.38 mbsf, which corresponded to the time interval from Chron C13r to C19n (Schneider and Kent, 1990) and zonal boundary NP19-20/NP21 (Okada, 1990).

The Eocene and Oligocene represent a critical time interval for paleoclimate and paleoceanography evolution. Deep-sea oxygen and carbon stable isotope records (e.g. Miller et al., 1991; Zachos et al., 2001, 2008) indicate that the climate system experienced progressive high-latitude cooling since the Early Eocene Climatic Optimum (EECO, ~50-52 Ma), which culminated in the oxygen isotopic (Oi-1) excursion (~34 Ma; Miller et al., 1991). Superimposed on this long-term cooling trend are climatic instabilities associated with warming (e.g., Bohaty and Zachos, 2003; Jovane et al., 2007; Bohaty et al., 2009; Sexton et al., 2011) and cooling events (e.g., Tripati et al., 2005). The largest warming event is the middle Eocene Climatic Optimum (MECO) (Bohaty and Zachos, 2003; Jovane et al., 2007; Luciani et al., 2010; Spofforth et al., 2010; Edgar et al., 2010), which is interpreted as a global warming event by Bohaty et al. (2009). The MECO event is characterized by a progressive long-term increase (~1.0‰) in benthic foraminiferal $\delta^{13}C$ values in several sites in the southern Ocean. This long-term trend began at ~40.7 Ma and ended at ~39.6 Ma (Bohaty et al., 2009). The large negative $\delta^{18}O$ shift at 40 Ma from several sites indicates that MECO was a global warming event (Bohaty et al., 2009). Bijl et al., 2010 reconstructed the pCO_2 and sea surface temperatures (SST) during the MECO suggesting a warming of ~5°C of the SST.

The Oi-1 event at the Eocene-Oligocene boundary was a pivotal event in the shift from greenhouse to icehouse climate state. The Oi-1 event was associated with an abrupt stepwise onset of Antarctic glaciation with global shifts in distribution of marine biogenic sediments, an overall increase in ocean fertility, a major drop in the CCD, and an onset of Atlantic thermohaline circulation (e.g., Coxall et al., 2005; Coxall and Wilson, 2011). The Oi-1 cooling event was associated with an abrupt increase (~1.5‰) in benthic foraminiferal $\delta^{18}O$ values, which is attributed to development of ice sheets on Antarctica, which grew to ≥50% near present day (e.g., Shackleton and Kennett, 1975; Coxall et al., 2005). Variations in the Earth's climate system are caused by changes in ocean circulation due to opening of Southern Ocean gateways (e.g., Kennett, 1977; Lyle et al., 2007), reduction of atmospheric greenhouse gases (DeConto and Pollard, 2003; Pagani et al., 2005; Merico et al., 2008; Liu et al., 2009), superimposed orbital forcing (Coxall et al., 2005) and closure of the Neo-Tethys ocean gateway at ~35 Ma (late Eocene) (e.g., Allen and Armstrong, 2008; Jovane et al., 2009).

In order to identify and provide new insight into the major Eocene and Oligocene climatic events, we developed a integrated high-resolution age model for Hole 711A. The

middle Eocene-to-lower Oligocene interval is well represented in sediments form this hole, and in this paper, we present new high-resolution magnetostratigraphy for this section. Previously published biostratigraphic results (Okada, 1990) from this site are used to constrain the correlation to the GPTS (Table 6.1). Magnetostratigraphic results have been previously reported for Hole 711A by Schneider and Kent (1990) and Touchard et al. (2003). However, these earlier studies do not cover the lower part of the section due to the proximity of the site to the equator and the difficulty envisioned in obtaining polarity data from these azimuthally-unoriented samples. Our new results from Hole 711A have important implications for identification and dating global climate change events (MECO, Oi-1), and for reconstructing CCD history of this site.
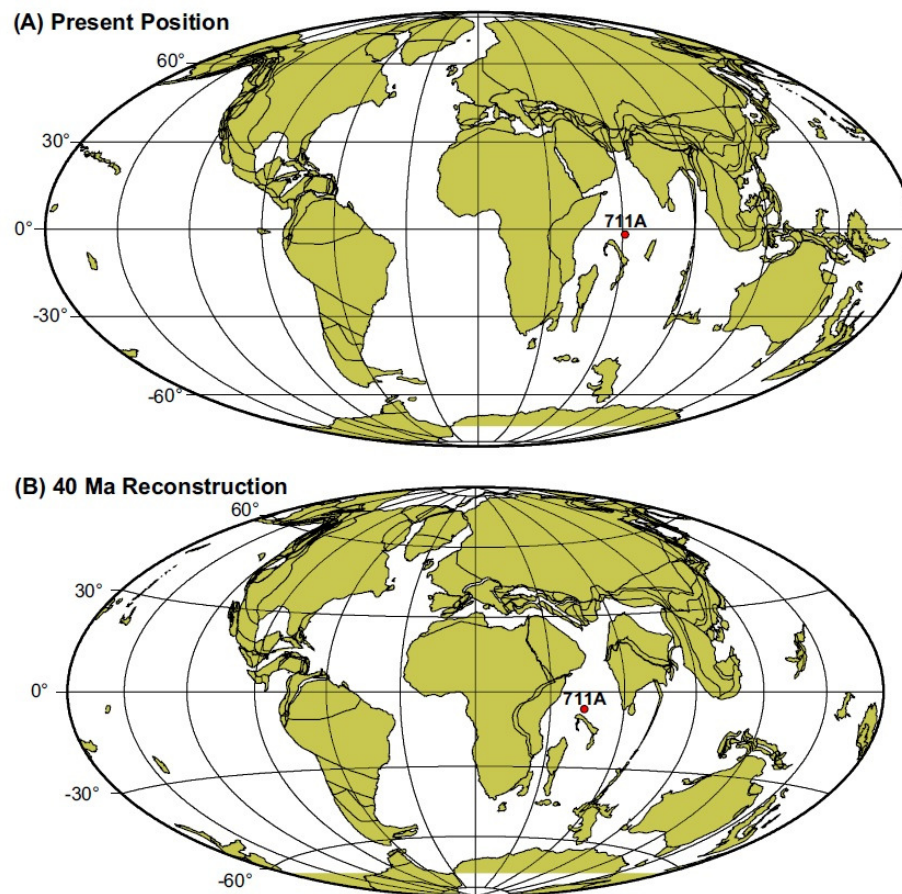

Figure 6.1. *(A) Location of ODP site 711 in the western equatorial Indian Ocean. (B) Paleogeographic reconstruction showing location of ODP site 711 at 40 Ma. The maps were generated from the Ocean Drilling Stratigraphic Network (GEOMAR, Kiel, Germany).*

6.2. Methods

Measurements were carried out in the paleomagnetic laboratory of the National Oceanography Centre Southampton (NOCS), University of Southampton, UK. All measurements were made using a 2G–Enterprises superconducting quantum interference device (SQUID) magnetometer (model 755R). To minimize sources of noise, the magnetometer is situated in a magnetically shielded room, which reduces the intensity of the ambient magnetic field. The sensitivity of the instrument corresponds to a rock magnetization of ~10^{-6} A/m. We measured the low–field mass magnetic susceptibility (χ) of all samples using a KLY–4 Kappabridge (Agico Ltd.), prior to measurement of the natural remanent magnetization (NRM).

In order to recognize and remove secondary NRM components we use alternating field (AF) demagnetization to isolate the characteristic remanent magnetization (ChRM). This process effectively randomizes the magnetization of grains with coercivities below the peak AF intensity, which allows the remanence of higher coercivity grains to be isolated. The NRM of all samples from the Hole 711A was measured after progressive stepwise AF demagnetization at 5, 10, 15, 20, 25, 30, 35, 40, 45, 50, 60, 70, and 80 milliTesla (mT).

In order to display stepwise demagnetization data, we use vector component diagrams (Zijderveld, 1967; Dunlop, 1979). The ChRM direction were determined using stereographic projections, orthogonal and demagnetizing intensity plots of stepwise demagnetization data, allowing the various remanence components that make up the NRM to be separately identified. The directions of these different components are then calculated using principal component analysis (Kirschvink, 1980). This method analyses the best-fit line through straight-line, single component line. This linearity can be assessed by calculating the maximum angular derivation (MAD). A good line fit is indicated by a MAD <15°. This method is only valid where linear components of the demagnetization path can be isolated. Principal component analyses were analyzed using the paleomagnetic data software package REMASOFT 3.0 (Chadima and Hrouda, 2006).

The rock-magnetic measurements consisted of hysteresis curves and IRM (isothermal remanence magnetization) performed at room temperature using a vibrating sample

magnetometer (VSM MicroMagTM 3900) and a Pulse Magnetizer (MMPM–9) at the National Oceanography Centre Southampton (NOCS), University of Southampton, UK. Hysteresis loops were measured in maximum field of 1 T and average time 500 ms. The rock samples were placed in progressively fields the IRM increasing to a maximum value of saturation (SIRM), in a maximum field of 1.5 T.

Furthermore, environmental magnetism and FORC diagrams were performad for investigate the variation of the magnetic mineralogy trough the section. We used the same methodology mensioned in the section 4.4.3 for MCA section.

6.3. Results

6.3.1. Paleomagnetic polarity zonation

A total of 375 discrete samples were analyzed using the SQUID magnetometer. Of the 375 analyzed samples, 248 (66%) had no reliable magnetic directions (MAD ≥15°) after AF demagnetization. The others 127 samples (34%) displayed stable paleomagnetic behavior upon stepwise AF demagnetization (Figure 6.2). The ChRM directions with MAD ≤15° display normal and reverse polarities defining a magnetic polarity zonation. In particular, several samples have inclination values that are intermediate between normal and reverse directions. For azimuthally-unoriented samples from sedimentary rocks that formed in low-latitudes, determining the polarity of sedimentary units may be difficult. The polarity ambiguity arises because the samples are azimuthally-unoriented, the declination cannot be used to determine polarity; the inclination is shallow near the equator, the angular distance between reversed and normal polarity inclinations is small; and the paleomagnetic inclinations from any samples will have some degree of dispersion about their mean inclination, it is likely that when the mean inclination is shallow, the sign of the inclination will not be indicative of the polarity (e.g., McFadden and Reid, 1982; Cox and Gordon, 1984). In our case, only two samples (163.7 and 193.7 mbsf) present inclinations less than 10 degrees. The sign of the inclination of these two samples cannot be used as a definitive estimate of magnetic polarity. The samples with MAD values ≥15° were discarded. Some of them were showing low

intensity due to low magnetic concentration the others can be interpreted as drilling-induced overprint.
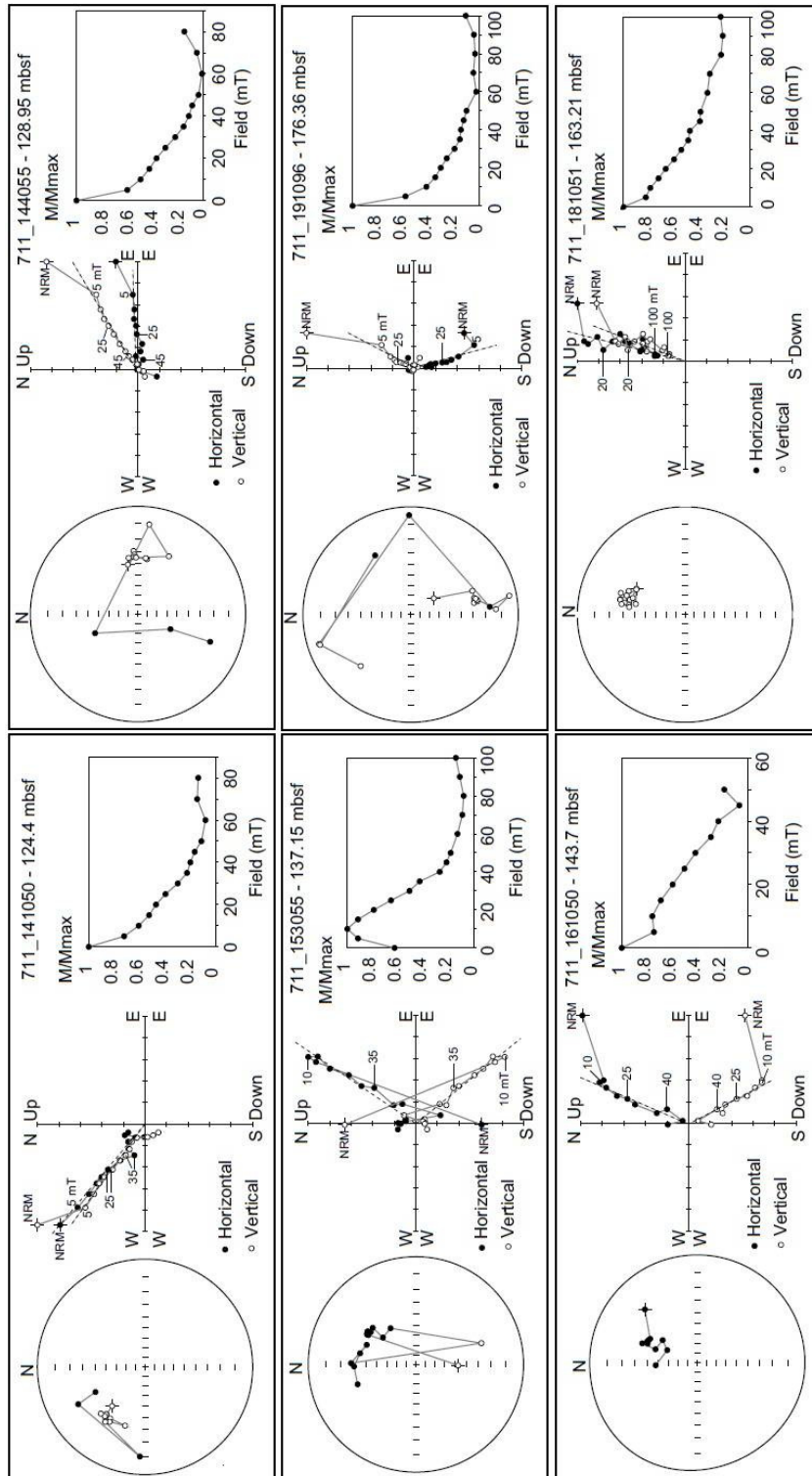

Figure 6.2. *Orthogonal and vector component diagrams (with normalized intensity decay plots) for alternating field (AF) demagnetization data for six representative specimens from*

Figure 6.3 illustrates the lithologic units of the middle Eocene-lower Oligocene sedimentary interval of Hole 711A. The abundance and preservation of the calcareous nannofossils varies from whole dissolved to moderate at Hole 711A (Backman et al., 1988; Okada, 1990; Wei et al., 1992). The NRM demagnetization paths of the 375 samples from Hole 711A have considerable variations that are attributed to the relatively low intensity of magnetizations (5.23×10^{-5} to 1.77×10^{-1} A/m with an arithmetic average of 5.27×10^{-3} A/m) (Figure 6.3). Several samples are characterized by high NRM intensity, which are associated with dished lithologies (186.92 and 187.01 mbsf), (e.g. very dark grayish brown clay-bearing radiolarian ooze). Arithmetic mean directions were computed separately for normal and reverse polarity populations and calculated following Jovane et al. (2008). The normal polarity samples have an arithmetic mean inclination of 29.0° (N = 59; α95 = 2.5) and the reverse polarity samples have an arithmetic mean inclination of -30.7° (N = 37; α95 = 2.6). These values show that our magnetostratigraphic record passes the reversal test. Our interpretation was compared with predicted paleolatitudes of the site 711A according to the absolute plate motion model based on fixed African hotspots (e.g., Duncan, 1981; Kidd et al., 1992). Based on these mean directions, the calculated mean paleolatitude of Hole 711A is 16° S. However, based on the reconstructed position of Hole 711A (see Figure 6.1B), the 40 Ma paleolatitude would be 9.5° S, and the expected inclination would be 19 degrees. The observed mean inclination is approximately 10 degrees steeper than the expected inclination. These inclinations are steeper than the present-day geocentric axial dipole inclination and it is attributed to three systematic error sources: method of calculating the mean inclination, drift of the hotspots, and a large non-dipole field (Schneider and Kent, 1990). This result is compatible with previous paleoreconstructions for the Eocene-Oligocene period (Schneider and Kent, 1990; Royer and Coffin, 1992; Zachos et al., 1992). However, our mean inclination is steeper than expected (according to the fixed hotspot models), and that this could be due to some unresolved combination of unaccounted for motion of the plate, long-term non-dipole fields, or effects of hotspot motion on the plate circuit models (Schneider and Kent, 1990b). Based on paleocenographic and paleomagnetic records have been reconstructing the globally

tectonic implications of the Site 711. The drill site has moved northward since the formation these sediments approximately 600 km.
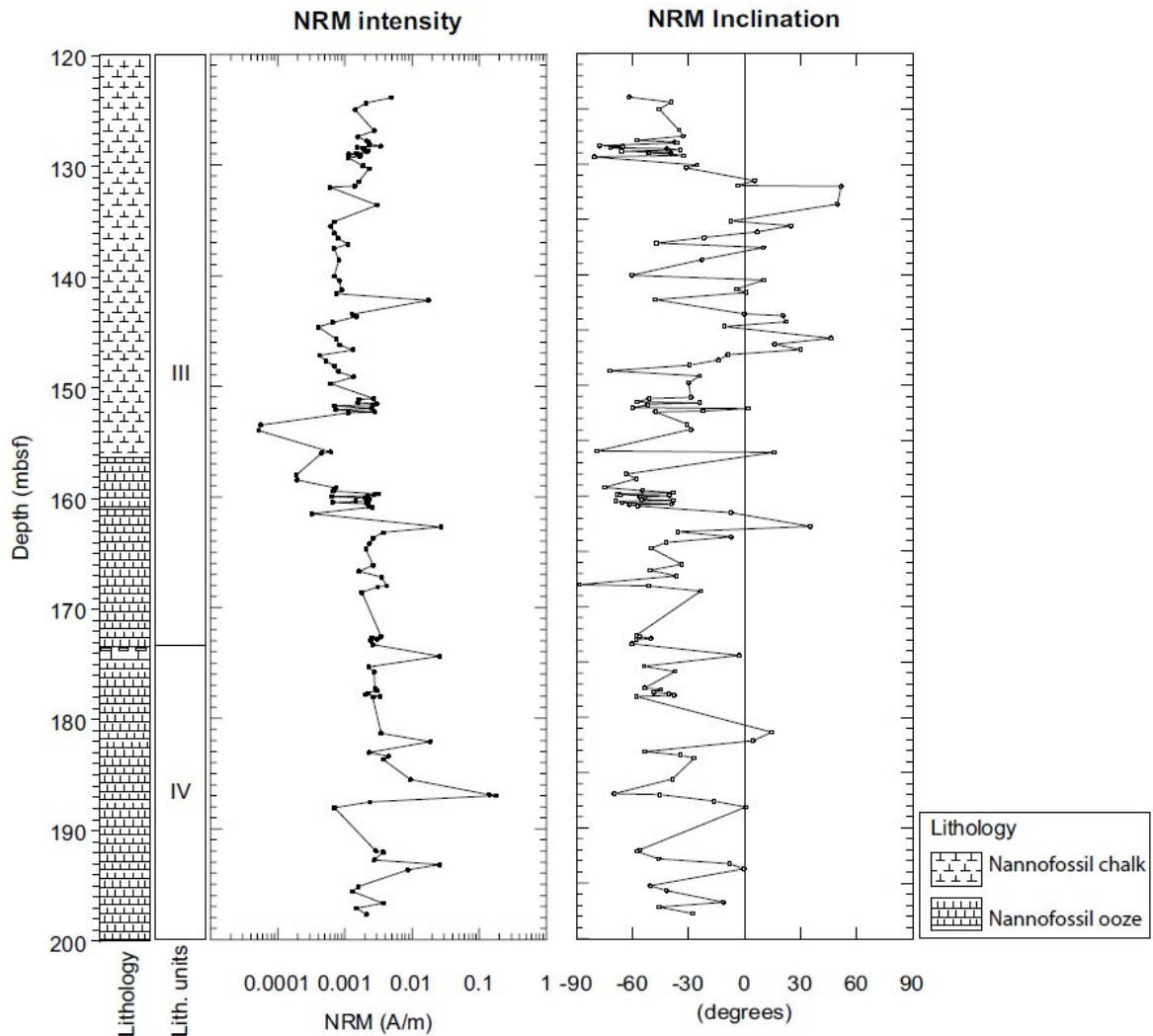
Figure 6.3. *Detailed lithostratigraphic column for ODP Hole 711A in the interval between 120 and 200 mbsf. The second column shows the lithostratigraphic units as defined in shipboard work (Backman et al., 1988), including Unit III (nannofossil oozes, clay-bearing nannofossil oozes, clay-bearing nannofossil chalks) and Unit IV (distinguished from unit III by the consistent occurrence of radiolarians). The third panel shows the stratigraphic variations of intensity and fourth panel shows the inclination of the natural remanent magnetization (NRM).*

The magnetic polarity record of the studied portion of Hole 711A can be subdivided into fourteen magnetozones (Figure 6.4). The magnetozones are defined as intervals with multiple, consecutive samples with polarities that are distinctly different from neighboring intervals. In only one case, at 142.23 mbsf, the sample has polarity opposite of the rest of the magnetozone, but it is not used to determine the polarity.
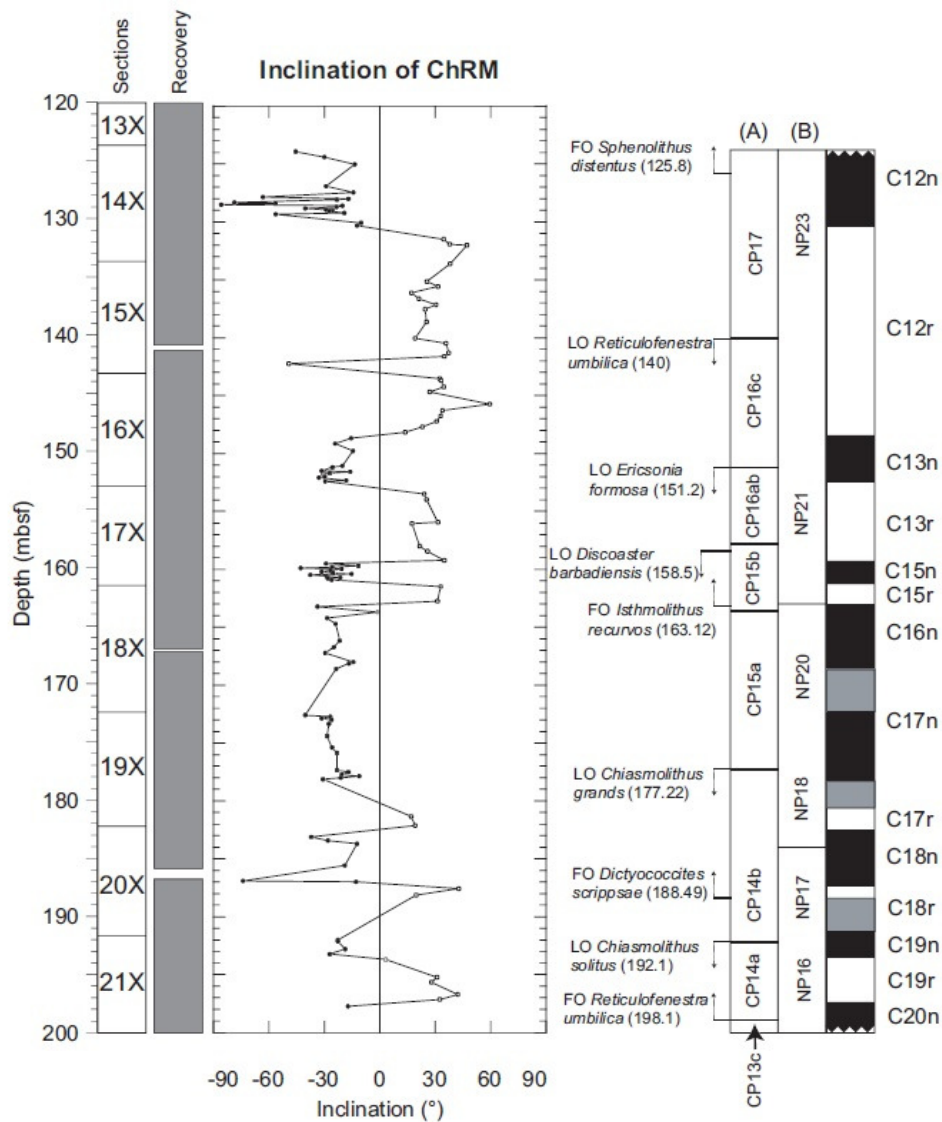
Figure 6.4. Core number (left), core recovery (gray bars), and variations in the declination and inclination in Hole 711. The magnetostratigraphic interpretation is show on the right side, which is constrained by the nannofossil biostratigraphy of Okada (1990). Nannofossil zones, using the zonal of both Okada and Bucky (1980) (A) Martini (1971) (B), are defined in the section. Inclination values steeper than 10 degree are black while values below 10 degree are grey points.

6.3.2. Rock magnetic properties

Isothermal remanent magnetization (IRM) acquisition curves were obtained for five representative samples of Hole 711A at fields up to 1.5 T (Figure 6.5). IRM acquisition experiments indicated that saturation magnetization (Ms) occur at field comprised between 60–80 mT, which typifies low- to medium coercivity remanence carrier such as magnetite and/or titanomagnetite (Ti–poor magnetite) (e.g. Dunlop and Özdemir, 1997). These results confirm previous published results from the lower Oligocene section of the Hole 711A (Touchard et al., 2003). The presence of a low–coercivity mineral is also confirmed from the rapid decrease in intensity of remanence during AF demagnetization (Figure 6.2).
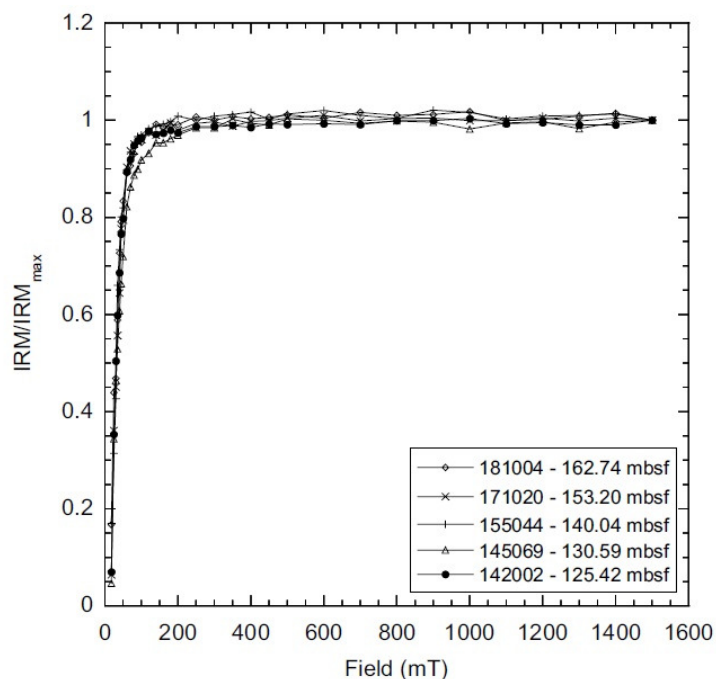
Figure 6.5. Isothermal remanent acquisition curves for five representative samples within the ODP Hole 711A study section (normalized intensities vs. applied magnetic field).

Hysteresis cycles for the twenty representative samples along of the eighty meters of section show a low coercivity behavior (Figure 6.6A), which is most likely indicated of the presence of magnetite and/or titanomagnetite (e.g., Dunlop and Özdemir, 1997; Krása et al.,

2011). The hysteresis standard parameters like Ms, saturation remanent magnetization (Mrs), coercive force (Hc), and coercivity of remanence (Hcr) are combined as ratio and approaching pseudo-single domain (PSD) values. Magnetic hysteresis data (Figure 6.6A) are characterized by stably magnetized samples that have moderate Hcr/Hc (1.74–2.10) and Mrs/Ms (2.61–3.61). Hysteresis ratios for samples from 711A indicate a pseudo-single domain (PSD) assemblage (Figure 6.6B) (Day et al., 1977) with the dominance of magnetite and/or titanomagnetite particles (e.g. Dunlop and Özdemir, 1997).
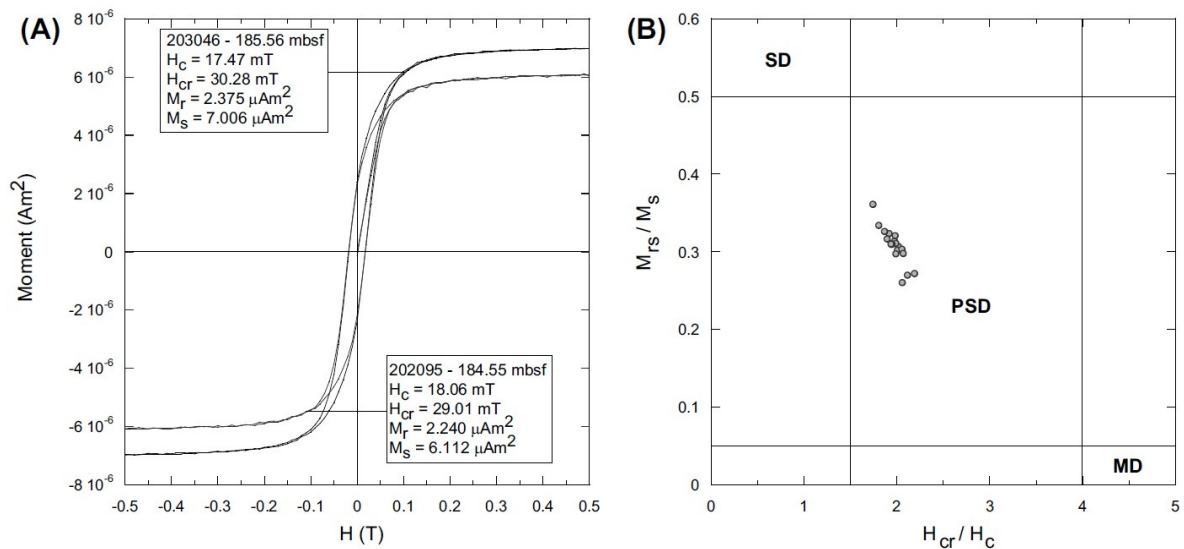
Figure 6.6. *(A) Hysteresis curves for two representative samples from Hole 711A indicating a similar magnetic behavior (low-coercivity behavior, magnetite and/or titanomagnetite). (B) Mrs/Ms versus Hcr/Hc plot for sediments from the Hole 711A. The magnetic grain size show a pseudo-single domain particles.*

6.3.3. Biostratigraphy

In order to obtain a high-resolution integrated age model, magnetostratigraphic data need to be combined with biostratigraphic datum in the same interval. Okada (1990) and Wei et al. (1992) conducted a biostratigraphic investigation on the Paleogene interval of the Site 711, studying calcareous nannofossil using biozones of Martini (1971) and Okada and Bukry (1980) (Figure 6.4).

The base of the studied section (198.1 mbsf), which defines the Zone CP14a, near the CP13c-CP14a zonal boundary of Okada and Bukry (1980) coinciding with the lower part of the Zone NP16-17 of Martini (1971), was characterized by the first occurrence (FO) of *Reticulofenestra umbilica* (Okada, 1990) (Table 6.1). The FO of *Dictyococcites scrippsae* at 188.49 mbsf occurs approximately in the CP14a-CP14b of Okada and Bukry (1980), which is defined by last occurrence (LO) of *Chiasmolithus solitus* (192.1 mbsf). The LO of *Chiasmolithus grands* (177.22 mbsf) occurs near the CP14b-CP15a zonal boundary of and NP18-NP20. The FO of *Isthmolithus recurvos* (163.12 mbsf) and the LO of *Discoaster barbadiensis* occur approximately at CP15a-CP15b boundary and CP15b-CP16ab boundary, respectively. The CP16ab-CP16c zonal boundary is characterized by LO of *Ericsonia formosa* (151.2 mbsf). The LO of *Reticulofenestra umbilica*, which marks the CP16c-CP17 zonal boundary, occur at 140 mbsf. The FO of *Sphenolithus distentus* (125.8 mbsf) occusr in the CP17 and NP23.

Table 6.1. *Calcareous nannofossil events and interpretation of Chrons boundaries for the Hole 711A. Calcareous nannofossil zonations of Jovane et al. (2010) (1) and Berggren et al. (1995) (3) and references therein. Magnetochron ages from Gee and Kent (2007) (2).*

Calcareous nannofossil events and chrons boundaries	Depth (mbsf)	Age (Ma)
FO *Reticulofenestra umbilica*	198.1	42.67 (C20n) (1)
C20n/C19r	197.3	42.356 (2)
C19r/C19n	193.5	41.521 (2)
LO *Chiasmolithus solitus*	192.1	40.4 (C18r) (3)
C19n/C18r	191.3	41.257 (2)
FO *Dictyococcites scrippsae*	188.49	39.86 (C18n.2n) (1)
C18r/C18n	187.3	40.13 (2)
C18n/C17r	182.7	38.426 (2)
C17r/C17n	180.07	38.113 (2)
LO *Chiasmolithus grands*	177.22	37.1 (C17n.1n) (3)
C17n/C16n	169	36.341 (2)
FO *Isthmolithus recurvos*	163.12	36 (C16n.2n) (3)
C16n/C15r	163.2	35.343 (2)
C15r/C15n	161.4	34.94 (2)
C15n/C13r	159.3	34.655 (2)
LO *Discoaster barbadiensis*	158.5	34.3 (C13r) (3)
C13r/C13n	153.2	33.545 (2)
LO *Ericsonia formosa*	151.2	32.8 (C12r) (3)
C13n/C12r	148.4	33.058 (2)
LO *Reticulofenestra umbilica*	140	32.3 (C12r) (3)
FO *Sphenolithus distentus*	125.8	31.5-33.1 (C12r) (3)
C12r/C12n	129.8	30.939 (2)

6.4. Discussion

6.4.1. Correlation to the geomagnetic polarity time scale

In this work, we present a new magnetic polarity record between 123.93 and 198.91 mbsf of Hole 711A. We recognize fourteen magnetozones in the middle Eocene-lower Oligocene interval following the published biostratigraphic of Okada (1990) (C12n-C20n; Figure 6.4). The new interpretation of the magnetic polarity pattern provides a correlation with geomagnetic polarity time scale (GPTS) of Gee and Kent (2007) and Jovane et al. (2010) between the top of Chron C12r (30.939–33.058 Ma) and the top of Chron C20n (42.536–43.789 Ma) (Figure 6.7). From 160 to 120 mbsf (late Eocene to early Oligocene) our interpretation is in good agreement with previous magnetostratigraphic results reported for Hole 711A (Touchard et al., 2003). However, below 160 mbsf our interpretation is completely new spanning approximately 8 myr.

Our new age interpretation following ages of Gee and Kent (2007) differs significantly of previously published data collected during the shipboard work (Backman et al., 1988) as well as subsequent works (Okada, 1990; Rio et al., 1990; Schneider and Kent, 1990). We use the GPTS of Gee and Kent (2007) and Jovane et al. (2010) – use of the Gradstein et al (2004) GPTS results in small changes in (less than 1 million years) in the age-depth relationships, and minor changes in the calculated sedimentation rate of the section (see Figure 6.8 and 6.9).
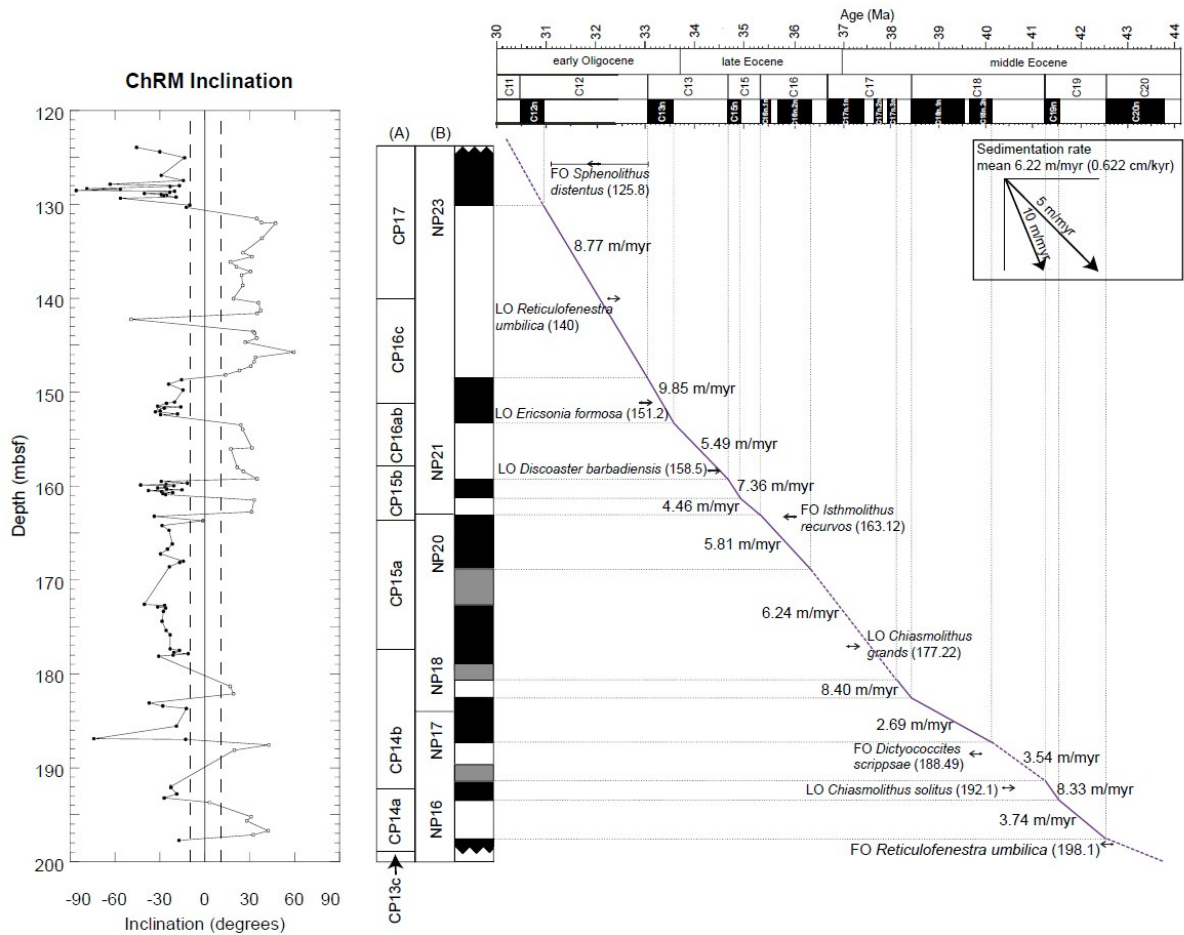
Figure 6.7. *Inclination of ChRM and age versus depth plot with correlation of the ODP Hole 711A polarity zonation to the geomagnetic polarity time scale of Gee and Kent (2007) and Jovane et al. (2010). Inclination values steeper than 10 degree are black while values below 10 degree are grey points and limited by dashed lines. Calcareous nannofossil and planktonic foraminiferal datums are used to constrain the interpretation. The biostratigraphic events from Okada (1990) are based on the calcareous nannofossil zonal schemes of Martini (1971) and Okada and Bukry (1980). The gray bars in the geomagnetic polarity zonation represent the uncertainties in the definition of polarity zonation in relationship with GPTS.*
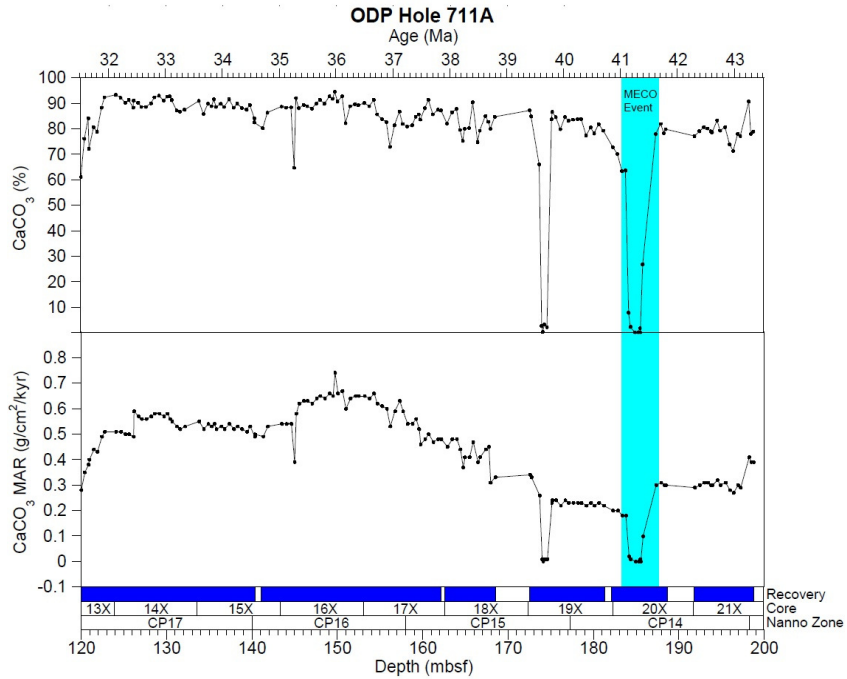
Figure 6.8*. Estimated ages of Peterson and Backman (1990), carbonate concentration data, and the calculated mass accumulation rates (MAR: g/cm²/kyr) for the middle Eocene to lower Oligocene interval of ODP Hole 711A between 120 and 200 mbsf.*
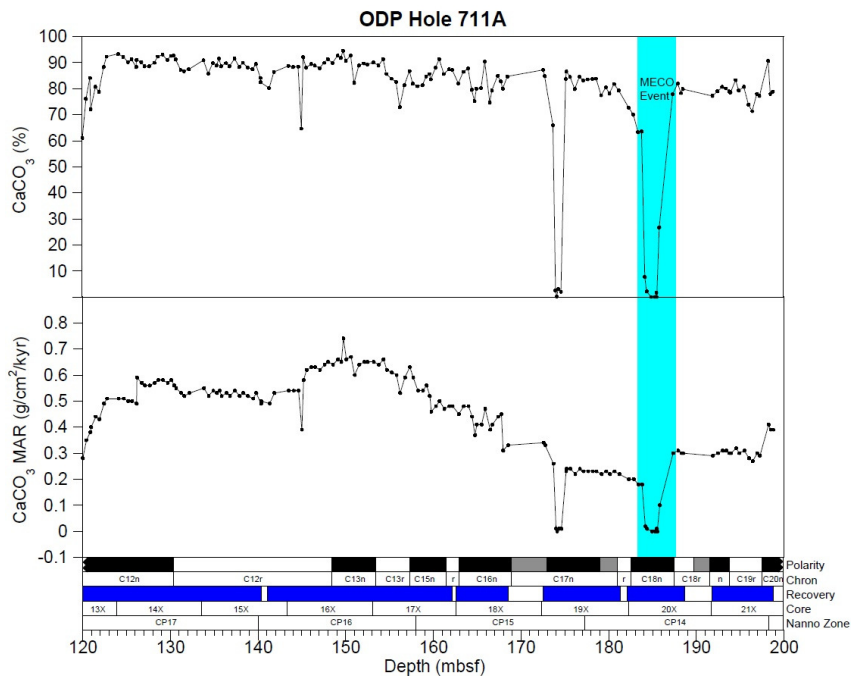
Figure 6.9*. Compilation of carbonate concentration and mass accumulation rates data from Peterson and Backman (1990) and paleomagnetic data used in this study.*

6.4.2. Age-Depth Model

With the aim of perform a new age model we correlated the twelve magnetozones with GPTS (Gee and Kent, 2007; Jovane et al., 2010). To constrain the magnetostratigraphic interpretation for the interval between 123.93 and 198.91 mbsf, we use nannofossil stratigraphy presented by Okada (1990). Overall the linear correlation between magnetostratigraphy and biostratigraphy for Hole 711A (Figure 6.7) show small uncertainties.

The age-depth curve for the middle Eocene to the lower Oligocene interval of Hole 711A is presented in Figure 6.7. The resulting sedimentation rates are relatively uniform and are consistent with biostratigraphic datum. The average sedimentation rate for the interval between 197.43 mbsf (base of Chron C19r) and 130.91 mbsf (top of Chron C12r) is 6.22 m/myr (0.622 cm/kyr) (Figure 6.10).
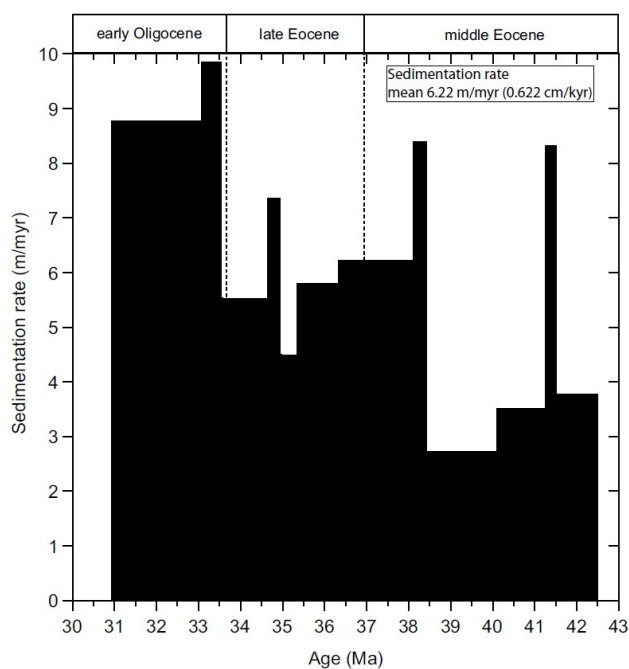
Figure 6.10. *Variation in sedimentation rate along the Middle Eocene-early Oligocene interval are shown as linear interpolation between the chron's boundary at Site 711. The average sedimentation rate is 6.22 m/myr. Age is from the Gee and Kent (2007) and Jovane et al. (2010) and depths are the meters below seafloor (mbsf).*

The new age model obtained in this study improves the dating of the bio-chronostratigraphical events during Eocene-Oligocene period. In this study we show that the Eocene-Oligocene boundary is placed approximately 33.7 Ma (~155 mbsf), at the top of the Chron C13r, which is in agreement with Touchard et al. (2003) and Jovane et al. (2006). Hole 711A represents the most complete and least disturbed paleomagnetic record from the northern Indian Ocean for the interval between from the middle Eocene to the early Oligocene. The defined age model for this section will allow further development of Eocene-Oligocene paleoceanographic records at this site with reliable age constraints. In particular, we are now able to define the Chrons C18n and C18r in Hole 711A, which span the interval of the MECO event (Bohaty and Zachos, 2003; Jovane et al., 2007; Bohaty et al., 2009; Edgar et al., 2010). We observe a decrease of the sedimentation rates along the Chron C18n, which can be easily related to the carbonate concentration data for the same interval (Peterson and Backman, 1990) showing that in this interval there is a decrease in carbonate mass accumulation rates (MARs) (Bohaty et al., 2009). We also observe an increase in sedimentation rates along Chrons 13n and 12r, which is attributed to deepening of the CCD (Coxall et al., 2005; Katz et al., 2008).

6.5. *Magnetic fingerprinting of the MECO event*

$CaCO_3$ data previously published by Bohaty et al. (2009) indicate a rapid shifts from high carbonate content (around 90 wt%) before and after the MECO event to very low carbonate contents (around zero) at its peak (Figures 6.8 and 6.9). The site 711A also records a distinct drop in carbonate MARs at 40.0 Ma. Bohaty et al. (2009) suggest that a shoaling of the CCD at the peak of the MECO event results in a total loss of the carbonate at the studied sections.

Environmental magnetic parameters for 310 samples were obtained at NOCS for the 70 m-thick interval of the Hole 711A (Figure 6.11). Magnetic susceptibility varies between 11.67 and 184.5×10^{-6} SI (Figure 6.11). A strong peak in the magnetic susceptibility is observed between ~180-190 mbsf, which is coincident with the MECO event. Magnetic

116

susceptibility is modulated by amount, but also by the grain size of ferromagnetic and ferrimagnetic materials in the sediments (e.g., Evans and Heller, 2003). In the same interval, a pronounced peak in the ARM data is observed. In contrats to the magnetic susceptibility, which is a bulk measurement influenced by all magnetic fractions and the paramagnetic matrix, the ARM is controlled only by the finest magnetic minerals (frequently SD grains). The ARM is thus a powerfull proxy for the concentration of fine magnetite (e.g., originated by eolian, biogenic, and impactoclastic processes) (Liu et al., 2012). The ARM/IRM$_{900mT}$ ratio shows a small increase during the MECO interval, indicanting an increase in magnetic grain size. HIRM values oscilate between 0.0006 and 0.9193 A/m along the studied section. This variation is very low and reflect the homogeneity of the magnetic mineral types across the section. This is corroborated by the S-ratio that varies in a narrow range between 0.96 and 1 consistent with the dominance of magnetite before, during, and after the the MECO event.
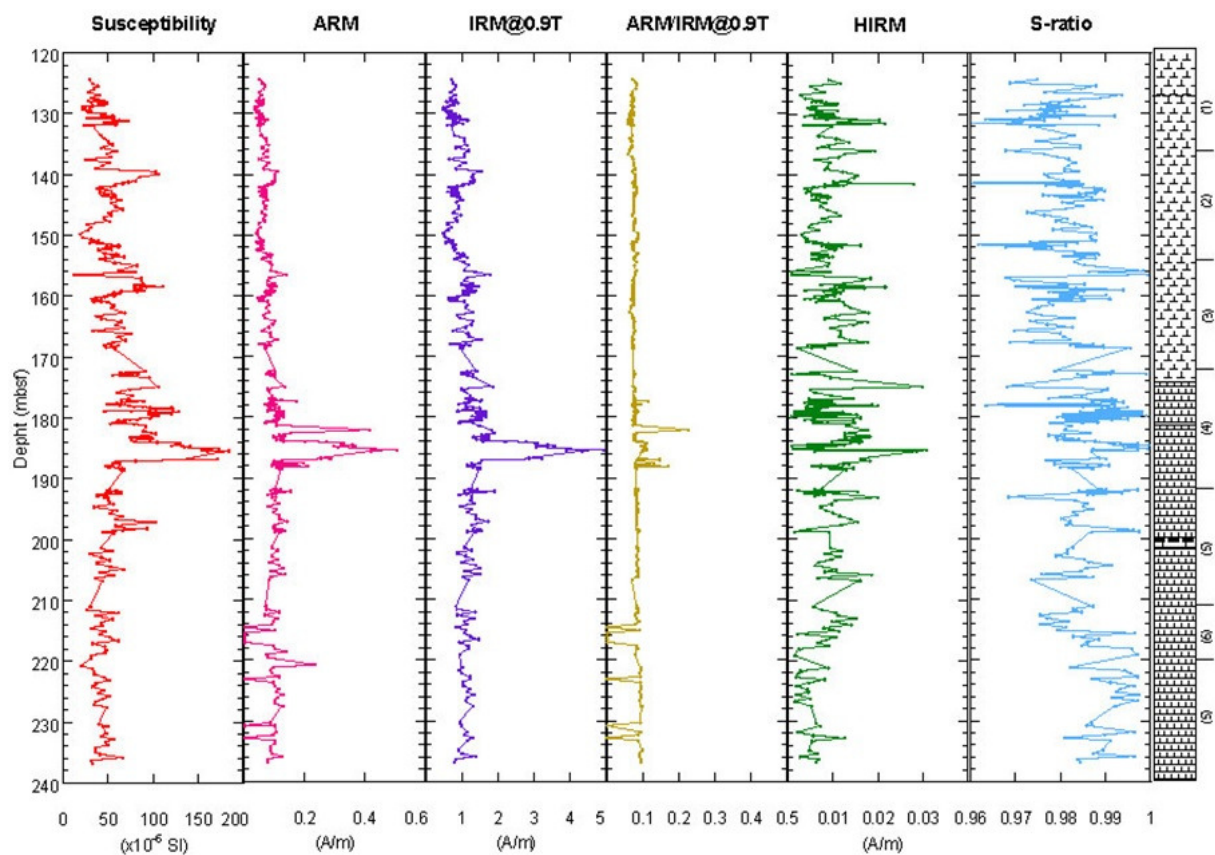
Figure 6.11. *Down-core variations in environmental magnetism parameters across the Eocene-Oligocene at ODP Hole 711A.*

The magnetic record of the ODP Hole 711A constrasts with that of the Monte Cagnero section, where magnetic and hematite were observed (see Chapter 4), with a characteristic increase in hematite at the MECO peak as evidenced by a distinctive incerase in HIRM. In ODP Hole 711A the HIRM does not show any significant peak coincident with the MECO interval. Hence, in this site the peak in magnetic properties at the MECO must be almost exclusively related to fine-grained magnetite. But is this magnetite related to magnetossomes? Recent data by Chang et al. (2012) posetively answer this question. Using transmission electron microscopy they reported giant bullet-shaped magnetite crystals (Figure 6.12) from ODP Hole 711A at the Middle Eocene Climatic Optimum (~40 Ma). Their results indicate a more widespread geographic, environmental, and temporal distribution of giant magnetofossils in the geological record with a link to "hyperthermal" events. They also suggest that enhanced global weathering during hyperthermals, and expanded suboxic diagenetic environments, probably provided more bioavailable iron that enabled biomineralization of giant magnetofossils. But in this case, the evidence for hematite dust and consequently of its potential as iron fertilizer is much weaker than in other sections.
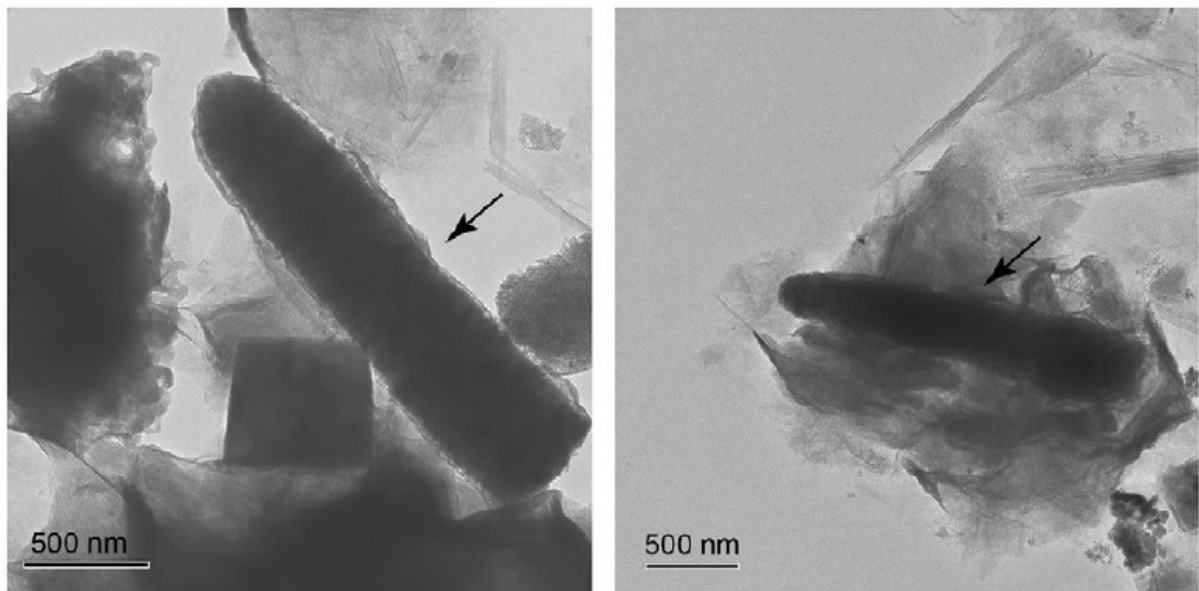
Figure 6.12. Transmission electron microscopy images of giant bullet-shaped magnetofossils during the MECO event extracted from Hole 711A (187.01 mbsf). Arrows indicate the giant bullet-shaped magnetites. The thinlayer surrounding the magnetite is amorphous silica (After Chang et al., 2012).

We performed FORC diagrams for samples from the same interval analyzed by Chang et al. (2012) in order to confirm the typical magnetic signal of the magnetossomes (Roberts et al., 2000; Egli et al., 2010). FORC distributions for these samples are nearly identical to those of the MCA samples at the MECO interval (Figure 6.13). These results further reinforce the widespread occurrence of magnetofossils throughout the MECO event, suggesting a link between the warming event and the increase in abundance of magnetotactic bacteria. Thereby, as previously proposed for the MCA section, the increase in magnetossome production may be related to enhanced global weathering and expanded suboxic diagenetic zones within sediments, providing more bioavailable iron to pelagic marine environments, which eased a key limiting factor for magnetite biomineralization and enabled growth of magnetofossils. The absence (or low-content) of hematite in ODP Hole 711A may suggest that in this case, local iron fertilization was not a necessary ingredient for magnetotactic blooming. Alternatively, it may also result from the complete consumption of this mineral for magnetossome production.
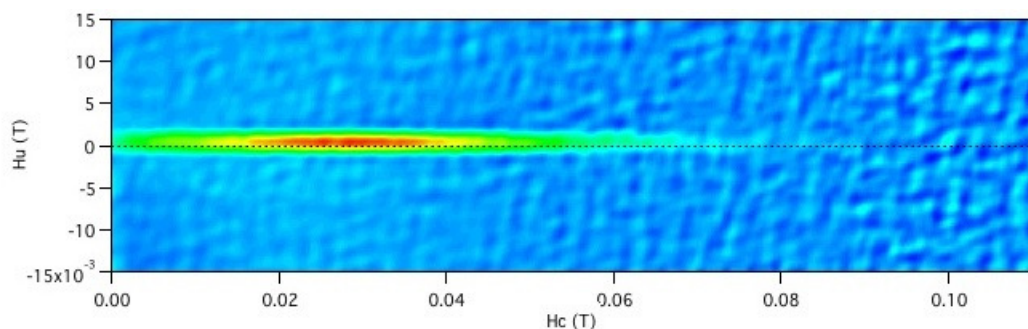
Figure 6.13. *Representative FORC diagram for a sample at 184.55 mbsf during the MECO event in ODP Hole 711A. FORC diagram indicate the presence of magnetostatically non-interacting SD magnetic particle assemblages that are typical of intact magnetite magnetofossil chains.*

6.6. Conclusions

We present a new magnetostratigraphic record and redefined age model for the middle Eocene-lower Oligocene interval of Indian Ocean ODP Hole 711A. The new

magnetostratigraphic results are integrated with published biostratigraphic results, and the integrated magnetozones are correlated to Chrons C19r to C12r, (~42.5 and 30.9 Ma). Our magnetostratigraphy provides the basis for further improvement based on cyclostratigraphy and astrochronology.

Isothermal remanence curves and hysteresis curves provide information on the magnetic mineralogy of the Hole 711A. The primary magnetic mineral carrier in pelagic sediments at this site is interpreted to be (titano)magnetite. Similar magnetic properties are observed throughout the study section.

Using our newly-developed age-depth model for the Eocene-Oligocene section of Hole 711A, it will be possible to document paleoceanographic variability within the middle Eocene-early Oligocene interval at this site. The Eocene-Oligocene transition and the MECO event, in particular, are present within continuous sections.

Our data indicate a decrease in the sedimentation rates at site 711 during the MECO event which may be related to the CCD shoaling inferred by Bohaty et al. (2009). In contrast, a considerable increase in the sedimentation rate during the Eocene-Oligocene transition is also observed in our magnetostratrigraphic data. This period is characterized by an abrupt stepwise onset of Antarctic glaciations, with a major deepening in the calcite compensation depth (CCD) (Coxall et al., 2005).

In addition to the previous report of magnetofossils in the ODP Hole 711A (Chang et al., 2012), we have identified the presence of magnetically non-interacting SD magnetic particles using FORC diagrams. Thereby, enhanced global weathering during warm climateseems to be responsible for enhanced magnetossome production worldwide. This may be related to the expansion of suboxic diagenetic zones within sediments, potentially providing in the pelagic marine environments more bioavailable iron, which is a key limiting factor for magnetite biomineralization (Roberts et al., 2011, Larrasoaña et al., 2012, Chang et al., 2012).

7. Conclusions and Perspectives

This thesis provides new insights into the magnetostratigraphy and paleoclimate fatures under the Peleogene period in the Neo-Tethys realm at the Umbria-Marche basin and the Indian Ocean. High-resolution integrated stratigraphy is used to stablish a robust temporal framework to correlate sections at inter-regional scale, and to unravel paleoceanographic and paleoclimatic signatures at the million years time scale. The main findings are:

➢ The Monte Cagnero section is the most complete and continuous stratigraphic sequence representing the middle Eocene to lower Oligocene interval (~55 to 28 Ma) currently identified in central Italy, spanning a time interval of at least ~13 Myr. New insights were obtained on the nature and age of these strata based on high-resolution magnetostratigraphic analyses and detailed calcareous nannofossil and planktonic foraminiferal analyses. These data form the basis of a new, robust age-depth model for the middle Eocene–lower Oligocene interval.

➢ The refined age information for this section, in addition to multi-disciplinary climatic proxy studies, that are currently ongoing, will allow reconstruction of environmental change across the greenhouse-icehouse transition. The Monte Cagnero section likely records the most important middle Eocene–early Oligocene climate events, such as the E-O climate transition at ~34 Ma and the MECO event at ~40 Ma. New insights into these events and related regional climate changes in the Tethys region will be obtained through future paleoclimatic studies of the Monte Cagnero section and application of the high-resolution integrated age-model presented here.

➢ An integrated and high-resolution analysis of stable isotopes, geochemistry, micropaleontology and environmental magnetism has been carried out in a 14 m-thick interval of the Monte Cagnero section corresponding to the ~40 Ma MECO. The data shows an interval of high productivity comprising the MECO climax and its aftermath marked by the presence of fossil magnetotactic bacteria. Intervals with higher concentration of magnetofossils correspond to those for which other proxies systematically point to an increase in productivity. In addition to the non-interacting SD magnetic fossils, hematite was recognized all along the MCA section with a peak

in the MECO interval and interpreted to be the result of aeolian dust transport. We speculate that this eolian hematite may have promoted iron fertilization of the oceans during the warming event increasing significantly the primary productivity in the ocean. This hypothesis must be tested on other coeval sections worldwide.

➤ The chapter 5 shows that the CHW–CR composite section offers a unique, complete and integrated record for the Palaeocene to early Eocene interval, thus providing a reference succession to study the early Palaeogene hyperthermals events and CIEs. Ongoing research on the magnetic signature of these events may provide clues for the mechanisms behind such climatic events and their biogeochemical feedbacks.

➤ We present a new magnetostratigraphic record and redefined age model for the middle Eocene-lower Oligocene interval of Indian Ocean ODP Hole 711A. The new magnetostratigraphic results are integrated with published biostratigraphic results, and the integrated magnetozones are correlated to Chrons C19r to C12r, (~42.5 and 30.9 Ma). We have identified the presence of magnetically non-interacting SD magnetic particles using FORC diagrams during the MECO event. The simultaneous occurrence of magnetofossils at the MECO intervals at ODP Hole 711A and Monte Cagnero, as well as the widespread occurrence of magnetofossils in other warming periods suggest a common mechanism linking climate warming and the enhancement of magnetossome production. Further work on hyperthermal intervals in the Umbria-Marche area were designed to test this correlation and to better understand the mechanisms behind it.

References

ACTON, G.D., OKADA, M., CLEMENT, B.M., LUND, S.P., WILLIAMS, T. 2002. Paleomagnetic overprints in ocean sediment cores and their relationship to shear deformation caused by piston coring. Journal of Geophysics Research. 107, 1–15.

ABRAJEVITCH, A. AND KODAMA, K. 2009. Biochemical vs. Detrital mechanism of remanence acquisition in marine carbonates: a lesson from the K–T boundary interval. Earth Planet. Sci. Lett. 286,269–277.

AGNINI, C., MUTTONI, G., KENT, D.V. and RIO, D. 2006. Eocene biostratigraphy and magnetic stratigraphy from Possagno, Italy: the calcareous nannofossil response to climate variability. Earth and Planetary Science Letters, 241, 815–830.

AGNINI, C., MACRÌ, P., BACKMAN, J., BRINKHUIS, H., FORNACIARI, E., GIUSBERTI, L., LUCIANI, V., RIO, D., SLUIJS, A. and SPERANZA, F., 2009. An early Eocene carbon cycle perturbation at ~52.5 Ma in the Southern Alps: chronology and biotic response. Paleoceanography, 24, PA209.

AITCHISON, J.C., ALI, J.R., and DAVIS, A.M. 2007. When and where did India and Asia collide?. Journal of Geophysical Research, 112, B05423.

ALLEN, M.B., JACKSON, J., and WALKER, R. 2004. Late Cenozoic reorganization of the Arabia-Eurasia collision and the comparison of shortterm and long-term deformation rates. Tectonics, 23, TC2008.

ALLEN, M.B. and ARMSTRONG, H.A. 2008. Arabia-Eurasia collision and the forcing of mid-Cenozoic global cooling. Palaeogeography, Palaeoclimatology, Palaeoecology, 265, 52-58.

ALVAREZ, W., ARTHUR, M. A., FISCHER, A. G., LOWRIE, W., NAPOLEONE, G., PREMOLI SILVA, I., AND ROGGENTHEN, W. 1977. Late Cretaceous-Paleocene geomagnetic reversal time scale: V. Type section in the pelagic limestone sequence at Gubbio, Italy. Geological Society of America Bulletin, 88, 383-389.

ALVAREZ, W. and MONTANARI, A. 1988. Geologic framework of the Northern Apennines pelagic carbonate sequence. In: I. PREMOLI SILVA, R. COCCIONI and A. MONTANARI (eds). The Eocene–Oligocene Boundary in the Marche–Umbria Basin (Italy). International Subcommission on Paleogene Stratigraphy Special Publication, Industrie Grafiche Fratelli Aniballi, Ancona, 13–30.

ANGORI, E., BERNAOLA, G. and MONECHI, S. 2007. Calcareous nannofossils assemblages and their response to the Paleocene–Eocene Thermal Maximum event at different latitudes: ODP Site 690 and Tethyan sections. In: MONECHI, S., COCCIONI, R. & RAMPINO, M.R. (eds) Large Ecosystem Perturbations: Causes and Consequences. Geological Society of America Special Paper, 424, 69–85.

ARENILLAS, I., MOLINA, E., ORTIZ, S. and SCHMITZ, B., 2008. Foraminiferal and δ^{13}C isotopic event–stratigraphy across the Danian–Selandian transition at Zumaya (northern Spain): chronostratigraphic implications. Terra Nova, 20, 38–44.

AUBRY, M.P. 1992. Late Paleogene calcareous nannoplankton evolution: a tale of climatic deterioration. In: Prothero, D.R., Berggren, W.A. (Eds.), Eocene-Oligocene climatic and biotic evolution. Princeton University Press, Princeton, New Jersey, 272–309.

AUBRY, M.P. 1995. Towards an upper Paleocene–lower Eocene high resolution stratigraphy based on calcareous nannofossil stratigraphy. Israel Journal of Earth–Sciences, 44, 239-253.

BARKER, P.F., FILIPPELLI, G.M., FLORINDO, F., MARTIN, E.E., AND SCHER, H.D. 2007. Onset and role of the Antarctic Circumpolar Current. Deep-Sea Research, Part II–Topical Studies in Oceanography. 54, 2388–2398.

BACKMAN, J. and HERMELIN, J.O.R. 1986. Morphometry of the Eocene nannofossil Reticulofenestra umbilicus lineage and its biochronological consequences. Palaeogeography, Palaeoclimatology, Palaeoecology, 57, 103–116.

BACKMAN, J., DUNCAN, R., MCDONALDS, A., BAKER, P., BAXTER, A., BOERSMA, A., CULLEN, J., DROXLER, A., FISK, M., GREENOUGH, J., HARGRAVES, R., HEMPEL, P., HOBART, M., HURLEY, M., JOHNSON, D., MIKKELSEN, N., OKADA, H., PETERSON, L., RIO, D., ROBINSON, S., SCHNEIDER, D., SWART, P., TATSUMI, Y., VANDAMME, D., VILKS, G., and VINCENT, E. 1988. Shipboard Scientific Party, Proceedings of the Ocean Drilling Program, 115.

BAINS, S., NORRIS, R.D., CORFIELD, R.M., FAUL, K.L., 2000.Termination of global warmth at the Palaeocene/Eocene boundary through productivity feedbacks. Nature, 407, 171–174.

BARRERA, E. and HUBER, B.T. 1993. Eocene and Oligocene oceanography and temperatures in the Antarctic Indian Ocean. In: Kennett, J.P., Warnke, D.A. (Eds.), The Antarctic paleoenvironment: a perspective on global change. AGU Ant. Res. Series, 60, 49–65.

BAUMANN, P., and ROTH, P.H., 1969. Zonierung des Obereozaens und Oligozaens des Monte Cagnero (Zentralapennin) mit planktonischen Foraminiferen und Nannoplankton, Eclogae Geologicae Helvetiae, 62, 303–323.

BAUMANN, P., 1970. Micropalaontologische und stratigraphische Untersuchungen der Obereozanen-Oligozanen Scaglia im zentralen Apennin (ltalien), Eclogae Geologicae Helvetiae, 63 (3), 1133–1211.

BAZYLINSKI, D.A. AND FRANKEL, R.B. 2003. Biologically controlled mineralization in prokaryotes. In: Weiner, S., Dove, P.M. (Eds.), Biomineralization, Mineralogical Society of America, Washington, DC., Rev. Mineral. 54, 95–114.

BAZYLINSKI, D.A. and FRANKEL, R.B. 2004. Magnetosome formation in prokaryotes. Nat. Rev. Microbiol. 2, 217–230.

BELLAGAMBA, M. and COCCIONI, R. 1990. Deep–water agglutinated foraminifera from the Massignano section (Ancona, Italy): A proposed stratotype for the Eocene–Oligocene boundary. In: HEMLEBEN, CH., KAMINSKI, M.A., KHUNT, W. and SCOTT D. (eds) Paleoecology, Biostratigraphy, Paleoceanography and Taxonomy of Agglutinated Foraminifera. Dordrecht, Netherlands, Kluwer, NATO ASI Series, 327, 883–921.

BERGGREN, W.A. and MILLER, K.G., 1989. Cenozoic bathyal and abyssal calcareous benthic foraminiferal zonation. Micropaleontology, 35, 308–320.

BERGGREN, W.A., KENT, D.V., SWISHER, C.C. and AUBRY, M.P. 1995. A Revised Cenozoic GeoChronology and Chronostratigraphy. In: BERGGREN, W.A., KENT, D.V., SWISHER III, C.C. and AUBRY, M.P. (eds) GeoChronology, Time and Global Stratigraphic Correlation. Special Publication–Society of Economic Paleontologist and Mineralogist SEPM (Society for Sedimentary Geology), Tulsa, OK, 54, 129–213.

BERGGREN, W.A. and PEARSON, P.N. 2005. A revised tropical to subtropical Paleogene planktonic foraminiferal zonation. Journal of Foraminiferal Research, 35, 279–298.

BERGGREN, W.A. and PEARSON, P.N. 2006. Tropical to subtropical planktonic foraminiferal zonation of the Eocene and Oligocene. In: PEARSON, P.N., OLSSON, R.K., HUBER, B.T. HEMLEBEN CH., and BERGGREN W.A. (eds) Atlas of Eocene Planktonic Foraminifera. Cushman Foundation Special Publication 41, 29–40.

BERNAOLA, G., BACETA, J.I., ORUE-EXTEBARRIA, X., ALEGRET, L., MARTIN-RUBIO, M., AROSTEGUI, J. and DINARE`S-TURELL, J., 2007. Evidence of an abrupt environmental disruption during the mid–Paleocene biotic event (Zumaia section, western Pyrenees). Geological Society of American Bulletin, 119, 785–795.

BESSE, J., and COURTILLOT, V., 1991. Revised and synthetic apparent polar wander paths of the African, Eurasian, North American and Indian plates, and true polar wander since 200 Ma. Journal of Geophysical Research, 96, 4029.

BICE, D.M. and MONTANARI, A. 1988. Magnetic stratigraphy of the Massignano section across the Eocene–Oligocene boundary. In: PREMOLI SILVA, I., COCCIONI , R. and MONTANARI, A. (eds). The Eocene/Oligocene Boundary in the Marche–Umbria Basin (Italy). International Subcommission on Paleogene Stratigraphy Special Publication, Industrie Grafiche Fratelli Aniballi, Ancona, 111–117.

BIJL, P. K., S. SCHOUTEN, ET AL. 2009. Early Palaeogene temperature evolution of the southwest Pacific Ocean. Nature, 461, 776-779.

BIJL, P.K., HOUBEN, A.J.P., SCHOUTEN, S., BOHATY, S.M., SLUIJS, A., REICHART, G-J., DAMSTE, J.S.S., and BRINKHUIS, H. 2010. Transient middle Eocene atmospheric CO_2 and temperature variations. Science, 330, 819-821.

BILLUPS, K. 2008, A tale of two climates. Nature Geoscience, 1, 294–295.

BLAKEMORE, R. 1975. Magnetotactic Bacteria. Science, 190, 377–379.

BLOEMENDAL, J., KING, J.W., HALL, F.R., DOH, S.-J. 1992. Rock magnetism of late Neogene and Pleistocene deep-sea sediments: relationship to sediment source, diagenetic processes, and sediment lithology. J. Geophys. Res. 97, 4361–4375.

BODISELITSCH, B., MONTANARI, A., KOEBERL, C. and COCCIONI, R. 2004. Delayed climate cooling in the late Eocene caused by multiple impacts: High resolution geochemical studies at Massignano, Italy. Earth and Planetary Science Letters, 223, 283–302.

BOHATY, S.M. and ZACHOS, J.C. 2003. Significant Sout 351 hern Ocean warming event in the late middle Eocene. Geology, 31, 1017-1020.

BOHATY, S.M., ZACHOS, J.C., FLORINDO, F. and DELANEY, M.L. 2009. Coupled greenhouse warming and deep-sea acidification in the middle Eocene. Paleoceanography, 24, PA2207, doi:10.1029/2008PA001676.

BOSELLINI, A. 1989. Dynamics of Tethyan carbonate platforms. In: CREVELLO, P., WILSON, J.L., SARG, R. and REED, R. (eds). Controls of carbonate platform and basin development. Society for Sedimentary Geology, Special Publication, 44, 3–14.

BOWEN, G.J., BRALOWER, T.J., DELANEY, M.K., DICKENS, G.R., KELLY, D.C., KOCH, P.L., KUMP, L.R., MENG, J., SLOAN, L.C., THOMAS, E., WING, S.L. and ZACHOS, J.C., 2006. Eocene hyperthermal event offers insight into greenhouse warming. EOS, 86, 165–169.

BOWN, P.R. and YOUNG, J.R. 1998. Techniques. In: Bown, P.R. (Eds.), Calcareous Nannofossil Biostratigraphy. Dordrecht, The Netherlands, Kluwer Academic Publications, 16–28.

BRINKHUIS, H. and BIFFI, U. 1993. Dinoflagellate cyst stratigraphy of the Eocene/Oligocene transition in central Italy. Marine Micropaleontology, 22, 131–183.

BRALOWER, T.J., PREMOLI SILVA, I. and MALONE, M.J., 2002. New evidence for abrupt climate change in the Cretaceous and Paleogene: an Ocean Drilling Program expedition to Shatsky Rise, northwest Pacific. Geol. Soc. Am. Today, 12, 4–10.

BROECKER, W.S. and CLARK, E., 1999. $CaCO_3$ size distribution: a paleocarbonate ion proxy? Paleoceanography, 14, 596–604.

BROECKER, W.S. and CLARK, E., 2001. Re-evaluation of the $CaCO_3$ size index paleocarbonate ion proxy. Paleoceanography, 16, 669–671.

BOWN, P.R., and YOUNG, J.R., 1998. Techniques. In Bown, P.R. (Ed.), Calcareous Nannofossil Biostratigraphy: Dordrecht, The Netherlands (Kluwer Academic Publisher), 16–28.

BRALOWER, T.J., PREMOLI SILVA, I. and MALONE, M.J., 2002. New evidence for abrupt climate change in the Cretaceous and Paleogene: an Ocean Drilling Program expedition to Shatsky Rise, northwest Pacific. Geol. Soc. Am. Today, 12, 4–10.

BROWN, R.E., KOEBERL, C., MONTANARI, A. and BICE D.M. 2009. Evidence for a change in Milankovitch forcing caused by extraterrestrial events at Massignano, Italy,

Eocene–Oligocene Boundary GSSP. In: KOEBERL, C. and MONTANARI, A. (eds). The Late Eocene Earth–Hothouse, Icehouse, and Impacts. Geological Society of America, Special Paper 452, 1–19.

CANDE, S.C. and KENT, D.V. 1995. Revised calibration of the geomagnetic polarity timescale for the Late Cretaceous and Cenozoic. Journal of Geophysical Research, 100, 6093–6095.

CENTAMORE, E., CHIOCCHINI, M., JACOBACCI, A., MANFREDINI, M. and MANGANELLI, P. 1980. The evolution of the Umbrian–Marchean Basin in the Apennine section of the Alpine orogenic belt (Central Italy). In: COGNE, J. and SLANSKY, M. (eds). Mémoire du Bureau de Recherches Géologiques et Minières, 108, 289–305.

CHANG, L., ROBERTS, A.P., WILLIAMS, W., FITZ GERALD, J.D., LARRASOAÑA, J.C., JOVANE, L., MUXWORTHY, A.R., 2012. Giant magnetofossils and hyperthermal events. Earth Planet. Sci. Lett. 351–352, 258–269.

CHANNELL, J.E.T., D'ARGENIO, B. and HORWATH, F. 1979. Adria, the African Promontory, in Mesozoic Mediterranean Palaeogeography. Earth Science Review, 15, 213–292.

CHANNELL, J.E.T., FREEMAN, R., HELLER, F., LOWRIE. W., 1982. Timing of diagenetic haematite growth in red pelagic limestones from Gubbio (Italy). Earth Planet. Science Letters, 58, 189-201.

CHANNELL, J.E.T., and McCABEL, C., 1994. Comparison of magnetic hysteresis parameters of unremagnetized and remagnetized limestones. Journal of Geophysical Research, 99, 4613-4623.

CHIARABBA, C., JOVANE, L. and DI STEFANO, R. 2005. A new view of Italian seismicity using 20 years of instrumental recordings. Tectonophyics, 395, 251–268.

COCCIONI, R., MONACO, P., MONECHI, S., NOCCHI, M. and PARISI, G. 1986. The Eocene/Oligocene boundary at Massignano (Ancona, Italy): Biostratigraphy based on calcareous nannofossils and planktonic foraminifera. Bulletin of Liaison and Information, International Geological Correlation Program Project 196, 6, 37–44.

COCCIONI, R., MONACO, P., MONECHI, S., NOCCHI, M. and PARISI, G. 1988. Biostratigraphy of the Eocene/Oligocene boundary at Massignano (Ancona, Italy). In: PREMOLI SILVA, I., COCCIONI, R. and MONTANARI, A. (eds). The Eocene–Oligocene Boundary in the Marche–Umbria Basin (Italy). International Subcommission on Paleogene Stratigraphy Special Publication, Industrie Grafiche Fratelli Aniballi, Ancona, 59–80.

COCCIONI, R., FRANCHI, R., NESCI, O., WEZEL, F.C., BATTISTINI, F. and PALLECCHI, P. 1989. Stratigraphy and mineralogy of the Selli Level (Early Aptian) at the base of the Marne a Fucoidi in the Umbro–Marchean Apennines, Italy. In: WIEDMANN J. (ed). Cretaceous of the Western Tethys. Proceedings 3rd International Cretaceous Symposium, Tübingen 1987, 563–584. E. Schweizerbart'sche Verlagsbuchhandlung, Stuttgart.

COCCIONI, R., MORANDI, N. and TATEO, F. 1994. The "Livello Raffaello" (early Miocene) in the Umbria–Marche Apennines, Italy: stratigraphy, paleontology, mineralogy, and geochemistry. In: COCCIONI, R., MONTANARI, A. and ODIN, G.S (eds). Miocene stratigraphy of Italy and adjacent regions. Giornale di Geologia, 56, 55–78.

COCCIONI, R., BASSO, D., BRINKHUIS, H., GALEOTTI, S., GARDIN, S., MONECHI, S. and SPEZZAFERRI, S. 2000. Marine biotic signal across a late Eocene impact layer at Massignano, Italy: evidence for long–term environmental perturbations? Terra Nova, 12, 258–263.

COCCIONI, R. and GALEOTTI, S. 2003. Deep–water benthic foraminiferal events from the Massignano Eocene/Oligocene boundary stratotype section and point (central Italy): Biostratigraphic, paleoecologic, and paleoceanographic implications. In: PROTHERO, D.R., IVANT, L.C. and NESBITT, E. (eds). From Greenhouse to Icehouse: The Marine Eocene–Oligocene Transition. New York, Columbia University Press, 438–452.

COCCIONI, R., MARSILI, A., MONTANARI, A., BELLANCA, A., NERI, R., BICE, D.M., BRINKHUIS, H., CHURCH, N., MACALADY, A., MCDANIEL, A., DEINO, A., LIRER, F., SPROVIERI, M., MAIORANO, P., MONECHI, S., NINI, C., NOCCHI, M., PROSS, J., ROCHETTE, P., SAGNOTTI, L., TATEO, F., TOUCHARD, Y., VAN SIMAEYS, S. and WILLIAMS, G.L. 2008. Integrated stratigraphy of the Oligocene pelagic sequence in the Umbria–Marche basin (northeastern Apennines, Italy): a potential Global Stratotype Section and Point (GSSP) for the Rupelian/Chattian boundary. Geological Society of America Bulletin, 120, 487–511.

COCCIONI, R., FRONTALINI, F. and SPEZZAFERRI, S. 2009. Late Eocene impact–induced climate and hydrological changes: Evidence from the Massignano global stratotype section and point (central Italy). Geological Society of America, Special Paper 452, 97–118.

COCCIONI, R., FRONTALINI, F., BANCALÀ, G., FORNACIARI, E., JOVANE, L. and SPROVIERI, M. 2010a. The Dan–C2 hyperthermal event at Gubbio (Italy): Global implications, environmental effects, and cause(s). Earth and Planetary Science Letters, 297, 298–305.

COCCIONI, R., BANCALÀ, G., CATANZARITI, R., FRONTALINI, F., JOVANE, L. and SPROVIERI, M., 2010b. The Selandian–Thanetian transition event (STTE): an abrupt environmental change at Contessa Road (Gubbio, Italy). Geoevents, Geological Heritage, and the Role of the International Geoscience Program. Caravaca de la Crux, Spain, 15th–18th September 2010, 121.

COCCIONI, R., BANCALÀ, G., CATANZARITI, R., FORNACIARI, E., FRONTALINI, F., GIUSBERTI, L., JOVANE, L., LUCIANI, V., SAVIAN, J., SPROVIERI, M., 2012. An integrated stratigraphic record of the Palaeocene–lower Eocene at Gubbio (Italy): new insights into the early Palaeogene hyperthermals and carbon isotope excursions. Terra Nova, 24, 380-386, doi: 10.1111/j.1365-3121.2012.01076.x.

COLOSIMO, A.B., BRALOWER, T.J. and ZACHOS, J.C., 2006. Evidence of lysocline shoaling at the Paleocene/Eocene Thermal Maximum on Shatsky Rise, northwest

Pacific. In: Bralower, T.J., et al. (Eds) Proc. Ocean Drilling Program, Sci. Res. 198, 1–36, College Station, Texas.

CORFIELD, R.M., CARTLIDGE, J.E., PREMOLI-SILVA, I., AND HOUSLEY, R.A. 1991. Oxygen and carbon isotope stratigraphy of the Palaeogene and Cretaceous limestones on the Bottaccione Gorge and the Contessa Highway sections, Umbria, Italy. Terra Nova, 3, 414–422.

COX, A., and GORDON, R.G. 1984. Paleolatitudes determined from paleomagnetic data from vertical cores. Reviews of Geophysics and Space Physics, 22, 47-72.

COXALL, H.K., WILSON, P.A., PÄLIKE, H., LEAR, C.H. and BACKMAN, J. 2005. Rapid stepwise onset of Antarctic glaciations and deeper calcite compensation in the Pacific Ocean. Nature, 433, 53-57.

COXALL, H.K. and WILSON, P.A. 2011. Early Oligocene glaciation and productivity in the eastern equatorial Pacific: Insights into global carbon cycling. Paleoceanography, 26, PA2221.

CHADIMA, M. and HROUDA, F. 2006. Remasoft 3.0 a user-friendly paleomagnetic data browser and analyzer. Travaux Géophysiques, XXVII, 20-21.

CRAMER, B.S., WRIGHT, J.D., KENT, D.V. and AUBRY, M.-P., 2003. Orbital climate forcing of $\delta^{13}C$ excursions in the late Paleocene–early Eocene (chrons C24n– C25n). Paleoceanography, 18, PA1097.

CRESTA, S., MONECHI, S. and PARISI, G. 1989. Stratigrafia del Mesozoico e Cenozoico nell'area umbro–marchigiana, Itinerari geologici sull'Appennino Umbro–Marchigiano (Italia). Memorie Descrittive della Carta Geologica d'Italia, 39, 1–185.

DAWBER, C., TRIPATI, A., 2011, Constraints on glaciation in the Middle Eocene (46-37 Ma) from Ocean Drilling Program (ODP) Site 1209 in the tropical Pacific Ocean, Paleoceanograph, 26, PA2208, doi:10.1029/2010PA002037.

DAY, R., FULLER, M. and SCHMIDT, V.A. 1977. Hysteresis properties of titanomagnetites: Grain-size and compositional dependence. Physics of the Earth and Planetary Interiors, 13, 260-267.

DeCONTO, R.M. and POLLARD, D. 2003. Rapid Cenozoic glaciations of Antarctic induced by declining atmospheric CO_2. Nature, 421, 245-249.

DERCOURT, J., RICOU, L.E., and VRIELYNCK, B., 1993, Atlas Tethys Paleoenvironmental Maps: Paris, Gauthiers-Villars, p. 1–307.

DICKENS, G.R., 1999. The blast in the past. Nature, 401,752–755.

DUNCAN, R. A., 1981. Hotspots in the southern oceans-an absolute frame of reference for motion of the Gondwana continents. Tectonophysics, 74, 29-42.

DUNCAN, R.A., BACKMAN, J. and PETERSON, L.C. 1990. Scientific Results, Proceedings of the Ocean Drilling Program, 115.

DUNLOP, D.J. 1979. On the use of Zijderveld vector diagrams in multicomponent paleomagnetic studies. Physics of the Earth and Planetary Interior, 20, 12-24.

DUNLOP, D.J. AND ÖZDEMIR, Ö. 1997. Rock magnetism: Fundamentals and frontiers, 573 pp, Cambridge University Press, Cambridge.

DUNLOP, D.J., 2002. Theory and application of the Day plot (Mrs/Ms versus Hcr/Hc) 1. Theoretical curves and tests using titanomagnetite data. J. Geophys. Res. 107 (B3), 2056.

EDGAR, K.M., WILSON, P.A., SEXTON, P.F., and SUGANUMA, Y., 2007. No extreme bipolar glaciation during the main Eocene calcite compensation shift. Nature, 44, 908-911. doi:10.1038/nature06053

EDGAR, K.M., WILSON, P.A., SEXTON, P.F., GIBBS, S.J., ROBERTS, A.P. and NORRIS, R.D. 2010. New biostratigraphy, magnetostratigraphy and isotopic insights into the Middle Eocene Climatic Optimum in low latitudes. Palaeogeography, Palaeoclimatology, Palaeoecology, 297, 670-682.

EGLI, R., 2004. Characterization of individual rock magnetic components by analysis of remanence curves, 1. Unmixing natural sediments. Stud. Geophys. Geod. 48, 391–446.

EGLI, R., CHEN, A.P., WINKLHOFER, M., KODAMA, K.P., HORNG, C.S., 2010. Detection of noninteracting single domain particles using first-order reversal curve diagrams. Geochem. Geophys. Geosyst. 11, Q01Z11, doi:10.1029/2009GC002916.

EVANS, M.E., HELLER, F., 2003. Environmental Magnetism. Principles and Applications of Enviromagnetics. Academic Press, pp. 299.

FAIVRE, D., SCHÜLER, D., 2008. Magnetotactic bacteria and magnetosomes. Chem. Rev. 108, 4875–4898.

FENNER, J. and MIKKELSEN, N. 1990. Eocene-Oligocene diatoms in the western Indian Ocean: taxonomy, stratigraphy, and paleoecology. Proceedings of the Ocean Drilling Program, 115, 433-466.

FLORINDO, F., FARMER, R.K., HARWOOD, D.M., CODY, R.D., LEVY, R., BOHATY, S.M., CARTER, L., WINKLER, A., 2013. Palaeomagnetism of sediments from Southern Ocean ODP Site 744 (southern Kerguelen Plateau): implications for early-to-middle Miocene climate in Antarctica, Global Planet. Change, in press.

FORNACIARI, E., RAFFI, I., RIO, D., VILLA, G., BACKMAN, J. and OLAFSSON, G. 1990. Quantitative distribution patterns of Oligocene and Miocene calcareous nannofossils from the western equatorial Indian Ocean. Proceedings of the Ocean Drilling Program, 115, 237-254.

FORNACIARI, E., GIUSBERTI, L., LUCIANI, V., TATEO, F., AGNINI, C., BACKMAN, J., ODDONE, M. and RIO, D. 2007. An expanded Cretaceous–Tertiary transition in a pelagic setting of the Southern Alps (central–western Tethys). Palaeogeography, Palaeoclimatology, Palaeoecology, 255, 98–131.

FORNACIARI, E., AGNINI, C., CATANZARITI, R., RIO, D., BOLLA, E.M., and VALVASONI, E., 2010. Mid-Latitude calcareous nannofossil biostratigraphy and biochronology across the middle to late Eocene transition. Stratigraphy, 7, 229-264.

FULLER, M., HASTEDT, M., and HERR, B., 1998. Coring induced magnetization of recovered sediments. In:Weaver, P.P.E., Schminke, H.-U., Firth, J.V., Duffield,W. (Eds.), Proceedings of the Ocean Drilling Program, 157. College Station, TX, 47–56 (Ocean Drilling Program).

GALEOTTI, S., ANGORI, E., COCCIONI, R., FERRARI, G., GALBRUN, B., MONECHI, S., PREMOLI SILVA, I., SPEIJER, R. and TURI, B. 2000. Integrated stratigraphy across the Paleocene/Eocene boundary in the Contessa Road section, Gubbio (central Italy). Bulletin de la Société Géologique de France, 171, 355–365.

GALEOTTI, S., KAMINSKI, M.A., SPEIJER, R. and COCCIONI, R. 2004. High resolution Deep Water Agglutinated Foraminiferal record across the Paleocene/Eocene transition in the Contessa Road section (central Italy). In: BUBIK, M. and KAMINSKI M.A. (eds). Proceedings of the 6th International Workshop on Agglutinated Foraminifera. Grzybowski Foundation Special Publication, 8, 83–103, Arti Grafiche Editoriali, Urbino.

GALEOTTI, S., KRISHNAN, S., PAGANI, M., LANCI, L., GAUDIO, A., ZACHOS, J.C., MONECHI, S., MORELLI, G. and LOURENS, L. 2010. Orbital Chronology of Early Eocene hyperthermals from the Contessa Road section, central Italy. Earth and Planetary Science Letters, 290, 192–200.

GARDIN, S., MONECHI, S., 1998. Palaeoecological change in middle to low latitude calcareous nannoplankton at the Cretaceous/Tertiary boundary. Bull. Soc. Geol. France. 169, 709–723.

GEE, J. S. and KENT, D. V. 2007. Source of oceanic magnetic anomalies and the geomagnetic polarity time scale. Geomagnetism. In: Kono, M. (ed.) Treatise on Geophysics. Elsevier, Amsterdam, 5, 455–507.

GIBBS, S.J., BRALOWER, T.J., BOWN, P.R., ZACHOS, J.C., BYBELL, L., 2006. Shelf-open ocean calcareous phytoplankton assemblages across the Paleocene–Eocene Thermal Maximum: implications for global productivity gradients. Geology 34, 233–236.

GIUSBERTI, L., COCCIONI, R., SPROVIERI, M. and TATEO, F. 2009. Perturbation at the sea floor during the Paleocene–Eocene Thermal Maximum: Evidence from benthic foraminifera at Contessa Road, Italy. Marine Micropaleontology, 70, 102–119.

GRADSTEIN, F.M., OGG, J.G. and SMITH, A.G. 2004. A Geologic Time Scale 2004. Cambridge University Press, Cambridge.

GUERRERA, F., MONACO, P., NOCCHI, M., PARISI, G., FRANCHI, R., VANNUCCI, S., and GIOVANNINI, G., 1988. La Scaglia Variegata Eocenica nella sezione di Monte Cagnero (bacino marchigiano interno): Studio litostratigrafico, petrografico e biostratigrafico. Bollettino Società Geologica Italiana, 107, 81–99.

HANCOCK, H.J.L., DICKENS, G.R., 2005. Carbonate dissolution episodes in Paleocene and Eocene sediment, Shatsky Rise, West-Central Pacific. Proc.Ocean Drilling Program, Sci. Res., College Station, Texas 198, pp. 1–58.

HANDLEY, L., O'HALLORAN, A., PEARSON, P.N., HAWKINS, E., NICHOLAS, C.J., SCHOUTEN, S., MCMILLAN, I.K., PANCOST, R.D., 2012. Changes in the hydrological cycle in tropical East Africa during the Paleocene-Eocene thermal maximum. Palaeogeogr. Palaeoclimatol. Palaeoecol. 329–330, 10–21.

HAQ, B.U., LOHMANN, G.P., 1976. Early Cenozoic calcareous nannoplankton biogeography of the Atlantic Ocean. Mar. Micropal. 1, 119–194.

HATCH, J.R., LEVENTHAL, J.S., 1992. Relationship between inferred redox potential of the depositional environment and geochemistry of the Upper Pennsylvanian (Missourian) Stark Shale Member of the Dennis Limestone, Wabaunsee County, Kansas, U.S.A. Chem. Geol. 99, 65–82.

HEMPEL, P. and BOHRMANN, G. 1990. Carbonate-free sediment components and aspects of silica diagenesis at Sites 707, 709, and 711 (Leg 115, western Indian Ocean). Proceedings of the Ocean Drilling Program, 115, 677-698.

HESLOP, D., DEKKERS, M.J., KRUIVER, P.P., VAN OORSCHOT, I.H.M., 2002. Analysis of isothermal remanent magnetisation acquisition curves using the expectation–maximization algorithm. Geophys. J. Int. 148, 58–64.

HESSE, P.P., 1994. Evidence for bacterial palaeoecological origin of mineral magnetic cycles in oxic and sub-oxic Tasman Sea sediments. Mar. Geol. 117, 1–17.

HOUSEN, B.A., MOSKOWITZ, B.M., 2006. Depth distribution of magnetofossils in near surface sediments from the Blake/Bahama Outer Ridge, western North Atlantic Ocean, determined by low-temperature magnetism. J. Geophys. Res. 111, G01005.

HROUDA, F., 1994. A technique for the measurement of thermal changes of magnetic susceptibility of weakly magnetic rocks by the CS-2 apparatus and KLY-2 Kappabridge. Geophysical Journal International, 118 (3), 604–612.

HROUDA, F., 2003. Indices for numerical characterization of the alteration processes of magnetic minerals taking place during investigation of temperature variation of magnetic susceptibility. Studia Geophysica et Geodaetica, 47, 847–861.

HYLAND, E., MURPHY, B., VARELA, P., MARKS, K., COLWELL, L., TORI, F., MONECHI, S., CLEAVELAND, L., BRINKHUIS, H., VAN MOURIK, C.A., COCCIONI, R., BICE, D. and MONTANARI, A. 2009. Integrated stratigraphy and astrochronologic calibration of the Eocene–Oligocene transition in the Monte Cagnero section (Northeastern Apennines, Italy): A potential parastratotype for the Massignano GSSP. In: KOEBERL, C. & MONTANARI, A. (eds) The Late Eocene Earth–Hothouse, Icehouse and Impacts. Geological Society of America, Special Paper 452, 303–322.

IVANY, L.C., LOHMANN, K.C., HASIUK, F., BLAKE, D.B., GLASS, A., ARONSON, R.B. and MOODY, R.M. 2008. Eocene climate record of a high southern latitude

continental shelf: Seymour Island, Antarctica. The Geological Society of America Bulletin, 120, 659– 678, doi:10.1130/B26269.1.

JOHNSON, D.A. 1990. Radiolarian biostratigraphy in the central Indian Ocean, Leg 115. Proceedings of the Ocean Drilling Program, 115, 395-410.

JONES, B., MANNING, D.A.C., 1994. Comparison of geochemical indices used for the interpretation of palaeoredox conditions in ancient mudstones. Chem. Geol. 111, 111–129.

JOVANE, L., FLORINDO, F. and DINARÈS–TURELL, J. 2004. Environmental magnetic record of paleoclimate change: revisiting the Eocene–Oligocene stratotype section, Massignano, Italy. Geophysical Research Letters, 31, doi: 10.1029/2004GL020554.

JOVANE, L., FLORINDO, F., SPROVIERI, M., and PÄLIKE, H. 2006. Astronomic calibration of the late Eocene/early Oligocene Massignano section (central Italy). Geochemistry Geophysics Geosystems, 7, p. Q07012, doi:10.1029/2005GC001195.

JOVANE, L., SPROVIERI, M., FLORINDO, F., ACTON, G., COCCIONI, R., DALL'ANTONIA, B. and DINARÈS-TURELL, J. 2007a. Eocene-Oligocene paleoceanography changes in the stratotype section, Massignano, Italy: clues from rock magnetism and stable isotopes. Journal of Geophysical Research, 112, B11101.

JOVANE, L., FLORINDO, F., COCCIONI, R., DINARÈS–TURELL, J., MARSILI, A., MONECHI, S., ROBERTS, A.P. and SPROVIERI, M. 2007b. The middle Eocene climatic optimum (MECO) event in the Contessa Highway section, Umbrian Apennines, Italy. Geological Society of America Bulletin, 119, 413–427.

JOVANE, L., ACTON, G., FLORINDO, F. and VEROSUB, K.L. 2008. Geomagnetic field behavior at high latitudes from a paleomagnetic record from Eltanin core 27-21 in the Ross Sea sector, Antarctica. Earth and Planetary Science Letters, 267, 435-443.

JOVANE, L., COCCIONI, R., MARSILI, A., FLORINDO, F., ACTON, G. and SPROVIERI, M. 2009. The late Eocene greenhouse–icehouse transition: Observations from the Massignano Global Stratotype Section and Point (GSSP). In: KOEBERL, C. & MONTANARI, A. (eds) The Late Eocene Earth–Hot House, Ice House, and Impacts. Geological Society of America, Special Paper 452, 149–168.

JOVANE, L., SPROVIERI, M., COCCIONI, R., FLORINDO, F., MARSILI, A. and LASKAR, J. 2010. Astronomical calibration of the middle Eocene Contessa Highway section (Gubbio, Italy). Earth and Planetary Science Letters, 298, 77–88.

JOVANE, L., FLORINDO, F., BAZYLINSKI, D.A., LINS, U., 2012. Prismatic magnetite magnetosomes from cultivated Magnetovibrio blakemorei strain MV-1: a magnetic fingerprint in marine sediments? Env. Microb. Rep.

JOVANE, L., SAVIAN, J., COCCIONI, R., FRONTALINI, F., BANCALÀ, G., CATANZARITI, R., LUCIANI, L., BOHATY, S., WILSON, P., AND FLORINDO, F. (2013). Integrated magnetobiostratigraphy of the middle Eocene-lower Oligocene interval from the Monte Cagnero section, central Italy. Geological Society, London, Special Publications, 373, first published March 25, 2013; doi 10.1144/SP373.13.

KATZ, M.E., MILLER, K.G., WHIGHT, J.D., WADE, B.S., BROWNING, J.V., CRAMER, B.S. and ROSENTHAL, Y. 2008. Stepwise transition from the Eocene greenhouse to the Oligocene icehouse. Nature Geoscience, 1, 329-334.

KENNETT, J.P., and SHACKLETON, N.J., 1976, Oxygen isotopic evidence for development of psychrosphere 38 Myr ago: Nature, 260, 513–515.

KENNETT, J.P. 1977. Cenozoic evolution of Antarctic glaciation, the Circum-Antarctic Ocean, and their impact on global paleoceanography. Journal of Geophysical Research, 82, 3843-3860.

KENNETT, J.P. and STOTT, L.D., 1991. Abrupt deep–sea warming, palaeoceanographic changes and benthic extinctions at the end of the Palaeocene. Nature, 353, 225–229.

KIDD, R.B., RAMSAY, A.T.S., SYKES, T.J.S., BALDAUF, J.G., DAVIES, T.A., JENKINS, D.G., and WISE. JR.S.W., 1992. An Indian Ocean framework for paleoceanographic synthesis based on DSDP and ODP results. Synthesis of Results from Scientific Drilling in the Indian Ocean, Geophysical Monograph 70, 403-422.

KIRSCHVINK, J.L. 1980. The least-squares line and plane and the analysis of palaeomagnetic data. Geophysical Journal of the Royal Astronomical Society, 62, 699-710.

KOPP, R.E., KIRSCHVINK, J.L., 2008. The identification and biogeochemical interpretation of fossil magnetotactic bacteria. Earth-Sci. Rev. 86, 42–61.

KRÁSA, D., MUXWORTHY, A.R. and WILLIAMS, W. 2011. Room and low-temperature magnetic properties of 2-D magnetite particles arrays. Geophysical Journal International, doi: 10.1111/j.1365-246X.2011.04956.x.

KRAUS, M.J., RIGGINS, S., 2007. Transient drying during the Paleocene–Eocene Thermal Maximum (PETM): analysis of paleosols in the Bighorn Basin, Wyoming. Palaeogeogr. Palaeoclimatol. Palaeoecol. 245, 444–461.

KRUIVER, P.P., DEKKERS, M.J., HESLOP, D., 2001. Quantification of magnetic coercivity components by the analysis of acquisition curves of isothermal remanent magnetization. Earth Planet. Sci. Lett. 189, 269–276.

LANCI, L., LOWRIE, W., AND MONTANARI, A., 1996, Magnetostratigraphy of the Eocene/Oligocene boundary in a short drill-core: Earth and Planetary Science Letters, 143, 37–48.

LANCI, L., and LOWRIE, W., 1997, Magnetostratigraphic evidence that 'tiny wiggles' in the oceanic magnetic anomaly record represent geomagnetic paleointensity variations: Earth and Planetary Science Letters, 148, 581–592.

LANCI, L., LOWRIE, W., and MONTANARI, A., 1998, Stratigrafi a magnetica ad alta risoluzione del limite Eocene-Oligocene nella successione Umbro-Marchigiana: Atti della Accademia Nazionale dei Lincei, Rendiconti diFisica dell'Accademia dei Lincei, 9, 109–129.

LARRASOAÑA, J.C., ROBERTS, A.P., CHANG, L., SCHELLENBERG, S.A., FITZ GERALD, J.D., NORRIS, R.D., ZACHOS, J.C., 2012. Magnetotactic bacterial response to Antarctic dust supply during the Paleocene-Eocene thermal maximum. Earth Planet. Sci. Lett. 333–334, 122–133.

LEAN, C.M.B., MCCAVE, I.N., 1998. Glacial to interglacial mineral magnetic and palaeoceanographic changes at Chatham Rise, SW Pacific Ocean. Earth Planet. Sci. Lett.163, 247–260.

LEAR, C.H., ELDERFIELD, H. and WILSON, P.A. 2000. Cenozoic deep-sea temperatures and global ice volumes from Mg/Ca in benthic foraminiferal calcite. Science, 287, 269-272.

LEON-RODRIGUEZ, L., DICKENS, G.R., 2010. Constraints on ocean acidification associated with rapid and massive carbon injections: the early Paleogene record at Ocean Drilling Program Site 1215, equatorial Pacific Ocean. Palaeogeogr. Palaeoclimatol. Palaeoecol. 298, 409–420.

LIRER, F., 2000. A new technique for retrieving calcareous microfossils from lithified lime deposits. Micropaleontology, 46, 365–369.

LIU, Q.S., ROBERTS, A.P., TORRENT, J., HORNG, C.S., LARRASOAÑA, J.C., 2007. What do the HIRM and S-ratio really measure in environmental magnetism? Geochem. Geophys. Geosyst. 8, Q09011, doi:10.1029/2007GC001717.

LIU, Q., ROBERTS, A.P., LARRASOAÑA, J.C., BANERJEE, S.K., GUYODO, Y., TAUXE, L., OLDIFIELD, F., 2012. Environmental magnetism: principles and applications. Rev. Geophys. 50, RG4002, doi:10.1029/2012RG000393.

LIVERMORE, R., NANKIVELL, A., EAGLES, G., and MORRIS, P., 2005, Paleogene opening of Drake Passage, Earth and Planetary Science Letters, 236, 459–470, doi: 10.1016/j.epsl.2005.03.027.

LOURENS, L.J., SLUIJS, A., KROON, D., ZACHOS, J.C., THOMAS, E., RÖHL, U., BOWLES, J. and RAFFI, I., 2005. Astronomical pacing of late Palaeocene to early Eocene global warming events. Nature, 435, 1083–1087.

LOWRIE, W., ALVAREZ, W., NAPOLEONE, G., PERCH–NIELSEN, K., PREMOLI SILVA, I. and TOUMARKINE, M. 1982. Paleogene magnetic stratigraphy in Umbrian pelagic carbonate rocks: The Contessa sections, Gubbio. Geological Society of America Bulletin, 93, 414–432.

LOWRIE, W. and LANCI, L. 1994. Magnetostratigraphy of Eocene–Oligocene boundary sections in Italy: No evidence for short subchrons within chrons 12R and 13R. Earth and Planetary Science Letters, 126, 247–258.

LUCIANI, V., GIUSBERT, L., AGNINI, C., FORNACIARI, E., RIO, D., SPOFFORTH, D.J.A. and PÄLIKE, H. 2010. Ecological and evolutionary response of Tethyan phanktonic foraminifera to the middle Eocene climatic optimum (MECO) from the Alano section (NE Italy). Palaeogeography, Palaeoclimatology, Palaeoecology, 292, 82-95.

LUNT, D.J., RIDGWELL, A., SLUIJS, A., ZACHOS, J., HUNTER, S. and HAYWOOD, A., 2011. A model for orbital pacing of methane hydrate destabilization during the Palaeogene. Nature Geoscience, 4, 775–778.

LUTERBACHER, H.P., ALI, J.R., BRINKHUIS, H., GRADSTEIN, F.M., HOOKER, J.J., MONECHI, S., OGG, J.G., POWELL, J., RÖHL, U., SANFILIPPO, A., and SCHMITZ, B., 2004. The Paleogene period, in Gradstein, F.M., Ogg, J.G., and Smith, A.G., eds., A geologic time scale: Cambridge University Press, Cambridge, 384–408.

LYLE, M.W., OLIVAREZ LYLE, A., BACKMAN, J., and TRIPATI, A., 2005. Biogenic sedimentation in the Eocene equatorial Pacific: the stuttering greenhouse and Eocene carbonate compensation depth, in Lyle, M., Wilson, P., and Firth, J., eds., Proceedings of the Ocean Drilling Program, Scientific Results, Volume 199: College Station TX, Ocean Drilling Program, 1-35 doi:10.2973/odp.proc.sr.199.219.2005. http://wwwodp.tamu.edu/publications/199_SR/219/219.htm

LYLE, M., GIBBS, S., MOORE, T.C. and REA D.K. 2007. Late Oligocene initiation of the Antarctic Circumpolar Current: evidence from the South Pacific. Geology, 35, 691-694.

MAHER, B.A., PROSPERO, J.M., MACKIE, D., GAIERO, D., HESSE, P.P., BALKANSKI, Y., 2010. Global connections between aeolian dust, climate and ocean biogeochemistry at the present day and at the Last Glacial Maximum. Earth Sci. Rev. 99, 61-97.

MARTINI, E. 1971. Standard Tertiary and Quaternary Calcareous Nannoplankton Zonation. In: FARINACCI, A. (ed). Proceedings of the Second Planktonic Conference, Rome 1970: Rome, Tecnoscienza, 2, 739–785.

MATTIAS, P., CROCETTI, G., BARRESE, E., MONTANARI, A., COCCIONI, R., FARABOLLINI, P. and PARISI, E. 1992. Caratteristiche mineralogiche e litostratigrafiche della sezione eo–oligocenica di Massignano (Ancona, Italia) comprendente il limite Scaglia Variegata–Scaglia Cinerea. Studi Geologici Camerti, 12, 93–103.

McFADDEN, P.L., and REID, A.B. 1982. Analysis of palaeomagnetic inclination data. Geophysical Journal of the Royal Astronomical Society, 69, 307-319.

MERICO, A., TYRRELL, T. and WILSON, P.A. 2008. Eocene/Oligocene ocean de-acidification linked to Antarctic glaciations by sea-level fall. Nature, 452, 979-983.

MIKKELSEN, N. 1990. Cenozoic diatom biostratigraphy and paleoceanography of the western equatorial Indian Ocean. Proceedings of the Ocean Drilling Program, 115, 411-432.

MILLER, K.G., WRIGHT, J.D. AND FAIRBANKS, R.G. 1991. Unlocking the ice house: Oligocene-Miocene oxygen isotopes, eustasy, and margin erosion. Journal of Geophysical Research, 96, 6829-6948.

MOLINA, E., ALEGRET, L., APELLANIZ, E., BERNAOLA, G., CABALLERO, F., DINARÈS–TURELL, J., HARDENBOL, J., HEILMANN–CLAUSEN, C., LARRASOAÑA, J.C., LUTERBACHER, H., MONECHI, S., ORTIZ, S., ORUE–ETXEBARRIA, X., PAYROS, A., PUJALTE, V., RODRÍGUEZ–TOVAR, F., J.,

TORI, F., TOSQUELLA, J. and UCHMAN, A. 2011. The Global Stratotype Section and Point (GSSP) for the base of the Lutetian Stage at the Gorrondatxe section, Spain. Episodes, 34, 86–108.

MONACO, P., NOCCHI, M. and PARISI, G. 1987. Analisi stratigrafica e sedimentologica di alcune sequenze pelagiche dell'Umbria sud–orientale dall'Eocene inferiore all'Oligocene inferiore. Bollettino della Società Geologica Italiana, 106, 71–91.

MONTANARI, A., CAREY, S., COCCIONI, R. and DEINO, A. 1994. Early Miocene tephra in the Apennine pelagic sequence: an inferred Sardinian provenance and implications for western Mediterranean tectonics. Tectonics, 13, 1120–1134.

MONTANARI, A., BICE, D.M., CAPO, R., COCCIONI, R., DEINO, A., DEPAOLO, D.J., EMMANUEL, L., MONECHI, S. RENARD, M. and ZEVENBOOM, D. 1997. Integrated stratigraphy of the Chattian to Mid–Burdigalian pelagic sequence of the Contessa Valley (Gubbio, Italy). In: MONTANARI, A., ODIN, G.S. and COCCIONI, R. Miocene Stratigraphy–An Integrated Approach. Developments in Palaeontology and Stratigraphy, 15, 249–277.

MONTANARI, A. and KOEBERL C. 2000. Impact stratigraphy–The Italian record. Lecture Notes in Earth Sciences, 93, Springer–Verlag, Berlin.

MORENO, A., NAVE, S., KUHLMANN, H., CANALS, M., TARGARONA, J., FREUDENTHAL, T., ABRANTES, F., 2002. Productivity response in the North Canary Basin to climate changes during the last 250 000 yr: a multi-proxy approach. Earth Planet. Sci. Lett. 196, 147–159.

MOSKOWITZ, B.M., BAZYLINSKI, D.A., EGLI, R., FRANKEL, R.B., EDWARDS, K.J., 2008. Magnetic properties of marine magnetotactic bacteria in a seasonally stratified coastal pond (Salt Pond, MA, USA). Geophys. J. Int. 174, 75–92.

MCNEILL, D.F., 1990. Biogenic magnetite from surface Holocene carbonate sediments, Great Bahama Bank. J. Geophys. Res. 95, 4363–4372.

NICOLO, M.J., DICKENS, G.R., HOLLIS, C.J. and ZACHOS, J.C., 2007. Multiple early Eocene hyperthermals: their sedimentary expression on the New Zealand continental margin and in the deep sea. Geology, 35, 699–702.

NOCCHI, M., PARISI, G., MONACO, P., MONECHI, S., and MADILE, M., 1988, Eocene and early Oligocene micropaleontology and paleoenvironments in SE Umbria, Italy: Palaeogeography, Palaeoclimatology, Palaeoecology, 67, 181–244.

ODIN, G.S. and MONTANARI, A. 1988. The Eocene–Oligocene boundary at Massignano (Ancona, Italy): A potential boundary stratotype. In: PREMOLI SILVA, I., COCCIONI, R. and MONTANARI, A. (eds). The Eocene–Oligocene Boundary in the Marche–Umbria Basin (Italy). International Subcommission on Paleogene Stratigraphy Special Publication, Industrie Grafiche Fratelli Aniballi, Ancona, 253–263.

OGG, J.G., OGG, G. and GRADSTEIN, F.M. 2008. The Concise Geologic Time Scale. Cambridge University Press, Cambridge.

OKADA, H. and BUKRY, D. 1980. Supplementary modification and introduction of code numbers to the low–latitude coccoliths biostratigraphic zonation (Bukry, 1973; 1975). Marine Micropaleontology, 5, 321–325.

OGG, J.G., 2012. Geomagnetic Polarity Time Scale. In: Gradstein, F.M., Ogg, J.G., Smith, A.G. (Eds.), A geologic time scale. Cambridge University Press, Cambridge, pp. 85–113.

OKADA, H. 1990. Quaternary and paleogene calcareous nannofossils, Leg 115. Proceedings of the Ocean Drilling Program, 115, 129-174.

PAGANI, M., ZACHOS, J.C., FREEMAN, K.H., TIPPLE, B. and BOHATY, S. 2005. Marked decline in atmospheric carbon dioxide concentrations during the Paleogene. Science, 309, 600-603.

PÄLIKE, H., ET AL., 2012. A Cenozoic record of the equatorial Pacific carbonate compensation depth. Nature 488, 609–615.

PARISI, G., GUERRERA, F., MADILE, M., MAGNONI, G., MONACO, P., MONECHI, S. and NOCCHI, M. 1988. Middle Eocene to early Oligocene calcareous nannofossil and foraminiferal biostratigraphy in the Monte Cagnero section, Piobbico (Italy). In: PREMOLI SILVA, I., COCCIONI, R. and MONTANARI, A. (eds). The Eocene–Oligocene boundary in the Marche–Umbria basin (Italy). International Subcommission on Paleogene Stratigraphy Special Publication, Industrie Grafiche Fratelli Aniballi, Ancona, 119–135.

PATTAN, J.N., MASUZAWA, T., DIVAKAR NAIDU, P., PARTHIBAN, G., YAMAMOTO, M., 2003. Productivity fluctuations in the southeastern Arabian Sea during the last 140 ka. Palaeogeogr. Palaeoclimatol. Palaeoecol. 193, 575–590.

PEARSON, P. N., AND PALMER, M. R., 2000. Atmospheric carbon dioxide concentrations over the past 60 million years, Nature, 406, 695-699.

PEARSON, P.N., OLSSON, R.K., HEMLEBEN, C., HUBER, B.T., and BERGGREN, W.A., 2006. Atlas of Eocene Planktonic Foraminifera. Cushman Foundation of Foraminiferal Research Special Publication, 41, 514 p.

PEARSON, P.N., FOSTER, G.L. and WADE, B.S. 2009, Atmospheric carbon dioxide through the Eocene-Oligocene climate transition. Nature, 461, 1110-1113. doi:10.1038/nature 08447.

PERCH-NIELSEN, K., 1985. Mesozoic calcareous nannofossils. In Bolli, H.M., Saunders, J.B., and Perch-Nielsen, K. (Eds.), Plankton Stratigraphy, Cambridge (Cambridge Univ. Press), 329–426.

PERSICO, D., VILLA, G., 2004. Eocene-Oligocene calcareous nannofossils from Maud Rise and Kerguelen Plateau (Antarctica): paleoecological and paleoceanographic implications. Mar. Micropal. 52, 153–179.

PETERMANN, H., BLEIL, U., 1993. Detection of live magnetotactic bacteria in South Atlantic deep-sea sediments. Earth Planet. Sci. Lett. 117, 223–228.

PETERSEN, N., VON DOBENECK, T., VALI, H., 1986. Fossil bacterial magnetite in deep-sea sediments from the South Atlantic Ocean. Nature 320, 611–614.

PETERSON, L.C. AND BACKMAN, J. 1990. Late Cenozoic carbonate accumulation and the history of the carbonate compensation depth in the western equatorial Indian Ocean. Proceedings of the Ocean Drilling Program, 115, 467-508.

PETRIZZO, M.R., 2005. An early late Paleocene event on Shatsky Rise, northwest Pacific Ocean (ODP Leg 198): evidence from planktonic foraminiferal assemblage. In: Proceeding Ocean Drilling Program, Scientific Results (T.J. BRALOWER, I. PREMOLI SILVA and M.J. MALONE, eds). ODP, 198, 1–29.

POLLING, M., HOUBEN, A.J.P., FIRTH, J., CAOXALL, H., ELDRETT, J., SCHOUTEN, S., REICHART, G-J., AND BRINKHUIS, H., 2011, The Middle Eocene Climatic Optimun (MECO) in the high latitudes of the North Atlantic: temperature and biotic change, in Egger, H., eds., Climate and Biota of Early Paleogene, Conference Program and Abstracts, Berichte der Geologischen Bundesanstalt, v. 85, p.130.

POPOV, S.V., RÖGL, F., ROZANOV, A.Y., STEININGER, F.F., SHCHERBA, I.G., AND KOVAC , M., 2004, Lithological-paleogeographic maps of Paratethys—10 maps Late Eocene to Pliocene: Frankfurt, Courier Forschungsinstitut Senckenberg, 250, 46 p., 10 maps.

PREMOLI SILVA, I. and JENKINS, D.G. 1993. Decision on the Eocene–Oligocene boundary stratotype: Episodes, 16, 379–382.

PROSS, J., HOUBEN, A.J.P., VAN SIMAEYS, S., WILLIAMS, G.L., KOTTHOFF, U., COCCIONI, R., WILPSHAAR, M. and BRINKHUIS H. 2010. Umbria–Marche revisited: A refined magnetostratigraphic calibration of dinoflagellate cyst events for the Oligocene of the Western Tethys. Review of Palaeobotany and Palynology, 158 213–235.

QUILLÉVÉRÉ, F., NORRIS, R.D., KROON, D. and WILSON, P.A., 2008. Transient ocean warming and shifts in carbon reservoirs during the early Danian. Earth and Planetary Science Letters, 265, 600–615.

RAFFI, I., BACKMAN, J. and PÄLIKE, H. 2005. Changes in calcareous nannofossil assemblages across the Paleocene/Eocene transition from the paleo–equatorial Pacific Ocean. Palaeogeography, Palaeoclimatology, Palaeoecology, 226, 93–126.

RAFFI, I., BACKMAN, J., ZACHOS, J.C., SLUIJS, A., 2009. The response of calcareous nannofossil assemblages to the Paleocene Eocene Thermal Maximum at the Walvis Ridge in the South Atlantic. Mar. Micropal. 70, 201–212.

REA, D.K., 1994. The paleoclimatic record provided by eolian deposition in the deep sea: the geologic history of wind. Rev. Geophys. 32, 159–195.

RIMMER, S.M., THOMPSON, J.A., GOODNIGHT, S.A., ROBL, T.L., 2004. Multiple controls on the preservation of organic matter in Devonian-Mississippian marine black shales: geochemical and petrography evidence. Palaeogeogr. Palaeoclimatol. Palaeoecol. 215, 125–154.

RIO, D., FORNACIARI, E. and RAFFI, I. 1990. Late Oligocene through early Pleistocene calcareous nannofossils from western equatorial Indian Ocean (Leg 115). Proceedings of the Ocean Drilling Program, 115, 175-236.

ROBERTS, A.P., STONER, J.S., RICHTER, C. 1996. Coring-induced magnetic overprints and limitations of the long-core paleomagnetic measiurment technique some observations from Leg 160 Eastern Mediterranean Sea. In: Emeis, K.-C., Robertson, A.H.F., Richter, C. (Eds.), Proceedings of the Ocean Drilling Program, Init. Repts. 160. College Station, 465 TX, 497-505 (Ocean Drilling Program).

ROBERTS, A.P., PIKE, C.R., VEROSUB, K.L., 2000. FORC diagrams: a new tool for characterizing the magnetic properties of natural samples. J. Geophys. Res. 105, 28461–28475.

ROBERTS, A.P., FLORINDO, F., VILLA, G., CHANG, L., JOVANE, L., BOHATY, S.M., LARRASOAÑA, J.C., HESLOP, D., FITZ GERALD, J.D., 2011. Magnetotactic bacterial abundance in pelagic marine environments is limited by organic carbon flux and availability of dissolved iron. Earth Planet. Sci. Lett. 310, 441–452.

ROBERTS, A.P., CHANG, L., HESLOP, D., FLORINDO, F., LARRASOAÑA, J.C., 2012. Searching for single domain magnetite in the "pseudo-single-domain" sedimentary haystack: implications of biogenic magnetite preservation for sediment magnetism and relative paleointensity determinations. J. Geophys. Res. 117, B08104, doi:10.1029/2012JB009412.

ROBERTSON, D.J., FRANCE, D.E., 1994. Discrimination of remanence-carrying minerals in mixtures, using isothermal remanent magnetisation acquisition curves. Phys. Earth Planet. Inter. 84, 223–234.

ROBINSON, S.G. 1990. Applications for whole-core magnetic susceptibility measurements of deep-sea sediments: Leg 115 results. Proceedings of the Ocean Drilling Program, 115, 737-772.

RÖHL, U., WESTERHOLD, T., MONECHI, S., THOMAS, E., ZACHOS, J.C. and DONNER, B., 2005. The Third and Final Early Eocene Thermal Maximum: characteristics, Timing and Mechanisms of the 'X' Event. Geol. Soc. Am., 37th Annual Meeting, Salt Lake City, USA, Abstract, 264.

RÖHL, U., WESTERHOLD, T., BRALOWER, T.J. and ZACHOS, J.C., 2007. On the duration of the Paleocene-Eocene thermal maximum (PETM). Geochemestry Geophysics and Geosystems, 8, Q12002.

ROMEIN, A.J.T., 1979. Lineages in early Paleogene calcareous nannoplankton. Utrecht Micropaleontological Bulletin, 22, 231.

ROYER, D. L., WING, S. L., BEERLING, D. J., JOLLEY, D. W., KOCH, P. L., HICKEY, L. J., AND BERNER, R. A., 2001. Paleobotanical evidence for near present-day levels of atmospheric CO_2 during part of the tertiary, Science, 292, 2310-2313.

ROYER, J.-Y and COFFIN, M.F., 1992. Jurassic to Eocene plate tectonic reconstructions in the Kerguelen Plateau Region. Proceedings of the Ocean Drilling Program Science Results, 120, edited by R. Schlich, S.W. Wise jr. et al., 917-928.

SAVIAN, J., JOVANE, L., BOHATY, S., WILSON, P., 2013. Middle Eocene to early Oligocene magnetostratigraphy of ODP Hole 711A (Leg 115), western equatorial Indian Ocean. Geological Society, London, Special Publications, 373, first published March 25, 2013; doi 10.1144/SP373.16.

SCHER, H.D., and MARTIN, E.E., 2004, Circulation in the Southern Ocean during the Paleogene inferred from neodymium isotopes: Earth and Planetary Science Letters, 228, 391–405.

SCHNEIDER, D.A. AND KENT, D.V. 1990a. Paleomagnetism of Leg 115 sediments: implications for Neogene magnetostratigraphy and paleolatitude of the Reunion Hotspot. Proceedings of the Ocean Drilling Program, 115, 717-736.

SCHNEIDER, D.A., and KENT, D.V., 1990b. Testing models of the Tertiary paleomagnetic field. Earth and Planetary Science Letters, 101, 260-271.

SCHULTE, P., SCHEIBNER, C., SPEIJER, R.P., 2011. Fluvial discharge and sea-level changes controlling black shale deposition during the Paleocene–Eocene Thermal Maximum in the Dababiya Quarry section, Egypt. Chem. Geol. 285, 167–183.

SCHUMANN, D., RAUB, T.D., KOPP, R.E., GUERQUIN-KERNE, J.-L., WUE, T.-D., ROUILLER, I., SMIRNOV, A.V., SEARS, S.Q., LÜCKEN, U., TIKOO, S.M., HESSE, R., KIRSCHVINK, J.L., VALI, H., 2008. Gigantism in unique biogenic magnetite at the Paleocene–Eocene Thermal Maximum. Proc. Natl. Acad. Sci. 105, 17648–17356.

SEXTON, P.F., NORRIS, R.D., WILSON, P.A., PÄLIKE, H., WESTERHOLD, T., RÖHL, U., BOLTON, C.T. AND GIBBS, S. 2011. Eocene global warming events driven by ventilation of oceanic dissolved organic carbon. Nature, 471, 349-353.

SHACKLETON, N.J. and KENNETT, J.P. 1975. Paleotemperature history of the Cenozoic and the initiation of Antarctic glaciation: oxygen and carbon isotope analyses in DSDP sites 277, 279, and 281. Initial Report of Deep Sea Drilling Project, 29, 743-755.

SLUIJS, A., BOWEN, G.J., BRINKHUIS, H., LOURENS, L.J. and THOMAS, E., 2007. The Palaeocene-Eocene Thermal maximum super greenhouse: biotic and geochemical signatures, age models and mechanisms of climate change. In: Deep Time Perspectives on Climate Change: Marrying the Signal from Computer Models and Biological Proxies (M. WILLIAMS, A.M. HAYWOOD, F.J. GREGORY and D.N. SCHMIDT, eds). Micropal. Soc. Spec. Publ., pp. 323–351. The Geological Society, London.

SMITH, J.J., HASIOTIS, S.T., KRAUS, M.J., WOODY, D.T., 2009. Transient dwarfism of soil fauna during the Paleocene–Eocene Thermal Maximum. Proc. Natl. Acad. Sci. USA 106, 17655–17660.

SPEZZAFERRI, S., BASSO, D. and COCCIONI, R. 2002. Late Eocene planktonic foraminiferal response to an extraterrestrial impact at Massignano GSSP (northeastern Apennines, Italy). Journal of Foraminiferal Research, 32, 188–199.

SPOFFORTH, D.J.A., AGNINI, C., PÄLIKE, H., RIO, D., FORNACIARI, E., GIUSBERT, L., LUCIANI, V., LANCI, L. and MUTTONI, G. 2010. Organic carbon burial following the middle Eocene climatic optimum in the central western Tethys. Paleoceanography, 25, PA3210.

STAP, L., LOURENS, L., VAN DIJK, A., SCHOUTEN, S. and THOMAS, E., 2010a. Coherent pattern and timing of the carbon isotope excursion and warming during Eocene Thermal Maximum 2 as recorded in planktic and benthic foraminifera. Geochemestry, Geophysics, Geosystems, 11, Q11011.

STAP, L., LOURENS, L.J., THOMAS, E., SLUIJS, A., BOHATY, S.M. and ZACHOS, J.C., 2010b. High-resolution deep-sea carbon and oxygen isotope records of Eocene Thermal Maximum 2 and H2. Geology, 38, 607–610.

TARDUNO, J.A., 1994. Temporal trends of magnetic dissolution in the pelagic realm: gauging paleoproductivity? Earth Planet. Sci. Lett. 123, 39–48.

TARDUNO, J.A., WILKISON, S., 1996. Non-steady state magnetic mineral reduction, chemical lock-in, and delayed remanence acquisition in pelagic sediments. Earth Planet. Sci. Lett. 144, 315–326.

THOMAS, E. and ZACHOS, J.C., 2000. Was the late Paleocene thermal maximum a unique event? Geol. För. Stock. för., 122, 169–170.

THOMAS, E., ZACHOS, J.C. and BRALOWER, T.J., 2000. Deep-sea environments on a warm Earth: latest Paleocene–early Eocene. In: Warm Climates in Earth History (B. HUBER, K. MACLEOD and S. WING eds), pp. 132–160. Cambridge University Press, Cambridge.

THOMAS, E., BRINKHUIS, H., HUBER, M. and RÖHL, U., 2006. An ocean view of the early Cenozoic Greenhouse World. Oceanography (Spec. Vol. Ocean Drilling), 19, 63–72.

TOFFANIN, F., AGNINI, C., FORNACIARI, E., RIO, D., GIUSBERTI, L., LUCIANI, V., SPOFFORTH, D.J.A., PÄLIKE, H., 2011. Changes in calcareous nannofossil assemblages during the Middle Eocene Climatic Optimum: clues from the central-western Tethys (Alano section, NE Italy). Mar. Micropal. 81, 22–31.

TOUCHARD, Y., ROCHETTE, P., AUBRY, M.P. AND MICHARD, A. 2003. High-resolution magnetostratigraphic and biostratigraphic study of Ethiopian traps-related products in Oligocene sediments from the Indian Ocean. Earth and Planetary Science Letters, 206, 293-508.

TREMOLADA, F., BRALOWER, T.J., 2004. Nannofossil assemblage fluctuations during the Paleocene–Eocene Thermal Maximum at Sites 213 (Indian Ocean) and 401 (North Atlantic Ocean): palaeoceanographic implications. Mar. Micropal. 52, 107–116.

TRIPATI, A., BACKMAN, J., ELDERFIELD, H. and FERRETTI, P. 2005. Eocene bipolar glaciation associated with global carbon cycle changes. Nature, 436, 341-346.

VALI, H., FÖRSTER, O., AMARANTIDIS, G., PETERSEN, N., 1987. Magnetotactic bacteria and their magnetofossils in sediments. Earth Planet. Sci. Lett. 86, 389–400.

VANDENBERGHE, N., HILGEN, F.J., SPEIJER, R.P., OGG, J.G., GRADSTEIN, F.M., HAMMER, O., HOLLIS, C.J., HOOKER, J.J., 2012. The Paleogene Period, Chapter 28, in Gradstein, F.M., Ogg, J.G., Smith, A.G., eds., A geologic time scale: Cambridge University Press, Cambridge, 855–941.

VERDUCCI, M. and NOCCHI, M. 2004. Middle to late Eocene main planktonic foraminiferal events in the Central Mediterranean area (Umbria–Marche Basin) related to paleoclimatic changes. Neues Jahrbuch für Geologie und Palaontologie Abhandlungen, 234, 361–413.

VIA, R.K., AND THOMAS, D.J., 2006, Evolution of Atlantic thermohaline circulation: Early Oligocene onset of deep-water production in the North Atlantic: Geology, 34, 6, 441–444.

VILLA, G., FIORONI, C., PEA, L., BOHATY, S., PERSICO, D., 2008. Middle Eocene–late Oligocene climate variability: calcareous nannofossil response at Kerguelen Plateau, Site 748. Mar. Micropal. 169, 173–192.

WADE, B.S., PEARSON, P.N., BERGGREN, W.A. and PÄLIKE, H. 2011. Review and revision of Cenozoic tropical planktonic foraminiferal biostratigraphy and calibration to the geomagnetic polarity and astronomical time scale. Earth–Science Reviews 104, 111–142.

WEI, W., VILLA, J., and WISE, JR., S.W. 1992. Paleoceanographic implications of Eocene-Oligocene calcareous nannofossils from sites 711 and 748 in the Indian Ocean. Proceedings of the Ocean Drilling Program, 120, 979-999.

WEI, G., LIU, Y., LI, X., CHEN, M., WEI, W., 2003. High-resolution elemental records from the South China Sea and their paleoproductivity implications. Paleoceanography 18, 1054.

VEIZER, J., HOEFS, J., 1976. The nature of 18O/16O and 13C/12C secular trends in sedimentary carbonate rocks. Geochim. Cosmochim. Acta 40, 1387–1395.

WESTERHOLD, T., RÖHL, U., LASKAR, J., BOWLES, J., RAFFI, I., LOURENS, L.J. and ZACHOS, J.C., 2007. On the duration of magnetochrons C24r and C25n and the timing of early Eocene global warming events: implications from the Ocean Drilling Program Leg 208 Walvis Ridge depth transect. Paleoceanography, 22, PA2201.

WESTERHOLD, T., RÖHL, U., RAFFI, I., FORNACIARI, E., MONECHI, S., REALE, V., BOWLES, J. and EVANS, H.F., 2008. Astronomical calibration of the Paleocene time. Palaeogeography, Palaeoclimatology, Palaeoecology, 257, 377–403.

WESTERHOLD, T., RÖHL, U., DONNER, B., MCCARREN, H.K. and ZACHOS, J.C., 2011. A complete high-resolution Paleocene benthic stable isotope record for the central Pacific (ODP Site 1209). Paleoceanography, 26, PA2216.

WING, S.L., HARRINGTON, G.J., SMITH, F.A., BLOCH, J.I., BOYER, D.M., FREEMAN, K.H., 2005. Transient floral change and rapid global warming at the Paleocene–Eocene boundary. Science 310, 993–996.

WITKOWSKI, J., BOHATY, S.M., MCCARTNEY, K., AND HARWOOD, D.M., 2012, Enhanced siliceous plankton productivity in response to middle Eocene warming at Southern Ocean ODP Sites 748 and 749: Palaeogeography, Palaeoclimatology, Palaeoecology, 326-328, 78-94.

YAMAZAKI, T., KAWAHATA, H., 1998. Organic carbon flux controls the morphology of magnetofossils in sediments. Geology 26, 1064–1066.

YAMAZAKI, T., 2008. Magnetostatic interactions in deep-sea sediments inferred from first-order reversal curve diagrams: implications for relative paleointensity normalization. Geochem. Geophys. Geosyst. 9, Q02005, doi:10.1029/2007GC001797.

YAMAZAKI, T., 2009. Environmental magnetism of Pleistocene sediments in the North Pacific and Ontong-Java Plateau: temporal variations of detrital and biogenic components. Geochem. Geophys. Geosyst. 10, Q07Z04, doi:10.1029/2009GC002413.

YAMAZAKI, T., 2012. Paleoposition of Intertropical Convergence Zone in the eastern Pacific inferred from glacial–interglacial changes in terrigenous and biogenic magnetic mineral fractions. Geology 40, 151–154.

YOUSSEF, M.A., 2009. High resolution calcareous nannofossil biostratigraphy and paleoecology across the Latest Danian event (LDE) in central Eastern Desert, Egypt. Marine Micropaleontology, 72, 111–128.

ZACHOS, J.C., REA, D.K., SETO, K., NOMURA, R. and NIITSUMA, N., 1992. Paleogene and early Neogene deep water paleoceanography of the Indian Ocean as determined from benthic foraminifer stable carbon and oxygen isotope records. Synthesis of Results from Scientific Drilling in the Indian Ocean, Geophysical Monograph 70, 351-385.

ZACHOS, J.C., QUINN, T.M. and SALAMY, K.A. 1996. High-resolution (104 years) deep-sea foraminiferal stable isotope records of the Eocene-Oligocene climate transitions. Palaeoceanography, 11, 251-266.

ZACHOS, J.C., PAGANI, M., SLOAN, L., THOMAS, E. AND BILLUPS, K. 2001. Trends, rhythms, and aberrations in global climate 65 Ma to present. Science, 292, 686-693.

ZACHOS, J.C., KROON, D., BLUM, P., BOWLES, J., GAILLOT, P., HASEGAWA, T., HATHORNE, E.C., HODELL, D.A., KELLY, D.C., JUNG, J.-H., KELLER, S.M., LEE, Y.S., LEUSCHNER, D.C., LIU, Z., LOHMANN, K.C., LOURENS, L., MONECHI, S., NICOLO, M., RAFFI, I., RIESSELMAN, C., RÖHL, U., SCHELLENBERG, S.A., SCHMIDT, D.N., SLUIJS, A., THOMAS, D.J., THOMAS, E. and VALLIUS, H., 2004. Proceedings of the Ocean Drilling Program, Initial Reports, 208.

ZACHOS, J.C., RÖHL, U., SCHELLENBERG, S.A., SLUIJS, A., HODELL, D.A., KELLY, D.C., THOMAS, E., NICOLO, M., RAFFI, I., LOURENS, L.J., MCCARREN, H. and KROON, D., 2005. Rapid acidification of the ocean during the Paleocene–Eocene thermal maximum. Science, 308, 1611–1615.

ZACHOS, J.C., DICKENS, G.R. AND ZEEBE, R.E. 2008. An early Cenozoic perspective on greenhouse warming and carbon-cycle dynamics. Nature, 451, 279-283.

ZACHOS, J.C., MCCARREN, H., MURPHY, B., RÖHL, U. and WESTERHOLD, T., 2010. Tempo and scale of late Paleocene and early Eocene carbon isotope cycles: implications for the origin of hyperthermals. Earth and Planetary Science Letters, 299, 242–249.

ZIJDERVELD, J.D.A., 1967. A.C. demagnetization of rocks. In: Collison, D.W., Creer, K.M. and Runcorn, S.K. (eds) Methods in Palaeomagnetism, Elsevier, 256-286.